8-2023

Injectable Immunomodulatory Strategies to Enhance Muscle Recovery Following Injury

Tai Huu Huynh
University of Arkansas-Fayetteville

Injectable Immunomodulatory Strategies to Enhance Muscle Recovery Following Injury

A dissertation submitted in partial fulfillment
of the requirements for the degree of
Doctor of Philosophy in Biomedical Engineering

by

Tai Huynh
University of Arkansas
Bachelor of Science in Chemical Engineering, 2013
University of Arkansas
Master of Science in Biomedical Engineering, 2021

August 2023
University of Arkansas

This dissertation is approved for recommendation to the Graduate Council.

_____
Jeffrey C. Wolchok, Ph.D.
Dissertation Director

_____
Kartik Balachandran, Ph.D.
Committee Member

_____
Nicholas P. Greene, Ph.D.
Committee Member

_____
Young Hye Song, Ph.D.
Committee Member

Abstract

Although skeletal muscle displays an astonishing regenerative capacity, injuries or diseases that resulted in bedridden or chronic muscle wasting can overwhelm this intrinsic feature of skeletal muscle and lead to functional deficit (range of motion and/or strength) and overall reduction in quality of life. Microenvironmental cues within injured skeletal muscle dictate regenerative and repair process which are tightly coordinated interplay among resident cells, cells recruitment and immune response following an assault in the muscle extracellular matrix (ECM). The successful regeneration of functional tissues requires both appropriate modulation of the inflammatory response, and activation of a variety of cell populations. Biomaterials offer unique opportunities to spatiotemporally control cytokine delivery and may provide significant benefits in the modulation of immune cells and muscle-immune micro-environment (MIME) to promote regeneration. The aim of this dissertation is to create injectable therapeutics that are capable of both modulating the inflammatory response and directly promoting muscle regeneration. In aim 1, we investigated the safety and therapeutic potential of human muscle derived decellularized ECM to promote muscle regeneration in mouse disuse and reloading hindlimb injury model and rabbit chronic rotator cuff tear muscle degenerative injury model. In aim 2, we investigated the therapeutic potential of delayed delivery of IL-10 to boost muscle regeneration when combined with progenitor cells repair (mined muscle grafts) in rat volumetric muscle loss injury model. Together, the findings of these two aims further our understanding of the role that pro-regenerative immune cells play in promoting endogenous mechanisms of tissue repair after muscle injury and present potential therapeutic avenues to modulate the MIME in aiding muscle repair and recovery.

Acknowledgments

I would like to thank my colleagues and lab-mates in the Regenerative Biomaterials Laboratory at the University of Arkansas, particularly John Kim, Kevin Roberts, Cassie Reed, Jacon Jacob Schluns, Chris Slaven. I thank Dr. Balachandran, Dr. Song, Dr. Greene as well as the students in their lab for their collaboration and assistance in these studies.

My deepest gratitude to Dr. Wolchok for providing me with invaluable support during my time in his lab. Dr. Wolchok not only helped me develop research skills, but he also allowed me to explore opportunities to broaden my scientific horizon. His mentorship has propelled me to this next stage of my scientific career and for that I am sincerely grateful.

I also want to thank my undergrad mentees Peyton Phelps, Alex Heffington, Jack Arp, and Zain Blackwell for the numerous hours of tedious lab work and for helping me become a better mentor. I would like to thank all my friends and family who have lend me incalculable support so I can complete this journey. Lastly, I would like to thank the public sources of funding without which this work would not be possible, including the National Institute of Health, and the Arkansas Biosciences Institute.

Dedication

I dedicate this work to my mother, and Brian for their love and support during this journey. I would not have achieved this goal without their sacrifices.

Table of Contents

List of Published Chapters

Chapter 2: Aim 1b

Huynh T, Kim JT, Dunlap G, Ahmadi S and Wolchok JC. In vivo testing of an injectable matrix gel for the treatment of shoulder cuff muscle fatty degeneration. *Journal of shoulder and elbow surgery*. 2020; 29: e478-e90 DOI: 10.1016/j.jse.2020.03.038.

Chapter 4: Aim 2

Huynh T, Reed C, Blackwell Z, Phelps P, Herrera LCP, Almodovar J, et al. Local IL-10 delivery modulates the immune response and enhances repair of volumetric muscle loss muscle injury. *Scientific reports*. 2023; 13: 1983 DOI: 10.1038/s41598-023-27981-x.

CHAPTER 1: Introduction

1.1 Skeletal muscle in health and injury

Skeletal muscle is a hierarchically organized tissue encompassing around 40% of total human body weight [1].The main functions of skeletal muscle are to maintain posture, to generate force and facilitate body movement. Muscle fibers, or myofibers, are the basic cellular building block of skeletal muscle and are multinucleated, post-mitotic cells that are arranged in bundles to form whole muscles[2]. In order to reliably produce contractile properties of muscle, these myofibers and muscles need support from blood vessels, nerve, resident muscle cells, non-contractile tissue (fat, and the extracellular matrix (ECM))[3]. The vascular system ensures a supply of nutrients, oxygen and removal of cellular waste and by-products. Nerves innervate the muscle, employing motoneurons that form the neuromuscular junction which is essential for muscle contractility. Cells of the immune system constitute a transient local environment in healthy muscle, though can be activated and further recruited by injury. Fibroblasts provide ECM and progenitor cells that are crucial to muscle maintenance[4]. The ECM functions to transmit forces between myofibers and tendons, localize soluble growth factors and glycoproteins, and guide the ancillary cells and structures that support contraction and satellite cells (predominant resident muscle progenitor cell activated during muscle repair and regeneration)[5].

The muscle satellite cells (MuSC) are named for their adjacency to myofibers- and were first identified by Alexander Mauro[6]. They were characterized by their anatomical position residing between the cell membrane (sarcolemma) of myofibers and the basal lamina of the basement membrane. These cells actively proliferate in the early postnatal phase but reserve a quiescent subpopulation that can be drawn upon from mature muscles[7]. In their quiescent state,

they express Pax3 and/or Pax7, two related paired-box transcription factors that provide useful markers for the identification of these cells. During muscle repair/regeneration, satellite cells can self-renew and differentiate into mature myofibers[8]. Upon muscle damage, satellite cells exit from the quiescent state, become activated and start to proliferate. During this period of proliferation, Pax7+/Myf5- satellite stem cells can produce two types of daughter cells. Some commit toward a myogenic fate by downregulating Pax7 expression and upregulating the myogenic regulatory factors (MRFs) Myf5, whereas others return to quiescence to replenish the pool of quiescent satellite cells[9]. The activated satellite cells and their progeny, also referred to as adult myoblasts, can migrate to sites of injury across relatively large distances both along and between myofibers[10,11]. Upon arriving at a site of injury, myoblasts undergo a program of differentiation, expressing MyoD, then fuse with each other to form immature myocytes termed myotubes. These myotubes, expressing MyoG, fuse to the sealed ends of existing damaged myofibers forming a nascent regenerating myofiber[12,13]. Together these MRFs (Myf5, MyoD, MyoG) control the specification and differentiation of skeletal muscle lineage[14].

Various stimuli can trigger satellite cell activation, which are thought to be released by damaged myofibers, immune cells, and fibroblasts after injury[15]. This sequence of events can be divided into roughly three phases. The first phase is the destruction and inflammatory phase in which damaged muscle fibers undergo necrosis and release damage-associate molecular patterns (DAMPs) that trigger an inflammatory response and the arrival of immune cells such as neutrophils, and inflammatory monocytes, and macrophages[16]. The second phase is the repair phase, in which the injury site debris is cleared by immune cells, and myoblasts proliferate and fuse to form new muscle fibers. During the repair phase, a provisional ECM scar is formed as a scaffold for infiltrating immune and stromal cells[17]. The third phase is the remodeling phase in

which newly regenerated muscle fibers are reorganized and the provisional scar tissue is remodeled, thus restoring tissue function. As many ancillary cells can shape the muscle microenvironment and secrete signals influencing cells with myogenic potential, dysregulation in any of these phases can result in atrophy, fibrosis, fatty infiltration and decrease in muscle function[18].

Immune cells including neutrophils, monocytes/macrophages, dendritic cells, and CD4+/CD8+/regulatory T cells are now known to significantly contribute to skeletal muscle regeneration; while mechanisms of immune cell involvement in muscle regeneration are understood mostly in broad terms, they are now intensely studied for the insight they may lend to myo-pathobiology and treatment[19]. The progression of inflammation during muscle regeneration is tightly associated with stages of reparative myogenesis[20]. The range of cells that make up the immunological repertoire changes in accordance with the repair state of the injured muscle, and influences not only satellite cell proliferation and differentiation, but also other recovery processes such as angiogenesis, nerve regeneration, and ECM deposition and remodeling.

Neutrophils (commonly immunophenotyped as CD11b+Ly6G+) are among the first immune cells initially infiltrating skeletal muscle following muscle trauma, peaking in the immediate hours post-injury and generally declining rapidly after one day [21]. Acting as the “first responders” to injury, neutrophils phagocytose apoptotic cells and debris, and secrete reactive oxygen species (ROS) as well as cytokines such as interferon-gamma (IFNγ) and tumor necrosis factor-alpha (TNF) that shifts the injury microenvironment towards a pro-inflammatory state and promotes endothelial cell activation for the subsequent recruitment of monocytes. Within 24 hours, the neutrophil quantities rapidly decline and are replaced with invading monocytes that ultimately transform into phagocytic macrophages, commonly referred to as M1 macrophages.

These inflammatory macrophages secrete inflammatory cytokines such interleukin (IL)-1 and IL-6 (among others), to further promote immune cell migration, activation of inflammatory signaling via NF-κβ, and furthering muscle damage via increased nitric oxide (NO) production[22].

Macrophages are among the longest-lived transient residents of injured and regenerating skeletal muscle, increasing rapidly in number roughly 2 days post-injury as neutrophils decline, and in some cases persisting for several weeks. In addition to their phagocytosis of cellular debris, M1 macrophages exert a pro-proliferative, anti-differentiating effect on satellite cells[23]. In typical mild muscle injury, the phagocytosis of apoptotic neutrophils stimulates macrophages to release mediators such IL-10 and TGF-β suppressing the inflammatory response[16]. Suppression of the initial inflammatory response is critical for subsequent tissue healing as many of the processes associated with acute inflammation can also cause collateral tissue damage[24]. For example, unresolved inflammation has been shown to inhibit the healing and significantly contribute to muscle wasting in muscular dystrophies[25]. This phenotypic transition toward a pro-constructive state is observed in the macrophage population several days post-injury. These anti-inflammatory (M2) macrophages that dominate the later stages of healing promote satellite cells differentiation, with IL-10 and IGF-1 identified as key molecules in the progression of late-stage myogenesis [26]. In additional to soluble factors, cell-cell contacts between macrophages and myogenic progenitor cells have been shown to protect these cells from apoptosis[27]. Though the categorization is helpful in studying macrophage programs in diseases and injuries, recent evidence suggests a spectrum of macrophage phenotypes rather than a Boolean metabolic switch. For example, examination of macrophage behavior following muscle laceration in mice revealed that the gene expression profiles of assessed macrophages did not correspond to the classical M1/M2 (Th1/Th2) paradigm observed in vitro; rather, they exhibited substantial heterogeneity[28].

Regardless of categorization, the general inflammatory-to-constructive macrophage transition in skeletal muscle is well attested[29]. Disruptions to the regulation of macrophage polarization have been shown to delay muscle regeneration in murine models. Deletion of microRNA-155, an miRNA that does not regulate satellite cells but rather regulates the balance between M1 and M2 macrophages, significantly inhibited the regeneration of muscle fibers [30]. Other studies have shown that conditional deletion of the IGF-1 gene, which inhibited M2 polarization, resulted in fewer regenerating myofibers in the muscle cross section and diminished myofiber cross sectional area (CSA) among the regenerating myofibers[31].

Adding to the complexity, activated wound healing ("M2") macrophages are further classified into a number of subtypes[32]. Two important subcategory of M2 macrophages are those stimulated in response to IL-4 and IL-13, typically referred to as wound-healing macrophages, or M2a (CD206) macrophages and those stimulated in response to glucocorticoids and IL- 10; typically referred to as regulatory macrophages, or M2c (CD163) macrophages[33]. In macrophages, IL-4 stimulates arginase metabolism ultimately leading to the production of polyamines and collagen, and contributing to the production of ECM, an important process in tissue regeneration[34]. Further, M2a macrophages express the decoy IL-1RII and IL-1 receptor antagonist, thereby directly suppressing inflammatory mechanisms promoted by the M1 phenotype[35]. Over expression of M2a macrophages, like over expression of M1 macrophages, can also be detrimental to the host. However rather than leading to tissue destruction, dysregulation of the M2a response leads to excessive fibrosis that can limit tissue function[36]. In contrast to M2a macrophages, M2c macrophages do not substantially contribute to extracellular matrix production. These macrophages produce high levels of IL-10, a potent inhibitor of inflammation, promote the ECM remodeling, angiogenesis and dampen inflammation.

Dysregulation of M2c macrophages can lead to inappropriate alterations in immune suppression, contribute to the progression of neoplasia[32]. Most notable, these macrophages can modulate the adaptive immune cells[37].

Specifically, among the adaptive immune cells, T-cells have been showed to play important roles in skeletal muscle regeneration. Burzyn *et al* showed that a population of ($CD4^+$, $CD25^+$, $ST2^+$) regulatory T cells (Tregs) within regenerating skeletal muscle displaying a transcriptome unique to the injury niche compared with Tregs isolated from lymphoid organs such as the spleen, accumulates precisely during the inflammatory-to-constructive macrophage transition[38]. The transcriptomic analysis revealed that these muscle Tregs overexpress IL-10, as well as the growth factors platelet-derived growth factor (PDGF) and Amphiregulin (AREG), compared to splenic Tregs ($ST2^-$, $CD4^+$, $Foxp3^+$) and conventional T-cells ($ST2^-$, $CD4^+$, and/or $CD8^+$) from either injured muscle or spleen. Apart from directly promoting the growth of muscle fiber via secretion of AREG, Tregs are also thought to govern the myeloid phenotype switch from inflammatory to pro-regenerative. Evidence indicates that their absence results in absence of the normal M1-M2 macrophage transition, causing chronic inflammation and fibrosis[39]. $CD8^+$ T-cells, other T-cells found at the site of muscle injury, have been shown to exert a positive impact on muscle regeneration through the secretion of monocyte chemoattractant protein-1 (MCP-1) that recruits inflammatory macrophages at the initial phase of muscle regeneration and the promotion satellite cell proliferation through the secretion of several cytokines[40]. On the other hand, depletion of $CD8^+$ and $CD4^+$ T-cells in dystrophic mice significantly reduces the skeletal muscle pathology seen in these animals [41]. Overall, the many the different roles and pathways that $CD8^+$ T-cells and $CD4^+$ T-cells exerted within muscle injury and regeneration largely remains unknown.

Perhaps the most poorly understood yet consequential cell population in skeletal muscle are the fibro-adipogenic progenitors (FAPs) ($Sca1^+$, $PDGFR\alpha^+$), a subpopulation of resident skeletal muscle stem cells arising from a distinct mesenchymal progenitors/stem cells (MSC) which have been shown to play an important role in response to both acute injury and chronic musculoskeletal disease[42]. In healthy adult skeletal muscle, FAPs primarily localize to the interstitial space of skeletal muscle and are quiescent. Following an acute skeletal muscle damage, FAPs proliferate in the interstitial space between myofibers and produce growth factors aiding in myofiber regeneration[43]. FAPs are responsible for the muscle ECM remodeling after damage, producing a transient ECM and supporting MuSC proliferation, differentiation, and self-renewal. In addition, FAPs can secrete Collagen VI, which specifically regulates MuSC quiescence [44]. FAPs also secrete various cytokines and growth factors, which directly induce myogenic cell proliferation and survival while blocking their differentiation[45]. Preventing FAP cells from proliferating and differentiation through Nilotinib treatment impairs regeneration of muscle from acute injury, possibly due to a contribution of FAPs to MuSC proliferation[46]. Since FAPs exhibit the capability to differentiate into fibroblasts and adipocytes and are the primary source of fibrosis and adipogenesis in some muscle injuries/diseases, dysregulation of FAPs regenerative program can lead to worsening muscle fatty degeneration and fibrosis[47]. In normal healing, FAPs and MuSC proliferate at immense rates following injury, progressively increasing their numbers after injury, when damage is resolved, they steadily return to their basal numbers. However, in pathological and chronic conditions, $PDGFR\alpha^+$ FAPs can be over-activated, accumulate in high numbers and differentiating toward multiple myopathic MSC lineages depending on the type and extension of the damage[45]. FAPs also exhibit crosstalk with immune cells to provide normal tissue assembly in regeneration[48]. Depletion of $CD11b^+$ cells via

diphtheria toxin, immediately post-cardiotoxin injury, resulted in elevated fat accumulation[49]. Thus the lack of crosstalk from macrophages promotes FAPs toward the adipogenic fate and induce adipogenesis[49]. On the other hand, depletion of Tregs shows altered regeneration with increased inflammation and fibrosis[50]. Thus, disruption of the Th1/Th2 transition promotes FAPs toward the fibrotic fate and induce fibrosis.

Taken together, MuSC, FAPs, and immune cells appear to influence one another to successfully repair and regenerate skeletal muscle after damage. Thus, therapies that leverage the pro-regenerative activities of these cells represent a promising strategy to promote the regeneration of not only muscle tissue, but also motor neurons and vasculature crucial to the proper function of skeletal muscle as a whole.

1.2 Skeletal muscle atrophy

Skeletal muscle atrophy, or loss, is a common side effect of many injuries and diseases. Characteristics of skeletal muscle atrophy are well described, including loss of muscle fiber number, size, innervation, and vascularization, as well as alterations in metabolic enzyme content[51]. While numerous investigations over the years have established a fair understanding of the functional manifestations of muscle atrophy, the underlying mechanisms that control this process are not well described. Due to the complexity of this atrophy programme, clinical trials using a wide range of treatments have shown mixed results depending on specific injuries or diseases and degrees of severity[52-54]. The maintenance of skeletal muscle mass occurs through balancing protein degradation and protein synthesis, which is mediated through both circulating systemic and local growth and growth-inhibitory factors (e.g., IGF-1 and myostatin) as well as, importantly, the mechanical load placed on the muscle[55]. In response to increased skeletal muscle loading or administration of growth factors, muscle fibers can hypertrophy or increase in

mass and fiber cross sectional area [56]. On the other hand, skeletal muscle can decrease in size (atrophy) in response to decreased muscle loading, certain growth-inhibitory factors such as inflammatory cytokines that are elevated during various disease conditions, or dysregulation in normal growth signaling pathways [57,58]. In response to atrophic stimuli, protein degradation through the ubiquitin proteasome system is elevated significantly, while protein synthesis declines, resulting in a net decrease in skeletal muscle contractile protein[59]. Numerous proteins and signaling pathways have been identified to regulate skeletal mass through modulating the balance between protein synthesis and protein degradation[56]. Among these, inflammatory factors can directly bind to certain receptors to activate signaling pathways, including muscle protein synthesis inhibition and proteolysis over-activation, that lead to skeletal muscle atrophy[60]. Inflammation can directly influence skeletal muscle through the activation of intramuscular signaling pathways, including the NF-κB, JAK/STAT, and p38MAPK pathways[60]. Studies have shown that inflammatory factors such as IL-6, TNF-α, and IL-1β are involved in the control of muscle mass. IL-1β secretion caused by central nervous system inflammation can cause hypothalamic/pituitary negative feedback dysregulation resulting in excessive steroids in the bloodstream, and eventually triggering muscle atrophy[61]. A single dose of TNF-α could increase muscle proteolysis and lead to anorexia in rats[62]. IL-6 secretion caused by cachexia can inhibit PPARα, resulting in hypoketosis, which ultimately led to increased glucocorticoid release and enhanced muscle proteolysis[63]. On the other hand, therapeutic inhibitors of those aforementioned pro-inflammatory cytokines displayed positive effects in alleviating atrophy in various atrophic models[64]. Furthermore, anti-inflammatory cytokines such IL-10, and IL-4 can also affect muscle atrophy. Injection of IL-4– or IL-10–conjugated nanoparticles improve muscle function, fiber size even in at the advanced stage of muscular dystrophy[65]. These cytokines seemed to reduce

chronic muscle inflammation and atrophy through modulating immune cells and FAPs cells [66].

While a variety of conditions (denervation, disuse, unloading, volumetric muscle loss, and aging) and pathological states (malnutrition, diabetes, cancer, viral and bacterial infections) can result in atrophy[67], I will focus on three animal models that are of interest to the scope of this study.

1.3 Animal models

1.3.1 Rotator cuff tear injury

Rotator cuff tears (RCTs) are among the most common injuries and represent the most encountered muscle-tendon tear in patients. Rotator cuff tendinopathy is typically a progressive disorder evolving from tendon inflammation to degeneration and ultimately rupture[68]. However, a subset of RC tendon ruptures occur acutely as the result of a traumatic event[69]. Progressive degeneration of the tendon, particularly tendon tearing, is associated with progressive muscle degeneration. During the progression of tendinopathy, atrophy in the affected muscle can range from minimal, to greater than 75% reduction in CSA in large and chronic tears involving multiple tendons[70]. The degree of muscle atrophy correlates with the size of the tendon tear, suggesting that progressive reduction in the mechanical load through the tendon is a likely driver of this effect[71]. As the tendon tears, the muscle retracts onto the scapula, reducing muscle length[72]. This retraction of muscle onto the scapula is important because muscle force production is length sensitive[73]. In addition to an overall reduction in muscle CSA and sarcomere length, large areas of connective tissue and fat develop between the fascicles and myofibers. These features, generally termed “fibrosis” and “fatty infiltration” (FI), are frequently seen in conjunction with muscle atrophy in patients with chronic RCT [74]. Studies in animal models suggest that fibrosis resulting from RC tears significantly stiffens the muscle, depositing more

non-contractile tissue than the muscle loss[75]. Histologic lipid stains of muscle after chronic and massive RCTs show high amounts of fat that correlate with levels of FI seen on CT or MRI imaging, and can be used to diagnose the severity of muscle degeneration induced by RCT[76,77]. The quantity of FI is important not only because of its effects on decreased muscle function but also because much of this FI is irreversible, even after tendon repair[78]. Despite the importance of FI in surgical outcomes of RC repairs, little is known about the underlying etiology of this process[79]. Understanding the molecular pathways responsible for FI will be imperative to determine potential pharmacologic interventions that can reverse these degenerative processes after RCTs. One of the central regulators of adipogenesis is peroxisome proliferator–activated receptor gamma (PPARγ); a transcription factor that plays an important role in controlling gene expression in multiple physiologic processes[80]. It was initially characterized as a central regulator of developing adipose cells but has now also been implicated in the control of cell proliferation, macrophage function, and immunity[81,82]. There is also ongoing debate over which cells generate the fatty response. In the muscle context, there are at least three confirmed sources of adipogenesis: transdifferentiation of MuSC, differentiation of non-MuSC myogenic progenitors, and differentiation of FAPs subpopulation into pre-adipocyte linage [83]. Due to this lack of knowledge in the pathology of the muscle degeneration in RCT injury, no clinically-approved treatments have successfully reversed the damages in affected cuff muscles[28]. While RCT surgical treatments have advanced over the years and have remained the most effective treatment strategy to repair small to large tears, the average re-tear rate remains high at approximately 30%[84]. Therefore, developing strategies to promote RC muscle regeneration in conjunction with tendon repair can greatly add to functional recovery in this type of injury. Understanding the complex array of cell types that control muscle homeostasis, regeneration, and

pathologic progression, will support bioengineering approaches to target and/or harness the endogenous cells as an important avenue for treating RC injuries[85]. Animal models are a practical means to elucidate the cellular and molecular pathways and pathology of rotator cuff tears and to develop new technologies to improve existing treatments [86].

The rabbit models provide some of the most important insights regarding muscular changes and functional recovery associated with RCT [87]. Atrophy and fatty accumulation occur in rabbit rotator cuff tears, as in humans. The rotator cuff in rabbits heals in a fashion that is similar to that of humans[87]. The supraspinatus and infraspinatus tendons have both been used as repair models in the rabbit, however the tendon of the supraspinatus muscle (SSP) is most susceptible to tear and damage due to its shortest fibers requiring it to operate over the greatest sarcomere length range[88]. This larger model of animal (compared to mouse and rat) also provides greater accuracy and reproducibility during surgical procedures (injury creation and repair). Furthermore, to study muscle atrophy, fatty infiltration, and retraction of the musculotendinous unit, several techniques has been developed to create a chronic RCT model by delaying the repair for up to 4 weeks[89,90]. Typically, during surgical repairs, the torn (tendonectomy) RC tendons are reattached to the humerus using sutures, and sometimes in conjunction with other biomaterials[91]. Previous studies in rabbits reaffirm that RCT repair does not reverse fatty degeneration[92,93]. Although, the source of adipocytes during fatty degeneration is still under scrutiny (resident cells vs. extra muscular sources), FAPs are believed to be the main source of intramuscular fibrosis and FI[94]. The exact mechanism by which FAPs are induced towards RC adipogenesis and fibrogenesis is not well defined but some contributing factors includes local signaling, gene expression, epigenetics changes and the local niche of FAP subpopulations[95]. Two important families of transcription factors involved in the differentiation of pre-adipocytes

into mature adipocytes are peroxisome proliferator–activated receptors (PPARs) and CCAAT/enhancer-binding proteins (C/EBPs). One study using of the rodent model of RCTs found that PPARg and C/EBPa levels were increased[74]. In addition, there was significantly more FI in the RC muscle than in the tibialis anterior two weeks after each muscle received an intramuscular injection of glycerol, suggesting different baseline characteristics of FAPs depending on local niches[96]. Recent studies have also highlighted the role of FAP–immune cell interactions and how the inflammatory milieu within injured muscle can influence FAP differentiation[97]. FAPs were shown to cluster near macrophages and that factors secreted by IL-4–polarized macrophages increased FAP adipogenesis[98]. TGFβ signaling, a known stimulator of FAP fibrogenesis, is upregulated in injured muscle, with macrophages being identified as a main source[99]. TGFβ has been shown to decrease muscle fiber size, reduce contractile force, and increase expression of atrogin-1, a muscle ubiquitin ligase protein involved in proteolysis and muscle atrophy[100]. Furthermore, administration of a TGFβ inhibitor that promoted FAP apoptosis (in a rodent RCT model) demonstrated 4-fold reduction in atrogin-1 and a 50% increase in supraspinatus wet weight[101]. To this end, modulating FAP number and activity could affect the amount of fibrosis and FI that develop after muscle injury, many studies have found some successes. For example, blocking TNF signaling halted FAP apoptosis, resulting in double the FAP quantity and twice as much fibrosis after muscle injury (notexin-induced injury in mice model)[102]. This study also demonstrated that use of small molecule inhibitor that targets the TGFβ signaling pathway, led to increased FAP apoptosis and a reduction in fibrosis. Pharmaceutical means such as the anti-fibrotic drug CWHM-12 (fibrosis inhibitor in liver, kidney, and lung tissue) was shown to decrease FAP fibrotic potential i*n vitro*[103]. Although it appears that reducing the overall FAP number and activity can mitigate their downstream

pathology, removing them from muscle tissue through pharmacologic means may blunt their beneficial roles, as it has been shown that FAPs are an integral part of muscle regeneration[104]. Another avenue that preserves and augments FAP initial beneficial functions rather than simply depleting them, is to modify their behavior towards a more useful phenotype. Some studies have successfully used histone deacetylase inhibitors and microRNAs to increase expression of FAP myogenic genes (e.g., MYOD) and activate FAP myogenic transcriptional programming to promote myotube formation in MuSC co-culture experiments[105]. Along the same line, engineered FAP cells that displayed PDGFRβ expression but no PDGFRα expression did not contribute to FI or fibrosis and resulted in a four-fold decrease in myofiber atrophy when transplanted into a mouse RCT injury model[106]. Although promising, most of these therapeutic strategies have not seen great success in human translation[83]. Additional studies are needed to assess the efficacy of different strategies of FAP modification to aid in RC regeneration as attempts to improve patient outcomes will likely require addressing the degenerative pathology caused by these cells.

1.3.2 Hindlimb unloading and reloading injury

The phenotype of muscle disuse atrophy as a result of mechanical unloading can be studied by tendon failure (in the case of RCT), though were complicated by other co-myopathies (as discussed earlier). One popular model to study muscle atrophy and the adaptation of skeletal muscles to decreased activity (plasticity) is hindlimb suspension/unloading (HU)[107]. In this model, the animal is suspended by the tail in such a way that its hindlimbs do not touch the floor of the cage, whereas it is able to freely move around the cage with its forelimbs. Thus, the model prevents bearing weight, but allows freedom of movement in the suspended limb. The disuse induced in this model begins with a rapid loss of muscle mass (first one to two weeks of

unloading) then precedes to a slow rate of the muscle loss period until muscle mass reaches a new lower but stable mass[108]. Muscle mass will remain at this new steady state until an anabolic stimuli, such as an increase in external loading, stimulates muscle regrowth. The maintenance of muscle mass is dependent on the balance of two processes: protein synthesis and protein degradation (previously discussed). Under atrophy conditions there is a shift in the balance of these two processes resulting is a net loss of muscle proteins. While decreases in the rate of protein synthesis have been measured following unloading, the cellular mechanisms responsible for the decline are poorly understood[109]. One pathway that has received limited investigation is the phosphorylation of glycogen synthase kinase-3β (GSK3β), which leads to its inhibition and an increase in global protein synthesis through an increase in the activity of eukaryotic initiation factor 2B (eIF2B)[110]. Although protein degradation may play a major role in disuse-induced atrophy, few studies have measured this *in vivo* protein degradation during disuse[111]. Some studies have inferred the changes in protein degradation through the measurement of activated genes associated with specific protein degradation pathways[112]. The major proteolytic pathways in skeletal muscle include the lysosomal system (i.e., cathepsins), Ca2+-dependent proteases (i.e., calpains), caspases, and the ubiquitin proteasome pathway (UPP). Distinct mechanisms of atrophic signaling in proteolytic pathways have emerged between muscle retraction due to tendon tears and disuse muscle[113]. For example, A study found that post tenotomy gastrocnemius (GAS) muscle atrophy was primarily characterized by a lysosomal/autophagic signature, in contrast to the classical ubiquitin-mediated proteasomal activity signature of the immobilized-disused GAS[114]. Two ubiquitin ligases MuRF1 (for Muscle Ring Finger 1) and MAFbx/atrogin-1 (Muscle Atrophy F-box) were found to be good markers for atrophy associated with HU as the gene expression pattern in this model shows a rapid increase upon unloading[115]. Other markers

such NF-kB transcription factors (Bcl3 and p50) have been shown to be upregulated in response to unloading[116]. Here the atrophy programme converges since NF-κB signaling is a critical component of many disparate atrophy models, though NFκB is capable of driving atrophy through various signaling pathways[117]. Due to the complexity of this atrophy programme, mitigating disuse-induced muscle atrophy required affecting multiple signaling pathways[118]. The loss of skeletal muscle due to unloading and inactivity can be reversed upon the return of normal weight bearing (or reloading) of the limbs but is delayed and often incomplete in older individuals[119]. In some muscles, such as the tibialis anterior (TA), there appears to be an injury response upon reloading with a loss of muscle mass for up to 7 days following reloading[120]. Interestingly, the flexor muscles (TA and EDL) suffered an increase in muscle injury and a lack of recovery in aged cohort following reloading[121]. Understanding of the cellular and molecular mechanisms regulating muscle loss in response to unloading and inactivity has increased substantially over the past decade; however, it remains incomplete. Additional research is needed to determine signaling pathways involved in causing the imbalance of protein synthesis and degradation during unloading and inactivity in the young, mature, and aging individual. Strategies for inhibiting the loss of muscle mass under conditions of inactivity (e.g., bed rest) and unloading (e.g., cast immobilization) can use this knowledge to target both the inhibition of protein degradation and/or stimulation of protein synthesis.

1.3.3 Volumetric muscle loss injury

Increased attention in recent years has been focused on severe musculoskeletal injuries from sports, car accidents, combat, and surgical resection that led to volumetric muscle loss (VML). Unlike the majority of muscle injuries which can recover or can be repaired, a blunt loss of muscle tissue (20% or more of the mass in the affected muscle) in VML injury often result in

a permanent loss of muscle tissue and chronic loss of strength and function[122]. As there are no surgical or regenerative standards of care for VML injury, physical rehabilitation is the only targeted therapy for VML-injured muscle, though these physical therapies have not promoted significant strength improvements [123]. Thus, there is a clear need for therapeutic strategies that can promote *de novo* regeneration of the removed muscle tissue to restore muscle and limb function.

Preclinical models of extremity VML have been developed in various species and all resulted in a chronic loss of muscle mass and muscle strength[124]. Generally, in VML, because of the significant loss of the native ECM together with resident myogenic progenitors, innervation and vascularity in the musculature, the ensuing innate muscle repair process does not yield sufficient new myofibers in time to prevent an excessive fibrotic response. Excessive fibrosis, in turn, may prevent adequate revascularization and reinnervation at the injury site, thus hindering the successful delivery of any postponed therapeutics. At the VML injury site, not only the fibrosis and scar formation override muscle regeneration, but chronic inflammatory responses are also sustained. These factors point to a VML muscle microenvironment that has been described as a myogenesis-inhibitive feedback loop[125]. This stipulation was attributed to a dysregulated and altered ECM as well as increases in expression of transcription factors that impede the convention of MRFs programme. Additionally, not only VML results in an immediate and persistent loss of isometric strength, but the strength deficits are also greater than the predicted level corresponding with the muscle loss. For example, VML models using quadriceps and TA muscle with 10 and 20% loss of muscle mass have presented strength deficits of ~33% and 65%, respectively [126,127]. Greater strength deficits than percent VML have also been observed in various animal models at extended recovery time points suggesting a suboptimal performance of

the remaining muscle mass which is not entirely explained by the initial loss of contractile tissue[124]. This exacerbated prolonged strength deficits has been attributed to the multifactorial pathophysiology of the VML injury. Our focus here will be immune microenvironment at the injury site.

Generally, an inflammatory immune response is a highly controlled/regulated process that subsides after initial flare of inflammation leading to the resolution of the inflammation[128]. However, in the case of VML, the injury overwhelms the repair programme resulting in chronic inflammation at the injured site. This unresolved inflammation can promote necrosis and degradation of skeletal muscle[129]. Immune cells populations (e.g., macrophages and T-cells) and cytokines (e.g., TGF-β and IL-1β) have been implicated to play important roles in the pathology of VML injury[16,130]. Thus, therapeutic modalities that incorporate immunomodulatory elements may nudge these cells and cytokines toward a more favorable environment for subsequent regenerative therapies, by removing debris and emitting soluble factors support regenerative programme. For example, Tacrolimus, an immunosuppression drug that can reduce macrophage and DC activity and inhibit IL-2 mediated activation of T cells, was used in combination with minced muscle grafts (MMGs) to repair VML injury[131]. Administration of systemic Tacrolimus with MMGs recovered 33% more of the muscle function compared to MMGs alone[131]. MMGs contain MuSCs and other cells residing in muscle tissue and have shown promising results functionally with *de novo* muscle tissue regeneration in both small to large animal VML models[132-134]. Furthermore, as an autologous source of MMGs can be easily accessed by repurposing the removed muscle during the VML injury creation, MMGs can be used as a default repair strategy when investigating novel co-delivery factors to improve functional recovery following VML injury. As mentioned earlier, local delivery of immunomodulatory

drugs in conjunction with bioconstructs have been a promising approach to enhance tissue regeneration. To control the inflammatory response at the dysregulated VML injury site, one strategy is to block inflammatory cytokines. For example, anti-TNF-α treatment can help decreased inflammation, apoptosis, and muscle loss in traumatic injury in rat soleus[135]. Different from suppression of pro-inflammatory factors, direct application of anti-inflammatory cytokines can also help modulate the injury site immune environment. For example, therapeutic myokine administration, such as interleukin-4 (IL-4) improves muscle function, adult myogenesis, and lifespan of cancer cachexia mice, while local intramuscular injection of IL-4 conjugated gold nanoparticles promoted regeneration and increased muscle strength [136,137]. Subcutaneous delivery of IL-10 was found to reduce inflammation and promote cardiac wound healing, while systemic upregulation of interleukin-10 (IL-10) using minicircle vector was shown to reduce vascular inflammation and mitigate abdominal aortic aneurysm[138,139]. Other research using biomaterials, vectors, and bioactive factors that can directly or indirectly increase IL-10 level have also shown promise in reducing inflammatory cytokines (e.g., TNF-α), and inhibiting NF-κB activation which affects important signaling pathways in immune response [140-142]. Though these strategies achieve therapeutic effect by influencing the immune cells, the underling mechanism in each immune cell population is not well studied. For example neutrophils, which are traditionally considered to be detrimental to tissue repair, have been shown to play a protective role to help resolve inflammation[143]. Macrophages have several subtypes involved in inflammation and subsequent regenerative processes in damaged tissue, while Tregs can modulate innate immune cells and conventional T cells to help tissue healing toward a regenerative pathway[144],[145]. However, controlling or modulating the behaviors of one or more of these immune cells populations in dysregulated MIMEs have seen mixed results[146]. In general, immunomodulation

for tissue regeneration involves very complicated physiological processes. We should further explore the underlying mechanisms with a view to harnessing the immune system to improve tissue repair. Although many methods can be employed to regulate immune response after tissue injury, precise modulation of specific immune cells awaits consideration of spatiotemporal strategies[147]. Since the immune response is a sequential multiple-step, dynamic, and context-dependent process, new generations of therapeutics should be engineered to be stimuli-responsive and programmable to harness different immune cells populations for better tissue regeneration.

1.4 Strategies for skeletal muscle regeneration

In recent years, *in vitro*, *in vivo*, and *in situ* muscle engineering approaches have been applied to produce and regenerate skeletal muscle. Each approach has its own advantages and disadvantages. The in vitro skeletal muscle engineering approach generally includes the *in vitro* differentiation of cells into myotubes[148]. This strategy aims to generate mature contractile functional constructs for transplantation. In addition, often a coculture of cells or multipotent cells is used to facilitate and support the formation of blood vessels and neuromuscular junctions (NMJs)[149]. Though this approach has seen some success in smaller animal models, the requirement for large cell density to induce differentiation into aligned myotubes for larger model and human (large constructs) continued to hinder the translation of this approach [150]. The *in vivo* strategy relies on the transplantation of cells with (injectable gel mixed or implantable constructs mixed with cells) or without (MMGs, progenitor cells injection) scaffold to generate a local niche at the transplantation site[151]. This strategy aims to stimulate the regeneration of muscle, vasculature, and MNJs *in vivo*. This strategy has been implemented in both small and large animal model with modest success[152-154]. The *in situ* strategy designed for in-surgery (pre-

made, moldable, or injectable bio-construct) or on-field deployment (3D-printed) can provide specific shapes, topographies, release bioactive and chemotactic molecules to attract, activate, and stimulate the recruitment/infiltration of cells to the injury site inducing tissue regeneration[152,155]. Depending on the type, the severity of injuries and other comorbidities of the patient, one or more of these strategies may be tailored to successfully promote muscle regeneration[156]. As our understanding of immune responses in muscle trauma progress, more studies have incorporated immunomodulation into the therapeutics to leverage the immune system toward aiding tissue repair. To this end, this project will focus on acellular injectable therapeutics that are immunomodulatory.

A simple method of creating immunomodulatory biomaterials is to incorporate immunomodulating small molecules into the material or co-delivered these molecules as an add-on treatment throughout the recovery process. For example, delivery of FTY720, an agonist of S1P (important regulator of the immune, cardiovascular, and nervous systems) [157], to injured muscle showed greater defect closure and more vascularization[158]. Inhibiting S1P in this case was shown to increase recruitment of non-classical monocytes (Ly6lo) and M2-like macrophages (CD206+) which promote tissue repair. Furthermore, delivery of some cytokines and growth factors have also been shown to provide positive outcomes in muscle injuries recovery by affecting a variety cells. For example, delivery of stromal cell derived factor-1 alpha (SDF-1α), improved the recruitment of cells expressing the SDF-1α receptor, CXCR4, and decreased mononuclear macrophage ($CD68^+$ cells) infiltration to muscle injury sites, resulting in subsequent improvement in vascularization[159]. Multiple cytokines regulate either the same or distinct aspects of regeneration and have also been used in parallel to promote the regeneration of muscle. For example, following a VML injury, muscles treated with hydrogels containing

both IGF-1 and FGF-2 showed significantly greater improvement in muscle function than the hydrogel containing only one factor likely through synergic effect of immunomodulation, progenitor cells recruitment and proliferation[160]. Therapies that make use of myokines (cytokines produced by myocytes) (e.g., IL-6, IL-4, IL10) have also gained some success in aiding muscle recovery[161 162,163]. To this end, IL-10 has gained some traction as an important immunomodulator that can affect muscle mass and function recovery. For example, IL-10 delivery was also shown to reduce myoblast necrosis in newborn rodents that had hypoxia-induced skeletal muscle injury[164]. IL-10 can also prevent muscle loss through suppressing pro-inflammatory cytokines in dysregulated inflammation[165]. Research on myoblasts shows that IL-10 can boost myogenin-induced myogenesis by inhibiting TNFα's JNK-mediated negative effects[166]. Furthermore, IL-10 may help direct immune cells toward pro-regenerative behaviors as researchers showed that IL-10 can enhance myoblast proliferation when macrophage was also co-cultured[167]. Compelling evidence provided by the study of cell restricted IL-10R deficiency has pointed to macrophages being the main targets of the IL-10 inhibitory effects[168,169]. IL-10 was shown to trigger a robust immune suppressive response in macrophages and other immune cells (neutrophils, T-cells, etc…) by modulating the local immune micro-environment[170]. However, anti-inflammatory response induced by IL-10 on different types of immune cells showed a divergent pattern. Specifically, in macrophages, IL-10 mostly inhibited NF-κB target genes, whereas in DCs and mast cells, an indirect disruption of IRF was proposed, and in neutrophils, IL-10 appeared to induce both IRF disruption and indirect NF-κB inhibition[171]. Interestingly, in context-dependent environment, IL-10 can either inhibit or stimulate responses of a variety of T-cells sub-populations[172,173]. Furthermore, IL-10 has been shown to regulate the ECMs and the non-immune cells (e.g., fibroblasts and epithelial cells) that are associated with wound repair[174]. In summary,

IL-10 has the potential to prevent muscle degeneration caused by dysregulated immune responses and aid in muscle recovery after injury and repair. Thus, therapeutic manipulation of this cytokine should be explored in the context of muscle recovery.

Alternatively, biomaterials which inherently promote a pro-regenerative immune microenvironment have also showed promise in aiding in muscle recovery[175]. There is a variety of natural and synthetic biomaterial that have been used in pre-clinal and clinical muscle repair. For example, synthetic materials containing methacrylic acid (MAA) have also been shown to be enhance early muscle regeneration (muscle fiber diameter) as well as vascularization at least partly through immunomodulation of macrophage population[176,177]. As for natural material, decellularized ECMs (dECM) have been widely evaluated as biomaterials for regeneration of various tissues and organs, including skeletal muscle, due to their off-the-shelf availability and immunomodulatory property[178]. Because of the specific structural and biochemical cues within ECM, these acellular grafts are hypothesized to create a regenerative environment within the injury that attracts and modulates the numerous cell types needed to orchestrate regeneration of functional muscle tissue[179]. One of the first FDA-approved dECM is derived from porcine small intestinal submucosa (SIS), but other types of dECM have been approved since then[180]. The sources and methods of processing tissues into dECM may result in different types and compositions of dECM. For example, muscle ECM (mECM) was found to contain growth factors, glycosaminoglycans (GAGs) and basement membrane structural proteins that differed from those present in the SIS ECM[181]. Preclinical animal studies using different species (e.g., mouse, rat, rabbit) and various muscle groups (e.g., tibialis anterior, quadriceps, latissimus dorsi) have demonstrated that xenogeneic and allogenic mECM scaffolds can support *de novo* muscle regeneration and vascularization[182-184]. Implantation of dECM alone in treating large animal and

human muscle injuries have seen mixed results on the capacity of ECMs to promote endogenous skeletal muscle regeneration and improve functional recovery[179,185,186]. dECM can also be formed into a hydrogel for use in injectable therapies[187]. For example, the injection of dECM gel in treating hindlimb ischemic injury produced a positive outcome in mass, force, and vascularization recovery[188,189]. The therapeutic benefit of dECM hydrogels has been attributed to the biochemical cues (i.e., proteins, peptides and proteoglycans) provided by the dECM-induced microenvironment at the injection site. The gel not only enhanced skeletal muscle progenitor cell recruitment, but also caused a shift in the inflammatory response, decreased cell death as well as increased blood vessel and muscle development indicated by the transcriptomic analysis[190]. These therapeutic properties of the dECM along with its off-the-self availability makes it an attractive option for treatment of skeletal muscle injuries.

1.5 Objectives

The goal of this research is to provide evidence to the following fundamental premise: Injectable therapy can promote functional tissue regeneration by modulating the muscle-immune micro-environment (MIME). Specifically, this research is exploring the use of immunomodulatory biomaterial (dECM) and cytokine (IL-10) to aid in muscle repair and recovery using different animal modalities (mouse, rat, and rabbit).

1) Examine the therapeutic potential of human muscle derived dECM gel in aiding muscle recovery following injury and repair/rehabilitation.

Hypothesis: local injection of solubilized human muscle derived dECM can modulate the local muscle immune microenvironment to ameliorate muscle atrophy and aid in muscle functional recovery from a) acute hindlimb unloading-induced atrophy and reloaded muscle injury and b) chronic fatty degenerative-induced atrophy and retracted muscle injury.

2) Examine the therapeutic potential of recombinant IL-10 in aiding muscle recovery following injury and repair.

Hypothesis: Local injection of delayed exogenous IL-10 can modulate the local muscle immune microenvironment to boost regenerative repair and enhance muscle functional recovery from traumatic muscle injury.

The use of injectable dECM as well as IL-10 in aiding muscle repair and recovery have been investigated by others as previously discussed. However, this project will add t regenerative tool kits by characterizing effects of these treatments on the different MIMEs using transcriptomic, proteomic, and a variety of new generation assays. Furthermore, we will use three different injuries (hindlimb unloading/reloading, chronic rotator cuff tear, and volumetric muscle loss) with three animal models (mouse, rabbit, rat) to sift out the unique immune responses to the treatments in each of these models. The results from this project will provide a deeper understanding by adding immuno-therapeutics to regenerative strategies and facilitate the translation of these pre-clinical medicines into helping patients in the clinic.

1.6 References

1. Frontera, W.R. & Ochala, J. Skeletal muscle: a brief review of structure and function. *Calcified tissue international* **96**, 183-195 (2015).

2. Gillies, A.R. & Lieber, R.L. Structure and function of the skeletal muscle extracellular matrix. *Muscle & nerve* **44**, 318-331 (2011).

3. Smith, L.R. & Meyer, G.A. Skeletal muscle explants: ex-vivo models to study cellular behavior in a complex tissue environment. *Connective tissue research* **61**, 248-261 (2020).

4. Tedesco, F.S., Moyle, L.A. & Perdiguero, E. Muscle Interstitial Cells: A Brief Field Guide to Non-satellite Cell Populations in Skeletal Muscle. *Methods in molecular biology* **1556**, 129-147 (2017).

5. Lepper, C., Partridge, T.A. & Fan, C.M. An absolute requirement for Pax7-positive satellite cells in acute injury-induced skeletal muscle regeneration. *Development* **138**, 3639-3646 (2011).

6. Mauro, A. Satellite cell of skeletal muscle fibers. *The Journal of biophysical and biochemical cytology* **9**, 493-495 (1961).

7. Le Grand, F. & Rudnicki, M.A. Skeletal muscle satellite cells and adult myogenesis. *Current opinion in cell biology* **19**, 628-633 (2007).

8. Zammit, P. & Beauchamp, J. The skeletal muscle satellite cell: stem cell or son of stem cell? *Differentiation; research in biological diversity* **68**, 193-204 (2001).

9. Zammit, P.S., *et al.* Muscle satellite cells adopt divergent fates: a mechanism for self-renewal? *The Journal of cell biology* **166**, 347-357 (2004).

10. Asfour, H.A., Allouh, M.Z. & Said, R.S. Myogenic regulatory factors: The orchestrators of myogenesis after 30 years of discovery. *Experimental biology and medicine* **243**, 118-128 (2018).

11. Schultz, E., Jaryszak, D.L. & Valliere, C.R. Response of satellite cells to focal skeletal muscle injury. *Muscle & nerve* **8**, 217-222 (1985).

12. Snow, M.H. An autoradiographic study of satellite cell differentiation into regenerating myotubes following transplantation of muscles in young rats. *Cell and tissue research* **186**, 535-540 (1978).

13. Wright, W.E., Sassoon, D.A. & Lin, V.K. Myogenin, a factor regulating myogenesis, has a domain homologous to MyoD. *Cell* **56**, 607-617 (1989).

14. Cornelison, D.D. & Wold, B.J. Single-cell analysis of regulatory gene expression in quiescent and activated mouse skeletal muscle satellite cells. *Developmental biology* **191**, 270-283 (1997).

15. Charge, S.B. & Rudnicki, M.A. Cellular and molecular regulation of muscle regeneration. *Physiological reviews* **84**, 209-238 (2004).

16. Tidball, J.G. Regulation of muscle growth and regeneration by the immune system. *Nature reviews. Immunology* **17**, 165-178 (2017).

17. Mann, C.J., *et al.* Aberrant repair and fibrosis development in skeletal muscle. *Skeletal muscle* **1**, 21 (2011).

18. Farup, J., Madaro, L., Puri, P.L. & Mikkelsen, U.R. Interactions between muscle stem cells, mesenchymal-derived cells and immune cells in muscle homeostasis, regeneration and disease. *Cell death & disease* **6**, e1830 (2015).

19. Pillon, N.J., Bilan, P.J., Fink, L.N. & Klip, A. Cross-talk between skeletal muscle and immune cells: muscle-derived mediators and metabolic implications. *American journal of physiology. Endocrinology and metabolism* **304**, E453-465 (2013).

20. Tu, H. & Li, Y.L. Inflammation balance in skeletal muscle damage and repair. *Frontiers in immunology* **14**, 1133355 (2023).

21. Tidball, J.G. Inflammatory cell response to acute muscle injury. *Medicine and science in sports and exercise* **27**, 1022-1032 (1995).

22. Tidball, J.G. Mechanisms of muscle injury, repair, and regeneration. *Comprehensive Physiology* **1**, 2029-2062 (2011).

23. Wang, H., *et al.* NF-kappaB regulation of YY1 inhibits skeletal myogenesis through transcriptional silencing of myofibrillar genes. *Molecular and cellular biology* **27**, 4374-4387 (2007).

24. Soehnlein, O. & Lindbom, L. Phagocyte partnership during the onset and resolution of inflammation. *Nature reviews. Immunology* **10**, 427-439 (2010).

25. Rosenberg, A.S., *et al.* Immune-mediated pathology in Duchenne muscular dystrophy. *Science translational medicine* **7**, 299rv294 (2015).

26. St Pierre, B.A. & Tidball, J.G. Differential response of macrophage subpopulations to soleus muscle reloading after rat hindlimb suspension. *Journal of applied physiology* **77**, 290-297 (1994).

27. Chazaud, B., *et al.* Satellite cells attract monocytes and use macrophages as a support to escape apoptosis and enhance muscle growth. *The Journal of cell biology* **163**, 1133-1143 (2003).

28. Novak, M.L., Weinheimer-Haus, E.M. & Koh, T.J. Macrophage activation and skeletal muscle healing following traumatic injury. *The Journal of pathology* **232**, 344-355 (2014).

29. Arnold, L., *et al.* Inflammatory monocytes recruited after skeletal muscle injury switch into antiinflammatory macrophages to support myogenesis. *The Journal of experimental medicine* **204**, 1057-1069 (2007).

30. Nie, M., *et al.* MicroRNA-155 facilitates skeletal muscle regeneration by balancing pro- and anti-inflammatory macrophages. *Cell death & disease* **7**, e2261 (2016).

31. Tonkin, J., *et al.* Monocyte/Macrophage-derived IGF-1 Orchestrates Murine Skeletal Muscle Regeneration and Modulates Autocrine Polarization. *Molecular therapy : the journal of the American Society of Gene Therapy* **23**, 1189-1200 (2015).

32. Mosser, D.M. & Edwards, J.P. Exploring the full spectrum of macrophage activation. *Nature reviews. Immunology* **8**, 958-969 (2008).

33. Bencze, M., *et al.* Proinflammatory macrophages enhance the regenerative capacity of human myoblasts by modifying their kinetics of proliferation and differentiation. *Molecular therapy : the journal of the American Society of Gene Therapy* **20**, 2168-2179 (2012).

34. Kreider, T., Anthony, R.M., Urban, J.F., Jr. & Gause, W.C. Alternatively activated macrophages in helminth infections. *Current opinion in immunology* **19**, 448-453 (2007).

35. Mantovani, A., *et al.* The chemokine system in diverse forms of macrophage activation and polarization. *Trends in immunology* **25**, 677-686 (2004).

36. Wang, Y., Wehling-Henricks, M., Samengo, G. & Tidball, J.G. Increases of M2a macrophages and fibrosis in aging muscle are influenced by bone marrow aging and negatively regulated by muscle-derived nitric oxide. *Aging cell* **14**, 678-688 (2015).

37. Edwards, J.P., Zhang, X., Frauwirth, K.A. & Mosser, D.M. Biochemical and functional characterization of three activated macrophage populations. *Journal of leukocyte biology* **80**, 1298-1307 (2006).

38. Burzyn, D., *et al.* A special population of regulatory T cells potentiates muscle repair. *Cell* **155**, 1282-1295 (2013).

39. Panduro, M., Benoist, C. & Mathis, D. T(reg) cells limit IFN-gamma production to control macrophage accrual and phenotype during skeletal muscle regeneration. *Proceedings of the National Academy of Sciences of the United States of America* **115**, E2585-E2593 (2018).

40. Zhang, J., *et al.* CD8 T cells are involved in skeletal muscle regeneration through facilitating MCP-1 secretion and Gr1(high) macrophage infiltration. *Journal of immunology* **193**, 5149-5160 (2014).

41. Spencer, M.J., Montecino-Rodriguez, E., Dorshkind, K. & Tidball, J.G. Helper (CD4(+)) and cytotoxic (CD8(+)) T cells promote the pathology of dystrophin-deficient muscle. *Clinical immunology* **98**, 235-243 (2001).

42. Joe, A.W., *et al.* Muscle injury activates resident fibro/adipogenic progenitors that facilitate myogenesis. *Nature cell biology* **12**, 153-163 (2010).

43. Natarajan, A., Lemos, D.R. & Rossi, F.M. Fibro/adipogenic progenitors: a double-edged sword in skeletal muscle regeneration. *Cell Cycle* **9**, 2045-2046 (2010).

44. Urciuolo, A., *et al.* Collagen VI regulates satellite cell self-renewal and muscle regeneration. *Nature communications* **4**, 1964 (2013).

45. Theret, M., Rossi, F.M.V. & Contreras, O. Evolving Roles of Muscle-Resident Fibro-Adipogenic Progenitors in Health, Regeneration, Neuromuscular Disorders, and Aging. *Frontiers in physiology* **12**, 673404 (2021).

46. Fiore, D., *et al.* Pharmacological blockage of fibro/adipogenic progenitor expansion and suppression of regenerative fibrogenesis is associated with impaired skeletal muscle regeneration. *Stem cell research* **17**, 161-169 (2016).

47. Malecova, B., *et al.* Dynamics of cellular states of fibro-adipogenic progenitors during myogenesis and muscular dystrophy. *Nature communications* **9**, 3670 (2018).

48. Sass, F.A., *et al.* Immunology Guides Skeletal Muscle Regeneration. *International journal of molecular sciences* **19**(2018).

49. Wang, H., *et al.* Altered macrophage phenotype transition impairs skeletal muscle regeneration. *The American journal of pathology* **184**, 1167-1184 (2014).

50. Villalta, S.A., *et al.* Regulatory T cells suppress muscle inflammation and injury in muscular dystrophy. *Science translational medicine* **6**, 258ra142 (2014).

51. Cruz-Jentoft, A.J. & Morley, J.E. Sarcopenia. 1 online resource. (Wiley-Blackwell,, Chichester, West Sussex, UK, 2012).

52. Howard, E.E., Pasiakos, S.M., Fussell, M.A. & Rodriguez, N.R. Skeletal Muscle Disuse Atrophy and the Rehabilitative Role of Protein in Recovery from Musculoskeletal Injury. *Advances in nutrition* **11**, 989-1001 (2020).

53. Mirzoev, T.M. Skeletal Muscle Recovery from Disuse Atrophy: Protein Turnover Signaling and Strategies for Accelerating Muscle Regrowth. *International journal of molecular sciences* **21**(2020).

54. Lev, R. & Seliktar, D. Hydrogel biomaterials and their therapeutic potential for muscle injuries and muscular dystrophies. *Journal of the Royal Society, Interface* **15**(2018).

55. Guttridge, D.C. Signaling pathways weigh in on decisions to make or break skeletal muscle. *Current opinion in clinical nutrition and metabolic care* **7**, 443-450 (2004).

56. Glass, D.J. Skeletal muscle hypertrophy and atrophy signaling pathways. *The international journal of biochemistry & cell biology* **37**, 1974-1984 (2005).

57. Jackman, R.W. & Kandarian, S.C. The molecular basis of skeletal muscle atrophy. *American journal of physiology. Cell physiology* **287**, C834-843 (2004).

58. Argiles, J.M., Busquets, S., Toledo, M. & Lopez-Soriano, F.J. The role of cytokines in cancer cachexia. *Current opinion in supportive and palliative care* **3**, 263-268 (2009).

59. Tawa, N.E., Jr., Odessey, R. & Goldberg, A.L. Inhibitors of the proteasome reduce the accelerated proteolysis in atrophying rat skeletal muscles. *The Journal of clinical investigation* **100**, 197-203 (1997).

60. Ji, Y., *et al.* Inflammation: Roles in Skeletal Muscle Atrophy. *Antioxidants* **11**(2022).

61. Braun, T.P., *et al.* Central nervous system inflammation induces muscle atrophy via activation of the hypothalamic-pituitary-adrenal axis. *The Journal of experimental medicine* **208**, 2449-2463 (2011).

62. Flores, E.A., *et al.* Infusion of tumor necrosis factor/cachectin promotes muscle catabolism in the rat. A synergistic effect with interleukin 1. *The Journal of clinical investigation* **83**, 1614-1622 (1989).

63. Flint, T.R., *et al.* Tumor-Induced IL-6 Reprograms Host Metabolism to Suppress Anti-tumor Immunity. *Cell metabolism* **24**, 672-684 (2016).

64. Dutt, V., Gupta, S., Dabur, R., Injeti, E. & Mittal, A. Skeletal muscle atrophy: Potential therapeutic agents and their mechanisms of action. *Pharmacological research* **99**, 86-100 (2015).

65. Raimondo, T.M. & Mooney, D.J. Anti-inflammatory nanoparticles significantly improve muscle function in a murine model of advanced muscular dystrophy. *Science advances* **7**(2021).

66. Schiaffino, S., Pereira, M.G., Ciciliot, S. & Rovere-Querini, P. Regulatory T cells and skeletal muscle regeneration. *The FEBS journal* **284**, 517-524 (2017).

67. Gomes, M.D., Lecker, S.H., Jagoe, R.T., Navon, A. & Goldberg, A.L. Atrogin-1, a muscle-specific F-box protein highly expressed during muscle atrophy. *Proceedings of the National Academy of Sciences of the United States of America* **98**, 14440-14445 (2001).

68. Yamaguchi, K., *et al.* Natural history of asymptomatic rotator cuff tears: a longitudinal analysis of asymptomatic tears detected sonographically. *Journal of shoulder and elbow surgery* **10**, 199-203 (2001).

69. Mall, N.A., *et al.* An evidenced-based examination of the epidemiology and outcomes of traumatic rotator cuff tears. *Arthroscopy : the journal of arthroscopic & related surgery : official publication of the Arthroscopy Association of North America and the International Arthroscopy Association* **29**, 366-376 (2013).

70. Goutallier, D., Postel, J.M., Bernageau, J., Lavau, L. & Voisin, M.C. Fatty muscle degeneration in cuff ruptures. Pre- and postoperative evaluation by CT scan. *Clinical orthopaedics and related research*, 78-83 (1994).

71. Iannotti, J.P., *et al.* Magnetic resonance imaging of the shoulder. Sensitivity, specificity, and predictive value. *The Journal of bone and joint surgery. American volume* **73**, 17-29 (1991).

72. Tomioka, T., *et al.* Sarcomere length of torn rotator cuff muscle. *Journal of shoulder and elbow surgery* **18**, 955-959 (2009).

73. Gordon, A.M., Huxley, A.F. & Julian, F.J. The variation in isometric tension with sarcomere length in vertebrate muscle fibres. *The Journal of physiology* **184**, 170-192 (1966).

74. Itoigawa, Y., Kishimoto, K.N., Sano, H., Kaneko, K. & Itoi, E. Molecular mechanism of fatty degeneration in rotator cuff muscle with tendon rupture. *Journal of orthopaedic research : official publication of the Orthopaedic Research Society* **29**, 861-866 (2011).

75. Safran, O., Derwin, K.A., Powell, K. & Iannotti, J.P. Changes in rotator cuff muscle volume, fat content, and passive mechanics after chronic detachment in a canine model. *The Journal of bone and joint surgery. American volume* **87**, 2662-2670 (2005).

76. Valencia, A.P., *et al.* Fatty Infiltration Is a Prognostic Marker of Muscle Function After Rotator Cuff Tear. *The American journal of sports medicine* **46**, 2161-2169 (2018).

77. Yang, Z., *et al.* Does the Fatty Infiltration Influence the Re-tear Rate and Functional Outcome After Rotator Cuff Repair? A Systematic Review and Meta-analysis. *Indian journal of orthopaedics* **57**, 227-237 (2023).

78. Gladstone, J.N., Bishop, J.Y., Lo, I.K. & Flatow, E.L. Fatty infiltration and atrophy of the rotator cuff do not improve after rotator cuff repair and correlate with poor functional outcome. *The American journal of sports medicine* **35**, 719-728 (2007).

79. Khair, M.M., Lehman, J., Tsouris, N. & Gulotta, L.V. A Systematic Review of Preoperative Fatty Infiltration and Rotator Cuff Outcomes. *HSS journal : the musculoskeletal journal of Hospital for Special Surgery* **12**, 170-176 (2016).

80. Ma, X., Wang, D., Zhao, W. & Xu, L. Deciphering the Roles of PPARgamma in Adipocytes via Dynamic Change of Transcription Complex. *Frontiers in endocrinology* **9**, 473 (2018).

81. Frey, E., *et al.* Adipogenic and myogenic gene expression in rotator cuff muscle of the sheep after tendon tear. *Journal of orthopaedic research : official publication of the Orthopaedic Research Society* **27**, 504-509 (2009).

82. Tontonoz, P. & Spiegelman, B.M. Fat and beyond: the diverse biology of PPARgamma. *Annual review of biochemistry* **77**, 289-312 (2008).

83. Meyer, G.A. & Ward, S.R. Developmental Biology and Regenerative Medicine: Addressing the Vexing Problem of Persistent Muscle Atrophy in the Chronically Torn Human Rotator Cuff. *Physical therapy* **96**, 722-733 (2016).

84. Colvin, A.C., Egorova, N., Harrison, A.K., Moskowitz, A. & Flatow, E.L. National trends in rotator cuff repair. *The Journal of bone and joint surgery. American volume* **94**, 227-233 (2012).

85. Zumstein, M.A., Ladermann, A., Raniga, S. & Schar, M.O. The biology of rotator cuff healing. *Orthopaedics & traumatology, surgery & research : OTSR* **103**, S1-S10 (2017).

86. Edelstein, L., Thomas, S.J. & Soslowsky, L.J. Rotator Cuff Tears: What have we learned from animal models? *Journal of musculoskeletal & neuronal interactions* **11**, 150-162 (2011).

87. Gupta, R. & Lee, T.Q. Contributions of the different rabbit models to our understanding of rotator cuff pathology. *Journal of shoulder and elbow surgery* **16**, S149-157 (2007).

88. Clark, J.M. & Harryman, D.T., 2nd. Tendons, ligaments, and capsule of the rotator cuff. Gross and microscopic anatomy. *The Journal of bone and joint surgery. American volume* **74**, 713-725 (1992).

89. Turner, A.S. Experiences with sheep as an animal model for shoulder surgery: strengths and shortcomings. *Journal of shoulder and elbow surgery* **16**, S158-163 (2007).

90. Gerber, C., Meyer, D.C., Schneeberger, A.G., Hoppeler, H. & von Rechenberg, B. Effect of tendon release and delayed repair on the structure of the muscles of the rotator cuff: an experimental study in sheep. *The Journal of bone and joint surgery. American volume* **86**, 1973-1982 (2004).

91. Namdari, S., *et al.* Factors affecting outcome after structural failure of repaired rotator cuff tears. *The Journal of bone and joint surgery. American volume* **96**, 99-105 (2014).

92. Matsumoto, F., Uhthoff, H.K., Trudel, G. & Loehr, J.F. Delayed tendon reattachment does not reverse atrophy and fat accumulation of the supraspinatus--an experimental study in rabbits. *Journal of orthopaedic research : official publication of the Orthopaedic Research Society* **20**, 357-363 (2002).

93. Rubino, L.J., Stills, H.F., Jr., Sprott, D.C. & Crosby, L.A. Fatty infiltration of the torn rotator cuff worsens over time in a rabbit model. *Arthroscopy : the journal of*

arthroscopic & related surgery : official publication of the Arthroscopy Association of North America and the International Arthroscopy Association **23**, 717-722 (2007).

94. Uezumi, A., Ikemoto-Uezumi, M. & Tsuchida, K. Roles of nonmyogenic mesenchymal progenitors in pathogenesis and regeneration of skeletal muscle. *Frontiers in physiology* **5**, 68 (2014).

95. Agha, O., *et al.* Rotator cuff tear degeneration and the role of fibro-adipogenic progenitors. *Annals of the New York Academy of Sciences* **1490**, 13-28 (2021).

96. Lee, C., *et al.* Rotator Cuff Fibro-Adipogenic Progenitors Demonstrate Highest Concentration, Proliferative Capacity, and Adipogenic Potential Across Muscle Groups. *Journal of orthopaedic research : official publication of the Orthopaedic Research Society* **38**, 1113-1121 (2020).

97. Biferali, B., Proietti, D., Mozzetta, C. & Madaro, L. Fibro-Adipogenic Progenitors Cross-Talk in Skeletal Muscle: The Social Network. *Frontiers in physiology* **10**, 1074 (2019).

98. Moratal, C., *et al.* IL-1beta- and IL-4-polarized macrophages have opposite effects on adipogenesis of intramuscular fibro-adipogenic progenitors in humans. *Scientific reports* **8**, 17005 (2018).

99. Davies, M.R., Lee, L., Feeley, B.T., Kim, H.T. & Liu, X. Lysophosphatidic acid-induced RhoA signaling and prolonged macrophage infiltration worsens fibrosis and fatty infiltration following rotator cuff tears. *Journal of orthopaedic research : official publication of the Orthopaedic Research Society* **35**, 1539-1547 (2017).

100. Mendias, C.L., *et al.* Transforming growth factor-beta induces skeletal muscle atrophy and fibrosis through the induction of atrogin-1 and scleraxis. *Muscle & nerve* **45**, 55-59 (2012).

101. Davies, M.R., *et al.* TGF-beta Small Molecule Inhibitor SB431542 Reduces Rotator Cuff Muscle Fibrosis and Fatty Infiltration By Promoting Fibro/Adipogenic Progenitor Apoptosis. *PloS one* **11**, e0155486 (2016).

102. Lemos, D.R., *et al.* Nilotinib reduces muscle fibrosis in chronic muscle injury by promoting TNF-mediated apoptosis of fibro/adipogenic progenitors. *Nature medicine* **21**, 786-794 (2015).

103. Jensen, A.R., *et al.* Neer Award 2018: Platelet-derived growth factor receptor alpha co-expression typifies a subset of platelet-derived growth factor receptor beta-positive progenitor cells that contribute to fatty degeneration and fibrosis of the murine rotator cuff. *Journal of shoulder and elbow surgery* **27**, 1149-1161 (2018).

104. Molina, T., Fabre, P. & Dumont, N.A. Fibro-adipogenic progenitors in skeletal muscle homeostasis, regeneration and diseases. *Open biology* **11**, 210110 (2021).

105. Saccone, V., *et al.* HDAC-regulated myomiRs control BAF60 variant exchange and direct the functional phenotype of fibro-adipogenic progenitors in dystrophic muscles. *Genes & development* **28**, 841-857 (2014).

106. Mosich, G.M., *et al.* Non-fibro-adipogenic pericytes from human embryonic stem cells attenuate degeneration of the chronically injured mouse muscle. *JCI insight* **4**(2019).

107. Morey-Holton, E.R. & Globus, R.K. Hindlimb unloading rodent model: technical aspects. *Journal of applied physiology* **92**, 1367-1377 (2002).

108. Bodine, S.C. Disuse-induced muscle wasting. *The international journal of biochemistry & cell biology* **45**, 2200-2208 (2013).

109. Goodman, C.A., *et al.* Novel insights into the regulation of skeletal muscle protein synthesis as revealed by a new nonradioactive in vivo technique. *FASEB journal : official publication of the Federation of American Societies for Experimental Biology* **25**, 1028-1039 (2011).

110. Kimball, S.R., Farrell, P.A. & Jefferson, L.S. Invited Review: Role of insulin in translational control of protein synthesis in skeletal muscle by amino acids or exercise. *Journal of applied physiology* **93**, 1168-1180 (2002).

111. Ochala, J., *et al.* Preferential skeletal muscle myosin loss in response to mechanical silencing in a novel rat intensive care unit model: underlying mechanisms. *The Journal of physiology* **589**, 2007-2026 (2011).

112. Tesch, P.A., von Walden, F., Gustafsson, T., Linnehan, R.M. & Trappe, T.A. Skeletal muscle proteolysis in response to short-term unloading in humans. *Journal of applied physiology* **105**, 902-906 (2008).

113. Meyer, G.A., Thomopoulos, S., Abu-Amer, Y. & Shen, K.C. Tenotomy-induced muscle atrophy is sex-specific and independent of NFkappaB. *eLife* **11**(2022).

114. Bialek, P., *et al.* Distinct protein degradation profiles are induced by different disuse models of skeletal muscle atrophy. *Physiological genomics* **43**, 1075-1086 (2011).

115. Bodine, S.C., *et al.* Identification of ubiquitin ligases required for skeletal muscle atrophy. *Science* **294**, 1704-1708 (2001).

116. Jackman, R.W., Cornwell, E.W., Wu, C.L. & Kandarian, S.C. Nuclear factor-kappaB signalling and transcriptional regulation in skeletal muscle atrophy. *Experimental physiology* **98**, 19-24 (2013).

117. Cai, D., *et al.* IKKbeta/NF-kappaB activation causes severe muscle wasting in mice. *Cell* **119**, 285-298 (2004).

118. Senf, S.M., Dodd, S.L., McClung, J.M. & Judge, A.R. Hsp70 overexpression inhibits NF-kappaB and Foxo3a transcriptional activities and prevents skeletal muscle atrophy.

FASEB journal : official publication of the Federation of American Societies for Experimental Biology **22**, 3836-3845 (2008).

119. Suetta, C., *et al.* Effects of aging on human skeletal muscle after immobilization and retraining. *Journal of applied physiology* **107**, 1172-1180 (2009).

120. Slimani, L., *et al.* The worsening of tibialis anterior muscle atrophy during recovery post-immobilization correlates with enhanced connective tissue area, proteolysis, and apoptosis. *American journal of physiology. Endocrinology and metabolism* **303**, E1335-1347 (2012).

121. Hwee, D.T. & Bodine, S.C. Age-related deficit in load-induced skeletal muscle growth. *The journals of gerontology. Series A, Biological sciences and medical sciences* **64**, 618-628 (2009).

122. Garg, K., *et al.* Volumetric muscle loss: persistent functional deficits beyond frank loss of tissue. *Journal of orthopaedic research : official publication of the Orthopaedic Research Society* **33**, 40-46 (2015).

123. Mase, V.J., Jr., *et al.* Clinical application of an acellular biologic scaffold for surgical repair of a large, traumatic quadriceps femoris muscle defect. *Orthopedics* **33**, 511 (2010).

124. Corona, B.T., Wenke, J.C. & Ward, C.L. Pathophysiology of Volumetric Muscle Loss Injury. *Cells, tissues, organs* **202**, 180-188 (2016).

125. Parker, M.W., *et al.* Fibrotic extracellular matrix activates a profibrotic positive feedback loop. *The Journal of clinical investigation* **124**, 1622-1635 (2014).

126. Corona, B.T., *et al.* Autologous minced muscle grafts: a tissue engineering therapy for the volumetric loss of skeletal muscle. *American journal of physiology. Cell physiology* **305**, C761-775 (2013).

127. Willett, N.J., *et al.* Attenuated human bone morphogenetic protein-2-mediated bone regeneration in a rat model of composite bone and muscle injury. *Tissue engineering. Part C, Methods* **19**, 316-325 (2013).

128. Fullerton, J.N. & Gilroy, D.W. Resolution of inflammation: a new therapeutic frontier. *Nature reviews. Drug discovery* **15**, 551-567 (2016).

129. Kim, H., *et al.* Mesenchymal stem cell 3D encapsulation technologies for biomimetic microenvironment in tissue regeneration. *Stem cell research & therapy* **10**, 51 (2019).

130. Corona, B.T., Rivera, J.C. & Greising, S.M. Inflammatory and Physiological Consequences of Debridement of Fibrous Tissue after Volumetric Muscle Loss Injury. *Clinical and translational science* **11**, 208-217 (2018).

131. Corona, B.T., Rivera, J.C., Wenke, J.C. & Greising, S.M. Tacrolimus as an adjunct to autologous minced muscle grafts for the repair of a volumetric muscle loss injury. *Journal of experimental orthopaedics* **4**, 36 (2017).

132. Ward, C.L., Ji, L. & Corona, B.T. An Autologous Muscle Tissue Expansion Approach for the Treatment of Volumetric Muscle Loss. *BioResearch open access* **4**, 198-208 (2015).

133. Corona, B.T., Henderson, B.E., Ward, C.L. & Greising, S.M. Contribution of minced muscle graft progenitor cells to muscle fiber formation after volumetric muscle loss injury in wild-type and immune deficient mice. *Physiological reports* **5**(2017).

134. Aguilar, C.A., *et al.* Multiscale analysis of a regenerative therapy for treatment of volumetric muscle loss injury. *Cell death discovery* **4**, 33 (2018).

135. Stratos, I., *et al.* Inhibition of TNF-alpha Restores Muscle Force, Inhibits Inflammation, and Reduces Apoptosis of Traumatized Skeletal Muscles. *Cells* **11**(2022).

136. Raimondo, T.M. & Mooney, D.J. Functional muscle recovery with nanoparticle-directed M2 macrophage polarization in mice. *Proceedings of the National Academy of Sciences of the United States of America* **115**, 10648-10653 (2018).

137. Costamagna, D., *et al.* Interleukin-4 administration improves muscle function, adult myogenesis, and lifespan of colon carcinoma-bearing mice. *Journal of cachexia, sarcopenia and muscle* **11**, 783-801 (2020).

138. Jung, M., *et al.* IL-10 improves cardiac remodeling after myocardial infarction by stimulating M2 macrophage polarization and fibroblast activation. *Basic research in cardiology* **112**, 33 (2017).

139. Adam, M., *et al.* Systemic Upregulation of IL-10 (Interleukin-10) Using a Nonimmunogenic Vector Reduces Growth and Rate of Dissecting Abdominal Aortic Aneurysm. *Arteriosclerosis, thrombosis, and vascular biology* **38**, 1796-1805 (2018).

140. Boehler, R.M., *et al.* Lentivirus delivery of IL-10 to promote and sustain macrophage polarization towards an anti-inflammatory phenotype. *Biotechnology and bioengineering* **111**, 1210-1221 (2014).

141. Mountziaris, P.M., *et al.* Intra-articular controlled release of anti-inflammatory siRNA with biodegradable polymer microparticles ameliorates temporomandibular joint inflammation. *Acta biomaterialia* **8**, 3552-3560 (2012).

142. Silverman, J.M., *et al.* Leishmania exosomes modulate innate and adaptive immune responses through effects on monocytes and dendritic cells. *Journal of immunology* **185**, 5011-5022 (2010).

143. Wang, J. Neutrophils in tissue injury and repair. *Cell and tissue research* **371**, 531-539 (2018).

144. Howard, E.E., Pasiakos, S.M., Blesso, C.N., Fussell, M.A. & Rodriguez, N.R. Divergent Roles of Inflammation in Skeletal Muscle Recovery From Injury. *Frontiers in physiology* **11**, 87 (2020).

145. Zhang, B., Su, Y., Zhou, J., Zheng, Y. & Zhu, D. Toward a Better Regeneration through Implant-Mediated Immunomodulation: Harnessing the Immune Responses. *Advanced science* **8**, e2100446 (2021).

146. Moon, S., Hong, J., Go, S. & Kim, B.S. Immunomodulation for Tissue Repair and Regeneration. *Tissue engineering and regenerative medicine* (2023).

147. Chen, Y., *et al.* Interactions Between Immunomodulatory Biomaterials and Immune Microenvironment: Cues for Immunomodulation Strategies in Tissue Repair. *Frontiers in bioengineering and biotechnology* **10**, 820940 (2022).

148. Gilbert-Honick, J., *et al.* Engineering functional and histological regeneration of vascularized skeletal muscle. *Biomaterials* **164**, 70-79 (2018).

149. Kim, J.H., *et al.* Neural cell integration into 3D bioprinted skeletal muscle constructs accelerates restoration of muscle function. *Nature communications* **11**, 1025 (2020).

150. Qazi, T.H., Mooney, D.J., Pumberger, M., Geissler, S. & Duda, G.N. Biomaterials based strategies for skeletal muscle tissue engineering: existing technologies and future trends. *Biomaterials* **53**, 502-521 (2015).

151. McCullen, S.D., Chow, A.G. & Stevens, M.M. In vivo tissue engineering of musculoskeletal tissues. *Current opinion in biotechnology* **22**, 715-720 (2011).

152. Quarta, M., *et al.* Bioengineered constructs combined with exercise enhance stem cell-mediated treatment of volumetric muscle loss. *Nature communications* **8**, 15613 (2017).

153. Ward, C.L., *et al.* Autologous Minced Muscle Grafts Improve Muscle Strength in a Porcine Model of Volumetric Muscle Loss Injury. *Journal of orthopaedic trauma* **30**, e396-e403 (2016).

154. Hotham, W.E. & Henson, F.M.D. The use of large animals to facilitate the process of MSC going from laboratory to patient-'bench to bedside'. *Cell biology and toxicology* **36**, 103-114 (2020).

155. Ostrovidov, S., *et al.* 3D Bioprinting in Skeletal Muscle Tissue Engineering. *Small* **15**, e1805530 (2019).

156. Carnes, M.E. & Pins, G.D. Skeletal Muscle Tissue Engineering: Biomaterials-Based Strategies for the Treatment of Volumetric Muscle Loss. *Bioengineering* **7**(2020).

157. Perez-Jeldres, T., Alvarez-Lobos, M. & Rivera-Nieves, J. Targeting Sphingosine-1-Phosphate Signaling in Immune-Mediated Diseases: Beyond Multiple Sclerosis. *Drugs* **81**, 985-1002 (2021).

158. San Emeterio, C.L., Olingy, C.E., Chu, Y. & Botchwey, E.A. Selective recruitment of non-classical monocytes promotes skeletal muscle repair. *Biomaterials* **117**, 32-43 (2017).

159. Rajabi, S., *et al.* Effect of chemical immobilization of SDF-1 into muscle-derived scaffolds on angiogenesis and muscle progenitor recruitment. *J Tissue Eng Regen M* **12**, E438-E450 (2018).

160. Passipieri, J.A., *et al.* Keratin Hydrogel Enhances In Vivo Skeletal Muscle Function in a Rat Model of Volumetric Muscle Loss. *Tissue engineering. Part A* **23**, 556-571 (2017).

161. Lee, J.H. & Jun, H.S. Role of Myokines in Regulating Skeletal Muscle Mass and Function. *Frontiers in physiology* **10**, 42 (2019).

162. Chen, Z., Qin, X., Zhang, X., Liu, B. & Chen, M. Upregulation of IL-4 signaling contributes to aerobic exercise-induced insulin sensitivity. *Biochemical and biophysical research communications* **525**, 662-667 (2020).

163. Leal, L.G., Lopes, M.A. & Batista, M.L., Jr. Physical Exercise-Induced Myokines and Muscle-Adipose Tissue Crosstalk: A Review of Current Knowledge and the Implications for Health and Metabolic Diseases. *Frontiers in physiology* **9**, 1307 (2018).

164. Ozturk, K., Demir, B., Oke, R. & Durmaz, H. Dose-related effects of recombinant human interleukin-10 on hypoxia-induced skeletal muscle injury in immature rats. *Journal of orthopaedic science : official journal of the Japanese Orthopaedic Association* **11**, 620-625 (2006).

165. Dagdeviren, S., *et al.* IL-10 prevents aging-associated inflammation and insulin resistance in skeletal muscle. *FASEB journal : official publication of the Federation of American Societies for Experimental Biology* **31**, 701-710 (2017).

166. Strle, K., *et al.* Novel activity of an anti-inflammatory cytokine: IL-10 prevents TNFalpha-induced resistance to IGF-I in myoblasts. *Journal of neuroimmunology* **188**, 48-55 (2007).

167. Deng, B., Wehling-Henricks, M., Villalta, S.A., Wang, Y. & Tidball, J.G. IL-10 triggers changes in macrophage phenotype that promote muscle growth and regeneration. *Journal of immunology* **189**, 3669-3680 (2012).

168. Shouval, D.S., *et al.* Interleukin-10 receptor signaling in innate immune cells regulates mucosal immune tolerance and anti-inflammatory macrophage function. *Immunity* **40**, 706-719 (2014).

169. Shouval, D.S., *et al.* Interleukin 10 receptor signaling: master regulator of intestinal mucosal homeostasis in mice and humans. *Advances in immunology* **122**, 177-210 (2014).

170. Moore, K.W., de Waal Malefyt, R., Coffman, R.L. & O'Garra, A. Interleukin-10 and the interleukin-10 receptor. *Annual review of immunology* **19**, 683-765 (2001).

171. Hutchins, A.P., Takahashi, Y. & Miranda-Saavedra, D. Genomic analysis of LPS-stimulated myeloid cells identifies a common pro-inflammatory response but divergent IL-10 anti-inflammatory responses. *Scientific reports* **5**, 9100 (2015).

172. Kamanaka, M., *et al.* Memory/effector (CD45RB(lo)) CD4 T cells are controlled directly by IL-10 and cause IL-22-dependent intestinal pathology. *The Journal of experimental medicine* **208**, 1027-1040 (2011).

173. Chaudhry, A., *et al.* Interleukin-10 signaling in regulatory T cells is required for suppression of Th17 cell-mediated inflammation. *Immunity* **34**, 566-578 (2011).

174. Saraiva, M., Vieira, P. & O'Garra, A. Biology and therapeutic potential of interleukin-10. *The Journal of experimental medicine* **217**(2020).

175. Andorko, J.I. & Jewell, C.M. Designing biomaterials with immunomodulatory properties for tissue engineering and regenerative medicine. *Bioengineering & translational medicine* **2**, 139-155 (2017).

176. Carleton, M.M. & Sefton, M.V. Injectable and degradable methacrylic acid hydrogel alters macrophage response in skeletal muscle. *Biomaterials* **223**, 119477 (2019).

177. Carleton, M.M., Locke, M. & Sefton, M.V. Methacrylic acid-based hydrogels enhance skeletal muscle regeneration after volumetric muscle loss in mice. *Biomaterials* **275**, 120909 (2021).

178. Badylak, S.F. The extracellular matrix as a biologic scaffold material. *Biomaterials* **28**, 3587-3593 (2007).

179. Sicari, B.M., *et al.* An acellular biologic scaffold promotes skeletal muscle formation in mice and humans with volumetric muscle loss. *Science translational medicine* **6**, 234ra258 (2014).

180. Hussey, G.S., Dziki, J.L. & Badylak, S.F. Extracellular matrix-based materials for regenerative medicine. *Nat Rev Mater* **3**, 159-173 (2018).

181. Wolf, M.T., Daly, K.A., Reing, J.E. & Badylak, S.F. Biologic scaffold composed of skeletal muscle extracellular matrix. *Biomaterials* **33**, 2916-2925 (2012).

182. Merritt, E.K., *et al.* Functional Assessment of Skeletal Muscle Regeneration Utilizing Homologous Extracellular Matrix as Scaffolding. *Tissue Eng Pt A* **16**, 1395-1405 (2010).

183. McClure, M.J., *et al.* Decellularized Muscle Supports New Muscle Fibers and Improves Function Following Volumetric Injury. *Tissue Eng Pt A* **24**, 1228-1241 (2018).

184. Perniconi, B., *et al.* The pro-myogenic environment provided by whole organ scale acellular scaffolds from skeletal muscle. *Biomaterials* **32**, 7870-7882 (2011).

185. Greising, S.M., *et al.* Unwavering Pathobiology of Volumetric Muscle Loss Injury. *Scientific reports* **7**, 13179 (2017).

186. Dziki, J., *et al.* An acellular biologic scaffold treatment for volumetric muscle loss: results of a 13-patient cohort study. *NPJ Regenerative medicine* **1**, 16008 (2016).

187. Serna, J.A., *et al.* Recent Advances on Stimuli-Responsive Hydrogels Based on Tissue-Derived ECMs and Their Components: Towards Improving Functionality for Tissue Engineering and Controlled Drug Delivery. *Polymers* **13**(2021).

188. DeQuach, J.A., *et al.* Injectable skeletal muscle matrix hydrogel promotes neovascularization and muscle cell infiltration in a hindlimb ischemia model. *European cells & materials* **23**, 400-412; discussion 412 (2012).

189. Ungerleider, J.L., *et al.* Extracellular Matrix Hydrogel Promotes Tissue Remodeling, Arteriogenesis, and Perfusion in a Rat Hindlimb Ischemia Model. *JACC. Basic to translational science* **1**, 32-44 (2016).

190. Zhang, W., Du, A., Liu, S., Lv, M. & Chen, S. Research progress in decellularized extracellular matrix-derived hydrogels. *Regenerative therapy* **18**, 88-96 (2021).

CHAPTER 2: In-vivo testing of an injectable matrix gel for the treatment of shoulder cuff muscle fatty degeneration

Submitted as an original article by:

Tai Huynh BS [a], John Taehwan Kim PhD [a], Grady Dunlap BS [a], Shahryar Ahmadi MD [b], Jeffrey C. Wolchok PhD [a b]

a Department of Biomedical Engineering, University of Arkansas

b College of Medicine, Orthopedic Surgery, University of Arkansas for Medical Science

2.1 Abstract

Introduction: Extracellular matrix (ECM) gels have shown efficacy for the treatment of damaged tissues, most notably cardiac muscle. We hypothesized that the ECM gel prepared from skeletal muscle could be used as a treatment strategy for fatty shoulder cuff muscle degeneration.

Methods: We conducted experiments to 1) evaluate host biocompatibility to ECM gel injection using a rat model; and 2) examine the effect of ECM gel injection on muscle recovery following delayed repair of a released supraspinatus (SSP) tendon using a rabbit model.

Results: The host biocompatibility to ECM gel was characterized by a transient rise (first two weeks only) in several genes associated with macrophage infiltration, matrix deposition, and inflammatory cytokine production. By eight weeks all genes had returned to baseline levels and no evidence of fibrosis or chronic inflammation was observed from histology. When gel injection was combined with SSP tendon repair, we observed a significant reduction (7%) in SSP muscle atrophy (24+3% reduction from uninjured) when compared to treatment with tendon repair only (31+7% reduction). While fatty degeneration was elevated in both treatment groups, fat content trended lower (2%) in response to combined tendon repair and intramuscular ECM injection (4.1+2.1%) when compared to tendon repair only (6.1+2.9%). Transcriptome analysis

revealed adipogenesis and osteoarthritis pathway activation in the repair only group. These key pathways were abrogated in response to treatment using combined repair plus gel.

Discussion: The findings suggest that ECM injection had a modest but positive effect on muscle mass, fatty degeneration, and key cellular signaling pathways.

2.2 Introduction

In selected cases, the surgical care for damaged rotator cuffs is reattachment of the torn tendon(s) to their original boney insertion sites on the humerus [1-3]. Despite significant progress with arthroscopic techniques and improved fixation devices, rotator cuff surgery failure rates remain high, reported to be around 30-35% [4-6]. The muscles of the rotator cuff undergo progressive fatty degeneration, also termed fatty infiltration, following tendon tear [7,8]. This pathological degeneration of shoulder muscle in patients with rotator cuff tears is shown to be a contributing factor to the high failure rate [9]. While surgical techniques have been developed to address the torn tendinous portion of the damaged rotator cuff, there are currently no effective methods to address fatty degeneration. Fatty degeneration remains a well-recognized but currently unaddressed pathological condition that limits the success of rotator cuff surgery [10-12]. Our goal is the development of an effective treatment for the repair of fatty degenerated rotator cuff muscle that could become an adjunct to the current tendon repair techniques.

Under the right conditions, skeletal muscle has a robust capacity for self-repair. Following mild muscle injury (for example: strains, contusions, and lacerations) cells may be injured, but the damaged underlying ECM persists at the site of injury and regeneration is robust and complete [13,14]. Growth factors released from injured muscle matrix promotes satellite cells residing between myofibers to migrate to sites of injury, reenter cell cycle, proliferate, and differentiate into myoblasts, which in turn, undergo fusion to form nascent myofibers [15,16].

However, when muscle tissue is lost, the structural cues produced by the ECM are missing and regeneration is instead marked by fibrosis and the formation of non-contractile scar tissue [17-19]. The differential response to mild and severe muscle injury suggests an important role for extracellular matrix as a trigger for muscle regeneration. To deliver extracellular matrix cues into fatty infiltrated muscle, we are proposing the utilization of an injectable, water-based, matrix gel prepared from skeletal muscle tissue. Our enthusiasm for a matrix gel approach as a muscle repair strategy was motivated not only by the recognized role of matrix during muscle healing, but also by the cardiac work of Dr. Christman's group at the University of California at San Diego. They have developed an injectable matrix gel using cardiac tissue and demonstrated that injection of the material into infarcted cardiac muscle tissue stimulated regeneration [1,20,21]. A possible mechanism of repair is ECM gel promotion of vessel formation/perfusion, endothelial cell/ muscle progenitor cell infiltration as well as muscle cell proliferation [22,23].We believe the same regenerative results that have been reported in infarcted cardiac muscle tissue could be translated to fatty degenerated skeletal muscle.

We conducted this study to deeply explore the safety and efficacy of an injectable ECM gel while also deciphering whether any key wound healing mechanisms were impacted by matrix gel implantation. Specifically, we designed the study to test the hypothesis that intra-muscular delivery of matrix gel triggers the activation of pro-myogenic wound healing pathways that ameliorate fatty muscle infiltration. To test this hypothesis, we conducted experiments to 1) examine the longitudinal host response (biocompatibility) to ECM gel injection into normal muscle using a rodent model and 2) test matrix gel regenerative performance in a well accepted [24-27] animal model of delayed rotator cuff repair (rabbit).

2.3 Methods

ECM gel preparation

Human quadriceps muscle (Science Care, US) was thawed, trimmed to remove fat and connective tissue, and decellularized in 1% (wt/vol) solution of sodium dodecyl sulfate (SDS) in phosphate buffered saline (PBS) with agitation and multiple solution exchanges for up to 2 weeks [23,28] (**Fig. 1a and b**). We then rinsed the tissue with deionized water and incubated in DNase/RNase solution overnight at 4°C with agitation. The remaining ECM was rinsed, lyophilized, flash-frozen using liquid nitrogen, and ground into fine powder. We digested the ECM powder using a pepsin solution (1 mg/ml pepsin in 0.1 M HCl) at a ratio of 10mg ECM/1ml pepsin at a pH of 2.4 (adjusted every 12h if necessary) for 48h at room temperature [23,29] (**Fig. 1c and d**). The solubilized ECM solution was neutralized (pH=7.4) and diluted to a concentration of 10mg/ml in phosphate buffered saline (PBS). Finally, we loaded the neutralized pre-gel solution into syringes and stored it at -20°C **(Fig. 1e and f)**.

Host Response

Adult (12-14-weeks old) Sprague Dawley rats (Harlan, Indianapolis, IN) (n=12), weighing approximately 325-350g, were used as the animal model to explore the host response to injected ECM. All animal procedures were approved by the Institutional Animal Care and Use Committee of the University of Arkansas (#19002). We used isoflurane for anesthesia with induction dosage of 4% and maintenance dosage of 2% in oxygen. Syringes containing ECM gel were thawed and injected (200 µL; 27 gauge needle) into the TA at five sites along its distal-to-proximal length intramuscularly through the skin. We injected the contralateral TA's with sterile PBS to serve as comparative controls. Post-operative analgesia consisted of 0.1mg/kg

buprenorphine administered subcutaneously via injection twice daily for two days. A single surgeon performed all procedures. Animals also had access to anti-inflammatory medication (Rimadyl; 2mg/day) via a dietary tablet (Rodent MD's, Bio Serv, Flemington, NJ). We added tablets daily to each cage for one week following surgery in accordance with IACUC approved protocols and housed animals individually in standard-sized cages with unrestricted movement. The animals were allowed to bear weight on the operative extremity as tolerated. All animals were housed for a 3, 14, or 56 day recovery period (n=4 animals / time point).

Rotator Cuff Repair

Adult (24-weeks old) male New Zealand white rabbits (pre-surgery mass ~3.5 kg) purchased commercially (Charles River) (n=14) were used to examine the effect of ECM gel injection on recovery from torn rotator cuff repair. All animal procedures were approved by the Institutional Animal Care and Use Committee of the University of Arkansas for Medical Sciences (#3655). The rotator cuff tear and delayed tendon repair surgeries were performed following published methods [30,31]. A trained orthopedic surgeon performed the surgeries. We used isoflurane for anesthesia with induction dosage of 5% and maintenance dosage of 3% in oxygen. The left shoulder was shaved and disinfected. A longitudinal incision was made over the shoulder, and dissection performed down to the deltoid. The deltoid was retracted to reveal the supraspinatus (SSP) tendon. The supraspinatus tendon was transected at its insertion onto the greater tuberosity. The cut end of the tendon was tagged with a non-resorbable No. 4-0 suture (Prolene, Ethicon, Somerville, NJ) for later identification. All attachments of the tendon to the surrounding tissues, including the infraspinatus, were released, allowing the tendon to retract freely away from its insertion site. The incisions were closed with interrupted, subcutaneous No.

3-0 Vicryl sutures (Ethicon), and the skin was closed with a running 4-0 monocryl suture (Ethicon). The contralateral shoulder remained untreated to serve as a comparative control. All animals were housed for a 12-week recovery period.

Following recovery, all animals underwent SSP tendon reattachment repair surgery. The free tendon edge was identified by use of the tag suture and double stitched to the humerus using a fiber wire suture. We randomly assigned half of the animals to receive 1 mL of muscle derived ECM gel injection into the SSP muscle at five locations along its length. Following repair, the surgeon closed surgical site with a suture as previously described. The animals were maintained in the animal facility for a recovery period of 12 weeks (n= 7 / treatment group). At the end of the recovery period, a veterinarian euthanized all animals via intracardiac injection of a commercial euthanasia solution. SSP muscles were harvested, weighed, imaged, and prepared for histological sectioning and gene expression testing.

Contractile Force Measurements (Rat Only)

At each post-injection time point (3, 14 and 56 days), we measured peak tetanic TA contractile torque *in-situ* using published methods familiar to our group [19]. The ankle was flexed to 90° and the foot was secured to the lever arm of a commercial muscle physiology system (Aurora Scientific, Ontario, Canada). We measured the TA peak isometric tetanic torque by stimulating the peroneal nerve with the aid of a physiological stimulator (Grass; S88) and determined Optimal voltage (2 – 5 V) using a series of te tanic contractions (150Hz, 0.1 ms pulse width, 400 ms train). We recorded raw peak tetanic contractile force (N) from both the treated and contralateral control limb of each animal. We calculated peak tetanic force for each animal using the average of four contractions and reported the animal weight normalized force data

(N/kg body weight) in the results. At the conclusion of electrophysiological testing, we harvested the TA muscles and euthanized the rats by carbon dioxide inhalation.

Histological Analysis

Muscle tissue (rat and rabbit) was flash frozen in isopentane (2-methylbutane) chilled in liquid nitrogen. Tissue was sectioned (8μm) with the aid of a cryostat (Leica BioSystems) and mounted onto microscopic slides. Slides were immuno-stained using primary antibodies (1:300, Novus Biologicals) directed against collagen III (IgG), or collagen I (IgG) with or without myosin heavy chain (MHC) co-stain, followed by incubation in the appropriate fluorescently labeled secondary antibodies (AlexaFluor, 1:300, Life Technologies). Additional tissue sections were stained using hematoxylin and eosin (H&E) or Oil red-O following manufacturer's guidelines (Sigma-Aldrich). All sections were digitally imaged (100X, Nikon CiL).

Tissue immunoreactivity to collagen I as a percentage of total tissue area (% collagen I) was calculated with the aid of image analysis software (ImageJ) using techniques familiar to our group [19]. Similar image analysis methods were used to compute fiber cross-sectional area (μm^2) using collagen III positive area. Oil red-O images were evaluated using an in-house developed MATLAB code to isolate oil red-O positive (fat) and negative (muscle) tissue regions within each section. The ratio of oil red-O positive tissue area to total tissue area was used to calculate the intramuscular fat area fraction (% area).

Gene Expression

RNA was extracted from tissue samples using the RNeasy Kit (Invitrogen). Commercially available TaqMan primers (Invitrogen) for Pax7, MyoD, MyoG, Col I, Col III,

TGF-β1, IL-6, IL-10, CD68 and 18s ribosomal housekeeping were used to quantify the expression of desired host-response genes from rat tissue. Expression was normalized to 18S and then referenced to the contralateral saline injected limb. Commercially available SYBR Green primers (Bio-Rad) for PPAR-γ, MURF1 (Trim63), Pax7, MyoG, and RPL4 housekeeping were used to quantify the expression rabbit muscle genes. Experimental sample group (n=6-7/group) expressions were normalized to RPL4 and then referenced to the contralateral uninjured limb. Gene expression levels are reported as fold change using the $2^{-(\Delta\Delta Ct)}$ method.

The full transcriptomes of representative repair only, repair plus ECM gel, and uninjured controls rabbit SSP muscle samples (n=5/ group) were analyzed using RNA-Seq. cDNA libraries were sequenced on the NextSeq500 platform (Illumina) to a mean depth of 20 million reads per library. RNA sequencing reads were mapped to the Oryctolagus cuniculus genome (OryCun2.0) from NCBI using the 2-pass STAR protocol[32]. Reads were quantified using FeatureCounts[3], followed by analysis of differential expression and normalization in edgeR[33]. Differential expression was selected using a maximum false discovery rate (FDR) of 0.25 and a minimum log fold change of 1.5. Pathway level analysis was also performed using Ingenuity Pathway Analysis (IPA) (Qiagen)[34].

Statistical Analysis

All data are presented as the mean and standard deviation unless otherwise noted. The effect of treatment on TA mass, TA contractile force, TA collagen I area (%), TA myofiber cross-sectional area, TA and SSP gene expression, as well as SSP mass reduction were evaluated using a two-sided Student's t-test. The effect of treatment SSP fat area fraction, SSP collagen I area fraction, and SSP myofiber area were evaluated using ANOVA with Tukey's post hoc test.

A standard $p<0.05$ level of significance was used as the threshold for all statistical tests.

2.4 Results

Host Response

All animals tolerated the ECM gel injection treatment well. Peak tetanic contractile force values for ECM gel injected TA muscle were statistically indistinguishable from PBS controls at three days (0.97+0.41 N/kg vs. 0.72+0.18 N/kg) and at 14 days (1.72+0.87 N/kg vs.1.34+0.56 N/kg) post-injection (**Fig. 2a**). However, at 56 days, the study endpoint, a statistically significant (p=0.048) increase in contractile force was detected for the ECM gel injection group. Mean gel injected TA contractile force values were on average 53+37% higher than PBS injected control values (3.25+0.41 N/kg vs. 2.25+0.70 N/kg). TA mass followed a similar trend to force. At 3 days (1.93+0.23 g/kg vs. 2.14+0.16 g/kg) and 14 days (2.03 + 0.08 g/kg vs. 2.09+0.09 g/kg) post-injection TA mass did not differ between the ECM gel and PBS injected groups respectively (**Fig. 2b and c**). Similar to force results, at 56 days there was a statistically significant (p=0.003) increase (18+8%) in TA mass for the ECM gel injection group (2.43+0.14 g/kg) when compared to PBS controls (2.05+0.07 g/kg).

Rat TA sections immunostained for collagen I exhibited no discernible differences between ECM gel injection and PBS controls across all time points (**Fig. 3a)**. There were no indications of abnormal inflammatory or fibrotic responses within any of the TA tissue sections examined. Fiber cross-sectional area as indicated by collagen III-positive regions were normal in appearance with spheroid muscle fiber cross sections observed for both groups (**Fig. 3b)**. H&E staining also appeared normal with tightly apposed bundles of myofibers and no evidence of hyperplastic regions within any of the TA sections (**Fig. 3c)**. Collagen I-positive area fraction

(**Fig. 3d)** and myofiber cross-sectional area (**Fig. 3e)** were not significantly different between either groups at any time point.

The expression levels of genes associated with ECM and ECM regulation: Col I (0.031), Col III (p=0.017), and TGF-ß1 (p=0.012) were all significantly upregulated (~10 fold) at 3 days post-injection (**Fig. 4a**). By 14 days post-injection, Col III (p=0.035) and TGF-ß1 (p=0.017) remained upregulated by approximately 5-fold in the gel injected groups compared to controls until returning to basal levels of expression by 56 days. We observed a similar trend in a panel of inflammatory genes, with IL-6 (p=0.033) and IL-10 (p=0.025) being expressed approximately 15-fold higher in response to gel injection at 3 days post-injection when compared to PBS controls, while CD68 (p=0.049), a macrophage specific marker, was expressed approximately 50-fold higher in the gel group compared to PBS controls at the same time point **(Fig. 4b)**. By 14 days all gene expression related to these targets returned to PBS control tissue levels. Myogenic gene expression (Pax7, MyoD, MyoG) is statistically indistinguishable between the two treatment groups at all post-injection time points (**Fig. 4c)**

Rotator Cuff Repair

All animals tolerated the RC surgery, bore weight normally on the treated limb by the end of the first post-operative week, and gained weight throughout the study period. Animal growth rate was examined during the twelve-weeks prior to and following SSP treatment. While growth generally slowed with increasing animal age, we did not detect any differences in growth rate between repair only and repair plus ECM gel groups during either the twelve weeks before repair or during the twelve weeks following repair. At the study endpoint (12 weeks after repair), a layer extramuscular fat remained on muscles harvested from both tendon repair only and

combined tendon repair plus ECM gel treatment animals (**Fig. 5a**). No accumulation of extramuscular fat was observed on any of the uninjured contralateral SSP muscles. While both treatment strategies resulted in significant muscle atrophy when compared to uninjured contralateral controls, combined tendon repair with ECM gel injection treatment had a positive effect on SSP mass to decrease atrophy. Treatment with tendon repair only resulted in a 31+7% reduction in SSP mass when compared to uninjured controls. Alternatively, treatment using combined tendon repair plus ECM gel injection resulted in a 24+3% reduction in SSP mass, a decrease of 7% when compared to the repair only (**Fig. 5b**). The SSP mass reduction between the repair only and the combined repair plus ECM injection groups was statistically significant.

Oil red-O staining of uninjured, repair only, and repair with ECM gel injection SSP sections revealed elevated levels of intramuscular lipids within muscle tissue collected from both treatment groups (**Fig. 6a**). The repair only and combined repair with ECM gel sections contained a gradient of intramuscular fat with the densest regions localized nearest the tendon injury site. Qualitative examination of sections immunostained for collagen I or collagen III revealed no notable differences between either of the treatment groups or differences from uninjured controls (**Fig. 6b and c**). Collagen I and III immunoreactivity was uniformly distributed around muscle fibers (collagen III primarily) and mutlifiber bundles (collagen I) for all treated and uninjured control muscles examined. We did not detect any abnormal changes to myofiber cross-sectional morphologies between the treatment groups. H&E sections from both treatment groups consistently exhibited a lack of tight myofiber apposition when compared to sections prepared from contralateral normal tissue and further confirmed fiber atrophy due the RCT (**Fig. 6d**).

Quantitative image analysis of oil red-O stained sections revealed that both repair and repair with ECM gel treatments resulted in significant increases in intramuscular fat area fraction when compared to uninjured contralateral controls. Fat fraction of repair only group was 6.1+2.9%, while repair plus ECM gel fat fraction was 4.1+2.1%, a reduction of 2% from repair only values. The difference in fat area fraction between the repair only and combined repair plus gel treatment group did not reach statistical significance (p=0.18) (**Fig. 6e**). The uninjured contralateral SSP fat content was minimal and similar within the repair only (0.6 +0.2%) and the combined repair plus ECM gel (0.7+0.6%) groups. No statistical difference was detected between these groups. We did not detect any abnormal fibrosis in any of the tissue examined. Specifically, the collagen I area fraction was not effected by either repair only or combined repair plus gel treatment, when compared to normal muscle sections (**Fig. 6f**). We did detect a significant difference in fiber cross-section area between treatment groups. Repair only treatment resulted in a 30+9.8% decrease in muscle fiber size when compared to uninjured contralateral controls, while combined tendon repair plus ECM gel injection resulted in a more modest decrease of 10+4.3% (p= 0.005) (**Fig. 6g**).

The mRNA abundance (fold change) of genes associated with muscle degeneration (PPAR-γ, MURF1) were sensitive to repair only treatment (**Fig. 7a**). PPAR-γ was significantly upregulated (3.15+2.44 fold change) (p= 0.040) while MURF1 was strongly downregulated (0.07+0.02 fold change) (p= 0.042) when compared to contralateral uninjured tissue. These genes were not significantly different from uninjured controls when examined in the combined repair plus gel injection group. The myogenic genes examined (Pax7, MyoG), were generally downregulated for both treatment groups (**Fig. 7b**). Pax7 was significantly downregulated in both the repair only (0.08+0.07 fold change) and combined repair plus ECM gel group

(0.05+0.04 fold change). However, although MyoD appeared downregulated when compared to uninjured controls tissue for both treatment groups, it only reached statistical significance for the repair only group (0.35+0.05 fold change).

Analysis of RNA-Seq data in EdgeR revealed a total of 40 differentially expressed genes (all upregulated) between the repair only group relative to uninjured controls, and 1 differentially expressed (downregulated) gene (DNAse1) between the combined repair plus gel group relative to control (**Supplementary Table 1**). Notably, in the repair only group, IPA detected the activation of the canonical adipogenesis pathway ($p<.0001$) due to four differentially expressed genes (PPAR-γ, LEP, KLF5, FABP4) and the activation of the canonical osteoarthritis pathway ($p<0.001$) due to four differentially expressed genes (LEP, MMP-12, PPAR-γ, SSP1). IPA did not detect the activation of any pathways in muscle tissue collected from the combined repair plus ECM gel injection group.

2.5 Discussion

Our host response findings using the rat model, which included functional, histological, and gene expression measures, suggest that intramuscular ECM gel injection was well tolerated. We detected a significant increase in the expression of inflammatory cytokines (IL-6, IL-1) and macrophage markers (CD68) at 3 days post ECM injection. This finding is consistent with normal muscle wound healing and while not a direct measure of macrophage presence, the increased expression of CD68 suggests macrophage infiltration in response to the presence of ECM fragments from the gel [35,36]. At 14 days post-injection, macrophage marker and inflammatory gene expression returned to basal levels suggesting that ECM injection did not elicit a foreign body response with chronic inflammation [37]. Future studies could benefit from a more extensive analysis of macrophage dynamics at the site of ECM gel injection. We did not

observe foreign body giant cells within tissue sections at any of the time points. Consistent with normal wound healing, specifically remodeling and repair, [38] we observed a characteristic upregulation of key matrix (CoL I and III) and matrix-regulatory (TGF-ß1) genes in response to intramuscular ECM matrix gel injection [39]. These genes remained upregulated into the second week but had returned to basal levels of expression at 56 days post-injection. Although matrix and matrix regulatory genes were upregulated in response to ECM injection, we did not observe any evidence of intramuscular fibrosis, suggesting normal matrix protein regulation during wound healing with balanced deposition of new matrix and degradation of damaged matrix [40]. Interestingly, we detected a significant increase in peak muscle force and mass in response to ECM gel injection. This outcome was unexpected, especially absent a finding of increased muscle fiber size, and warrants continued investigation.

The shoulder cuff repair findings indicate that the combination of tendon repair with ECM gel injection can have a positive effect on muscle atrophy. Although significant SSP atrophy occurred within both treatment groups when compared to contralateral uninjured SSP muscle, the use of combined tendon repair with ECM injection significantly reduced the amount of atrophy when compared to the tendon repair only group. Histological evaluation revealed that the repair only group had significantly smaller myofiber cross-sectional area when compared to uninjured controls, which is consistent with the pathological effect of muscle atrophy in other chronic rotator cuff injury models [41,42]. Alternatively, combining tendon repair with ECM gel injection resulted in the preservation of myofiber cross-sectional area in the SSP. Gene expression analysis using RT-qPCR provides a potential explanation for the differences in SSP atrophy and fiber size observed between the two treatments. We detected a reduction in MURF1, a well-known regulator of atrophy that acts as an important rate-limiting enzyme in protein

degradation in skeletal muscle [43], gene expression within the repair only group, while the expression was equivalent to normal uninjured muscle when examined in combined tendon repair with ECM gel injection tissue. The downregulation of MURF1 in the repair group, coupled with the absence of mass preservation of the SSP suggests that tendon repair alone may be insufficient to sustain hemostasis of muscle protein synthesis in chronic RCT injury. Examination of genes related to myogenesis revealed that Pax7, a marker of satellite cell activation, was significantly downregulated in both treatment groups. These results suggest that atrophic signaling may be inhibiting myogenic signaling in both treatment groups, which has been previously demonstrated in models of chronic RTC injury [44].

Although it did not reach the level of statistical significance, fatty infiltration was modestly reduced (2%) in response to treatment with combined tendon repair with a single round of ECM gel injection. Cell signaling pathway analysis conducted using the transcriptome profiling results of both treated and uninjured SSP tissue detected the activation of key canonical signaling pathways in the repair only group while none were found to be activated in uninjured SSP tissue or the ECM gel injection group. This suggests that ECM gel injection is possibly having a dampening effect on muscle tissue cellular signaling. In particular, within the adipogenic signaling pathway, four distinct transcription factors (PPAR-γ, LEP, KLF5, FABP4) were found to be significantly upregulated in response to tendon repair only treatment. These results are consistent with the observed increase in adipogenic gene expression in the repair only group with PCR. This story is further corroborated by a similar finding in the upregulation of FABP4 for the repair group, a protein that is involved in fatty acid uptake, transport, and muscle metabolism [45,46]. Interestingly, FABP4 has also been identified to be one of the key transcription factors affecting marbling in cattle meat, a condition with similarities to muscle fatty infiltration

following rotator cuff injury [47]. An understanding of the transcriptional changes in FABP4 and abrogation of the adipogenesis pathway in response to ECM gel injection may explain the reduced level of fatty degeneration that we observed. In turn, it may provide a candidate target for combinatorial therapies that could be incorporated into ECM gels in order to enhance their efficacy.

Interestingly, we also detected upregulation of the canonical osteoarthritis (OA) pathway in the repair only group, but not in the ECM injection or uninjured SSP muscle groups. Specifically, matrix metalloproteinase-12 (MMP-12) was significantly upregulated in response to tendon repair only. MMPs in general, and MMP-12 specifically, are associated with a number of degenerative diseases including rheumatoid arthritis [48-50]. In addition to degrading a wide range of substrates including those that compose the basal lamina, MMP-12 has also been shown to activate other matrix MMPs, further promoting matrix degradation and mechanical instability of the shoulder region [48,51]. This suggests that current repair techniques could potentially have the unintended consequence of creating tissue degradation and a mechanical environment that is associated with poor post-operative outcomes [52]. Abrogation of the OA pathway in the combined tendon repair with ECM injection group may warrant further investigation as it would appear to exert a protective effect on not just the injected muscle but the shoulder joint as well. We also detected significant downregulation of DNase1 within the ECM injection group. While there have been no published findings concerning the role of DNase1 in rotator cuff injuries, the finding may be significant as DNase1 delivery has been shown to reduce extracellular traps (ET) that promote inflammatory and thrombosis cascades [53] which could play a role in shoulder health.

A limitation to this study that deserves discussion was the lack of an early post-injection time point in the rabbit model. The 12-week endpoint examined in this study, while appropriate for the examination of recovery, did not allow us to make longitudinal comparisons between the repair only and repair plus ECM gel groups. As such, we can not conclude whether the reduction in muscle atrophy that we observed in response to combined repair plus ECM gel treatment was the result of gel induced muscle growth or simply a decrease in the rate of muscle atrophy when compared to repair only. Future studies will incorporate early post-injection time points in order to examine atrophy kinetics, as well as cellular (macrophages and other immune cells) and soluble factor (cytokines and growth factors) responses that may be responsible for the muscle atrophy differences we observed. Lastly, we did not utilize a sham injection as part of the repair only treatment group. As such we cannot separate the effect of the injection site injury from the presence of the ECM gel itself. However, the response to a sham PBS injection in the rat model was negligible, suggesting that the changes we observed in the rabbit model were predominately in response to the presence of the ECM gel.

To sum, its well accepted that chronic rotator cuff tears are associated with a variety of pathological changes to the skeletal muscle, including atrophy, fibrosis, and fatty infiltration [34,54,55]. While means to repair chronically torn shoulder cuff tendons exist, unaddressed muscle pathologies can decrease the capacity for tendon healing, prevent full recovery of shoulder function, and are generally associated with poor outcomes [54]. We envision the use of the ECM gel material explored in this study as an adjunct to existing tendon repair strategies, in order to address both tendon and muscle injury in patients with chronically torn rotator cuffs. It is worth noting that the clinical use of ECM materials in muscle is not without precedent. Acellular ECM scaffolds have been used in to improve the strength and range of motion in patients with

volumetric muscle loss injuries [56]. While we do not yet know the mechanism responsible for the improvement in muscle atrophy we observed, the ECM gel injection results when explored in a delayed SSP repair model were encouraging and warrant continued pre-clinical investigation in order to firmly establish safety and efficacy.

2.6 Conclusion

ECM gel injection elicited a host response that resulted in the elevation of wound repair gene expression at early time points, but did not lead to any pathological changes in muscle architecture, suggesting tolerance by the host environment. Furthermore we detected a significant increase in muscle mass and contractile force in response to ECM gel injection, which warrants continued exploration. When examined in a delayed SSP repair model we observed a modest but measurable effect when ECM gel was used in combination with tendon repair. Specifically, intramuscular ECM gel injection mitigated SSP atrophy and abrogated the activation of key adipogenic and osteoarthritic signaling pathways. The results suggest that the short-term activation of wound healing pathways observed in the rat model are complemented by a longer-term positive effect on muscle atrophy and cellular signaling.

2.7 Figure and table

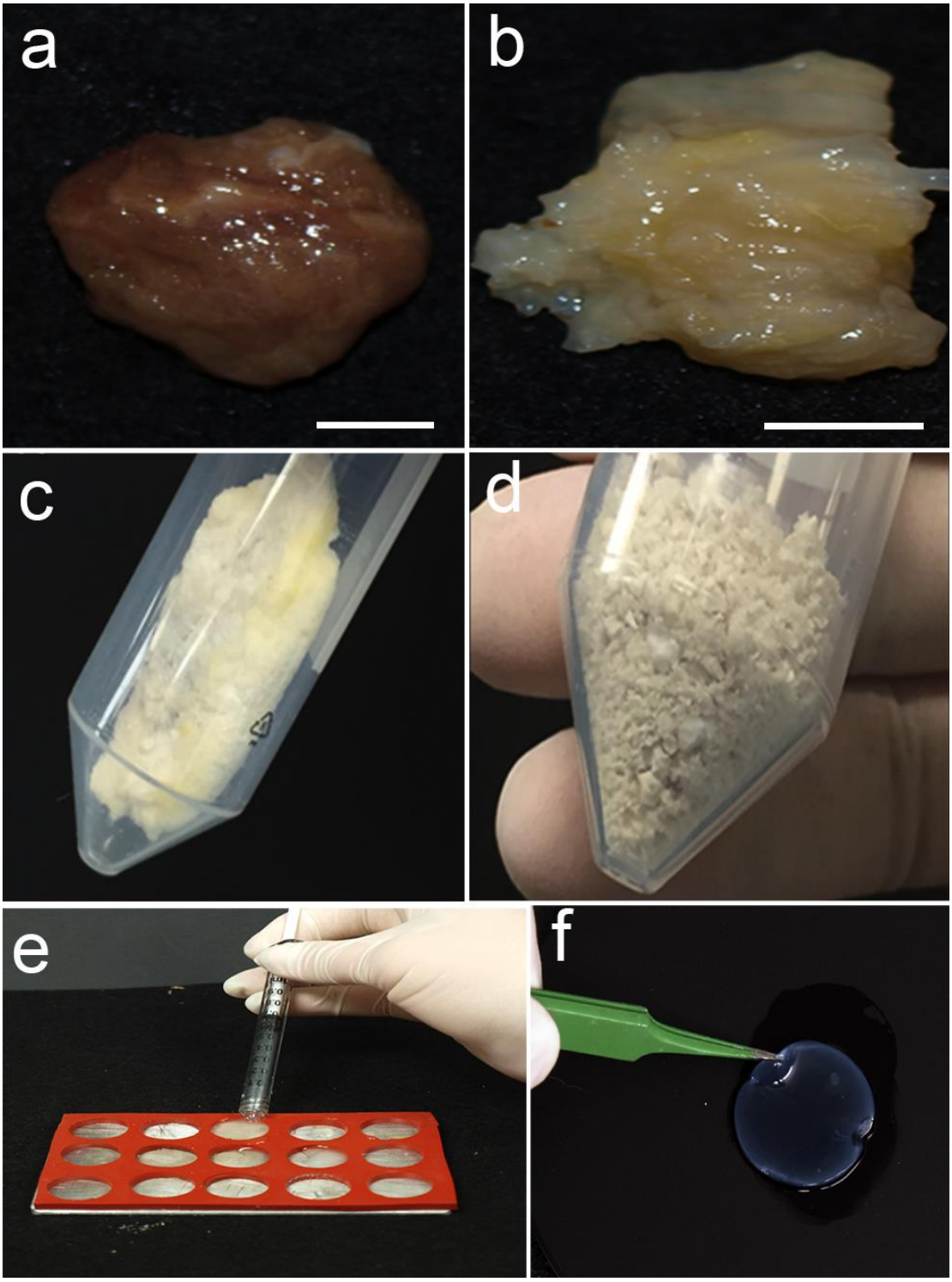

Figure 1: (a) Human quadriceps muscle was (b) decellularized, (c) lyophilized, (d) ground into a fine powder and (e) pepsin digested to create an injectable pre-gelled matrix solution. (f) The pregelled muscle matrix solution forms a gel when warmed to 37°C.

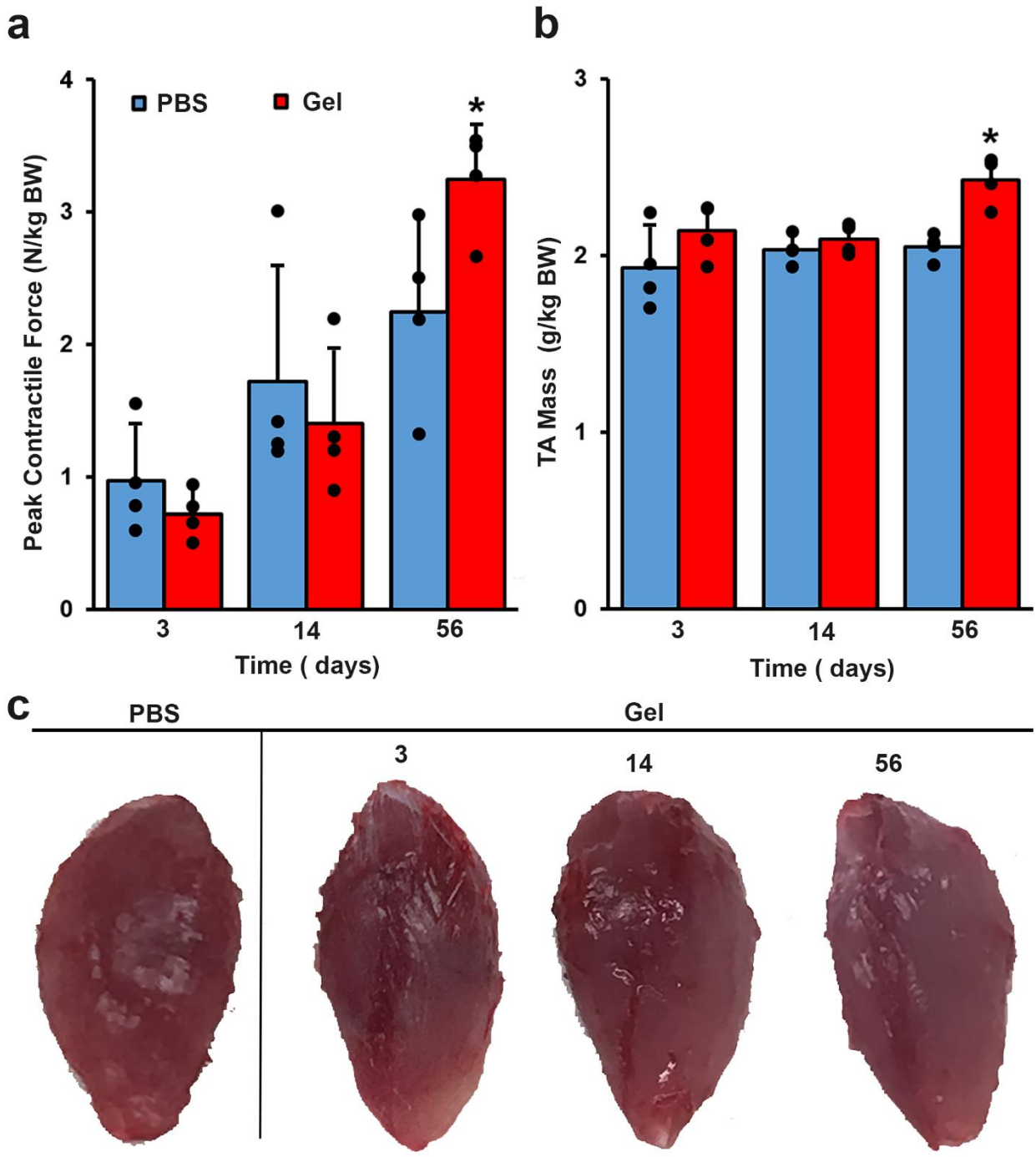

Figure 2: (a) TA muscle peak contractile force (N/kg body weight) and (b) wet weight (g/kg body weight) data normalized to animal weight. (c) Gross morphology of TA muscles 56 days post PBS injection (left) and 3, 14, and 56 days post ECM gel injection (right). Data is presented as group means + SD; n=4/group; * denotes statistically significant ($p<0.05$) differences from controls.

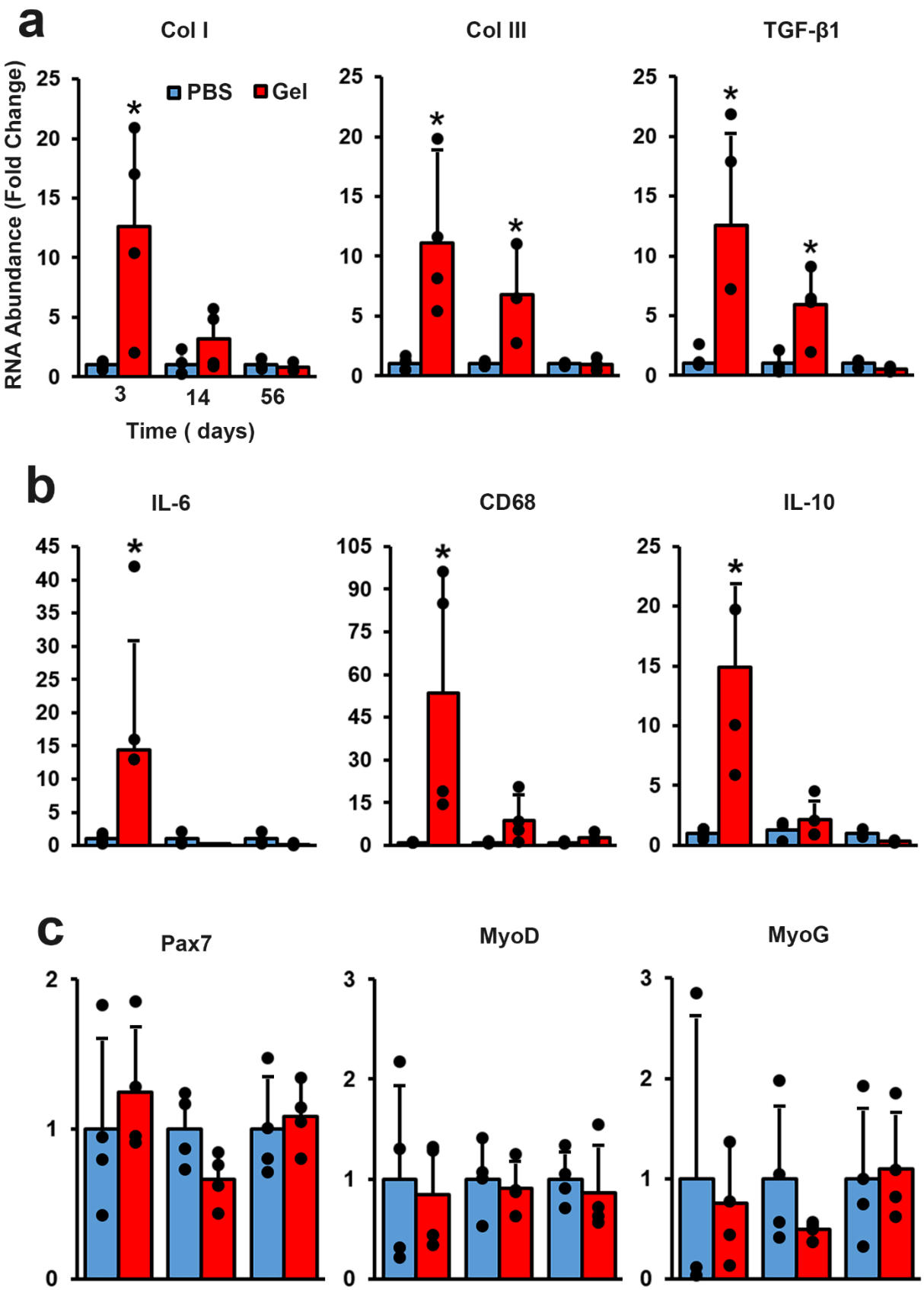
a
Col I
Col III
TGF-β1
PBS
Gel
RNA Abundance (Fold Change)
Time (days)
3
14
56
b
IL-6
CD68
IL-10
c
Pax7
MyoD
MyoG

Figure 3: TA muscle cross-sections were stained for (a) collagen I (green), b) collagen III (red), and with (c) Hematoxylin and Eosin. Representative 56 days post PBS injection (left) and 3, 14, and 56 days post ECM gel injection TA cross-sections are presented. Scale bar = 100μm unless noted. Cross-sections were quantified for (d) collagen I area fraction and (e) muscle fiber cross-sectional area. Group means + SD are presented; n=4/group.

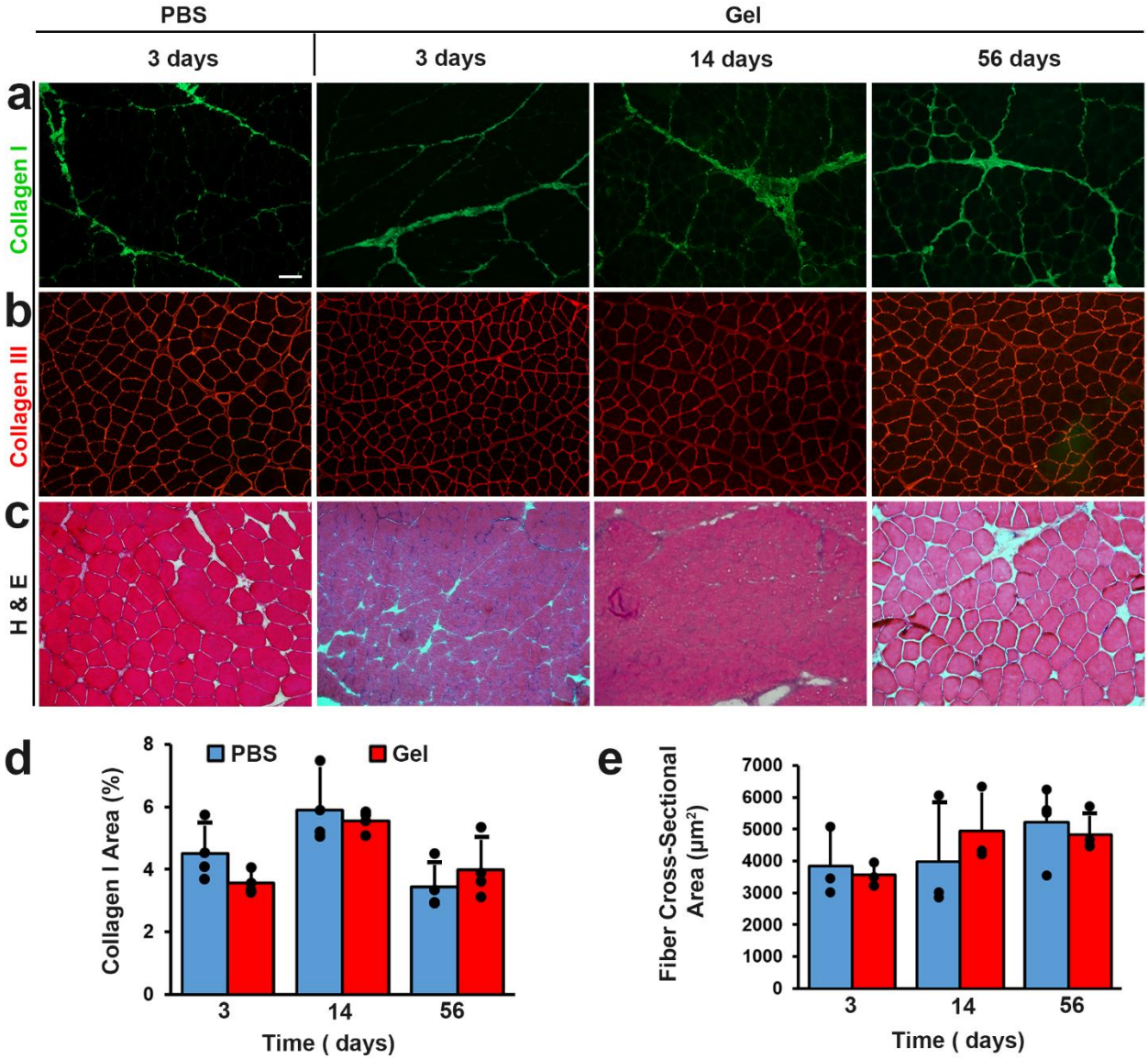

Figure 4: Comparison of relative gene expression for PBS and ECM gel injected groups determined using qRT-PCR. The expression of (a) ECM (Col I and Col III), ECM regulatory (TGFβ1), (b) inflammation (IL-6), anti-inflammation (IL-10), macrophage marker (CD68) and (c) myogenic (Pax7, MyoD, MyoG) genes were measured using muscle tissue harvested from the TA of each animal tested. Expression is presented as fold change normalized to PBS injected muscle expression. Group means + SD are presented, n=3-4/group. * denotes statistically significant ($p<0.05$) differences from controls.

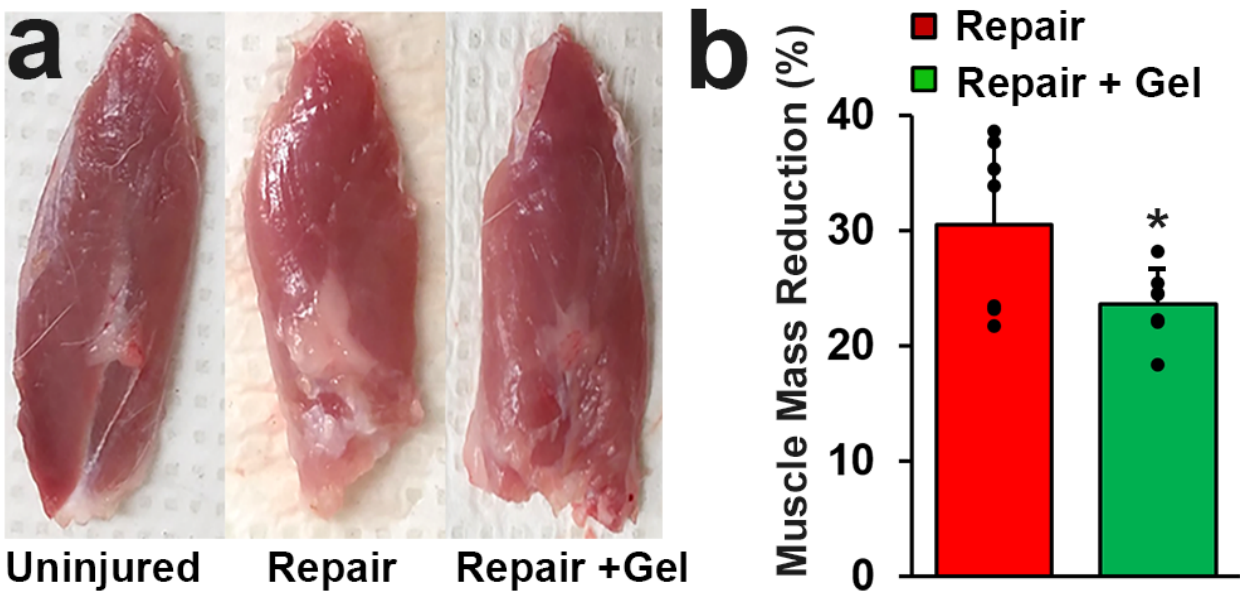

Figure 5: (a) Gross morphology of representative SSP muscles from uninjured, repair only, and combined repair plus ECM gel groups are presented to show the appearance of surface fat accumulation on injured muscles. (b) SSP muscle wet weight data (% of uninjured) for repair only and combined repair plus ECM gel groups. Data is presented as group means + SD; n=7/group; * denotes statistically significant ($p<0.05$) differences between groups.

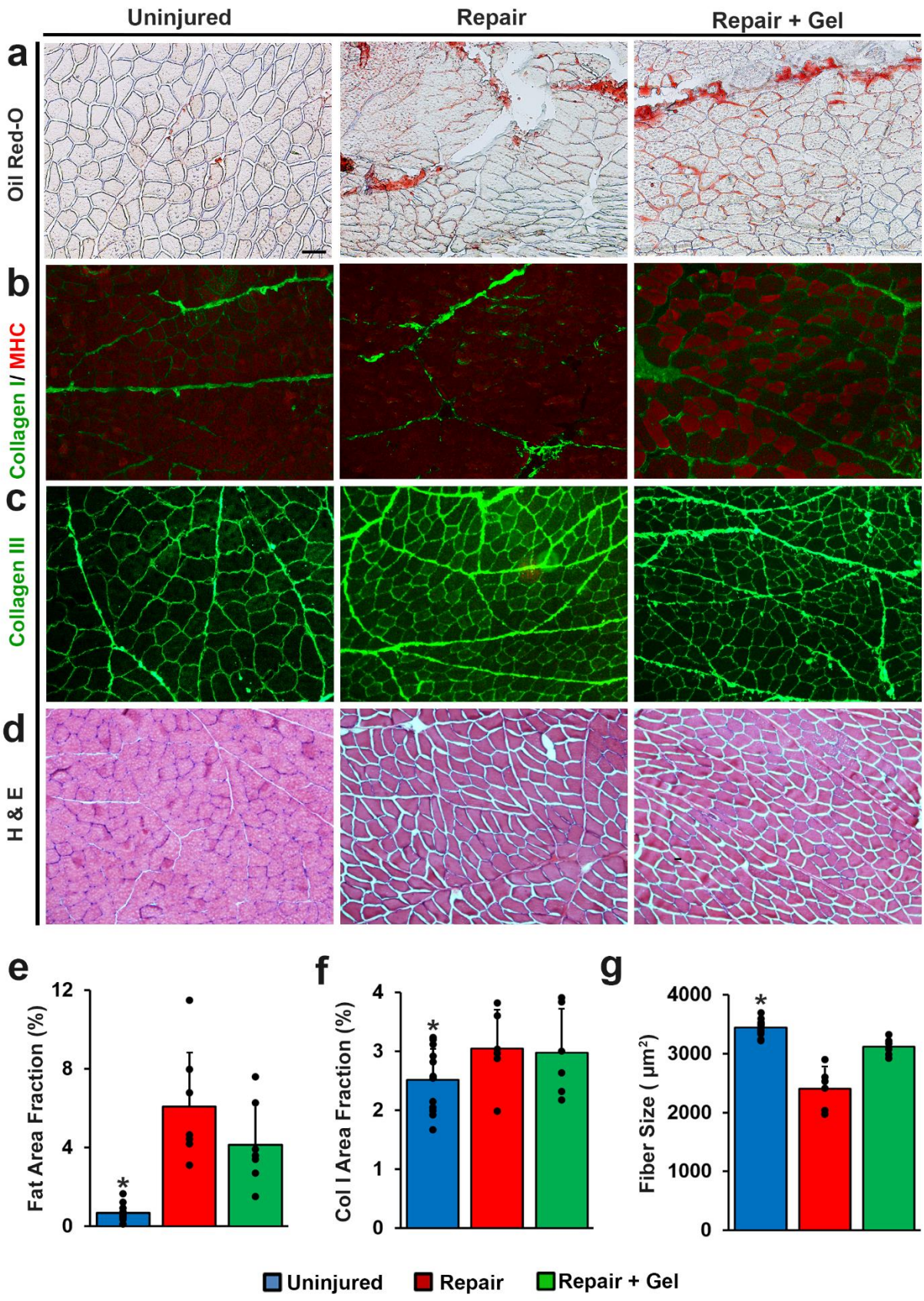
Uninjured
Repair
Repair + Gel
a
Oil Red-O
b
Collagen I/ MHC
c
Collagen III
d
H & E
e
Fat Area Fraction (%)
12
8
4
0
*
f
Col I Area Fraction (%)
4
3
2
1
0
*
g
Fiber Size (µm²)
4000
3000
2000
1000
0
*
Uninjured
Repair
Repair + Gel

Figure 6: SSP muscle cross-sections were stained for (a) Oil red-O, (b) collagen I (green) counterstained with MHC (red), (c) collagen III (green), and (d) hematoxylin and eosin. Representative 12 weeks post SSP repair images for uninjured, repair only, and combined repair plus gel groups are presented. Scale bar = 100μm unless noted. Repair only and combined repair plus ECM gel cross-sections were quantified to determine (e) area fraction collagen I, (f) area fraction oil red-O, and (g) muscle fiber cross-sectional area (μm^2). Group means + SD are presented; n=6-7/group. * denotes statistically significant ($p<0.05$) differences between groups.

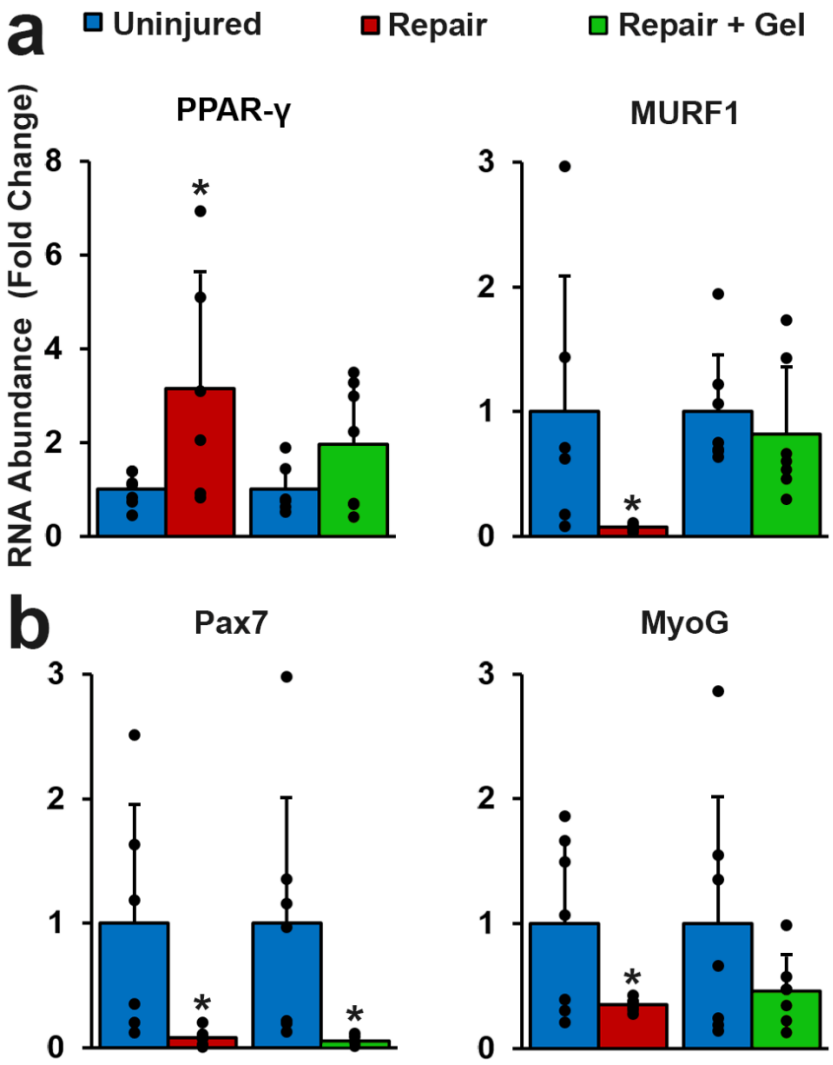

Figure 7: Comparison of relative gene expression for repair only and combined repair plus ECM gel injected groups using RT-PCR. The expression of (a) adipogenesis (PPAR-γ), muscle synthesis (MURF1), (b) satellite cell dynamics (Pax7) and myogenesis (MyoG) were measured using muscle tissue harvested from the SSP of each animal tested. Expression is presented as fold change normalized to contralateral uninjured muscle expression. Group means + SD are presented, n=6-7/group. * denotes statistically significant ($p<0.05$) differences from uninjured controls.

Supplementary Table 1: Differentially expressed (compared to uninjured) genes detected (RNA-Seq) within the repair only group. Only one (DNAse1) differentially expressed gene was detected in the repair plus ECM gel injection group. ($p<0.05$, log ratio >1.5, and FDR>0.25).

ID	Symbol	Entrez Gene Name	Location	Expr Log Ratio
TGM5	TGM5	transglutaminase 5	Cytoplasm	6.606
MLPH	MLPH	melanophilin	Cytoplasm	5.862
LRRC15	LRRC15	leucine rich repeat containing 15	Plasma Membrane	5.85
MMP12	MMP12	matrix metallopeptidase 12	Extracellular Space	5.416
CLSTN2	CLSTN2	calsyntenin 2	Plasma Membrane	4.461
NELL1	NELL1	neural EGFL like 1	Extracellular Space	4.404
UTS2	UTS2	urotensin 2	Extracellular Space	4.296
MCEMP1	MCEMP1	mast cell expressed membrane protein 1	Cytoplasm	4.051
PRR32	PRR32	proline rich 32	Other	4.048
FAM180B	FAM180B	family with sequence similarity 180 member B	Other	4.009
FBLN7	FBLN7	fibulin 7	Extracellular Space	3.844
SLC7A10	SLC7A10	solute carrier family 7 member 10	Plasma Membrane	3.597
CORIN	CORIN	corin, serine peptidase	Plasma Membrane	3.124
LEP	LEP	leptin	Extracellular Space	3.064
KCNK12	KCNK12	potassium two pore domain channel subfamily K member 12	Plasma Membrane	3.055
IGFBP2	IGFBP2	insulin like growth factor binding protein 2	Extracellular Space	2.881
SPP1	SPP1	secreted phosphoprotein 1	Extracellular Space	2.584
SMOC1	SMOC1	SPARC related modular calcium binding 1	Extracellular Space	2.572
PCK2	PCK2	phosphoenolpyruvate carboxykinase 2, mitochondrial	Cytoplasm	2.525
THRSP	THRSP	thyroid hormone responsive	Nucleus	2.409
UCP2	UCP2	uncoupling protein 2	Cytoplasm	2.401
GPR88	GPR88	G protein-coupled receptor 88	Plasma Membrane	2.36
GPNMB	GPNMB	glycoprotein nmb	Plasma Membrane	2.326
CIDEC	CIDEC	cell death inducing DFFA like effector c	Cytoplasm	2.241
CIDEA	CIDEA	cell death-inducing DFFA-like effector a	Cytoplasm	2.237
CCDC173	CCDC173	coiled-coil domain containing 173	Other	2.223
PTGER3	PTGER3	prostaglandin E receptor 3	Plasma Membrane	2.206
ADAMTSL1	ADAMTSL1	ADAMTS like 1	Extracellular Space	2.117
TMEM45A	TMEM45A	transmembrane protein 45A	Plasma Membrane	1.909
SLC36A2	SLC36A2	solute carrier family 36 member 2	Plasma Membrane	1.896
MFAP4	MFAP4	microfibril associated protein 4	Extracellular Space	1.858
CD53	CD53	CD53 molecule	Plasma Membrane	1.793
KLF5	KLF5	Kruppel like factor 5	Nucleus	1.752
TRABD2B	TRABD2B	TraB domain containing 2B	Plasma Membrane	1.706
PPARG	PPARG	peroxisome proliferator activated receptor gamma	Nucleus	1.67
FST	FST	follistatin	Extracellular Space	1.624
PRLR	PRLR	prolactin receptor	Plasma Membrane	1.618
AEBP1	AEBP1	AE binding protein 1	Nucleus	1.59
PLSCR5	PLSCR5	phospholipid scramblase family member 5	Other	1.55
FABP4	FABP4	fatty acid binding protein 4	Cytoplasm	1.549

2.8 References

1. Garofalo, R.S., *et al.* Severe diabetes, age-dependent loss of adipose tissue, and mild growth deficiency in mice lacking Akt2/PKB beta. *The Journal of clinical investigation* **112**, 197-208 (2003).

2. Gonzalez, E. & McGraw, T.E. The Akt kinases Isoform specificity in metabolism and cancer. *Cell Cycle* **8**, 2502-2508 (2009).

3. Liao, Y., Smyth, G.K. & Shi, W. featureCounts: an efficient general purpose program for assigning sequence reads to genomic features. *Bioinformatics* **30**, 923-930 (2014).

4. Chen, W.S., *et al.* Growth retardation and increased apoptosis in mice with homozygous disruption of the akt1 gene. *Genes & development* **15**, 2203-2208 (2001).

5. Garofalo, R.S., *et al.* Severe diabetes, age-dependent loss of adipose tissue, and mild growth deficiency in mice lacking Akt2/PKB beta. *Journal of Clinical Investigation* **112**, 197-208 (2003).

6. Easton, R.M., *et al.* Role for Akt3/Protein kinase B gamma in attainment of normal brain size. *Molecular and cellular biology* **25**, 1869-1878 (2005).

7. Rotwein, P. Variation in Akt protein kinases in human populations. *American journal of physiology. Regulatory, integrative and comparative physiology* **313**, R687-R692 (2017).

8. Gerber, C., Meyer, D.C., Schneeberger, A.G., Hoppeler, H. & von Rechenberg, B. Effect of tendon release and delayed repair on the structure of the muscles of the rotator cuff: an experimental study in sheep. *The Journal of bone and joint surgery. American volume* **86**, 1973-1982 (2004).

9. Akgumus, G., Chang, F. & Li, M.M. Overgrowth Syndromes Caused by Somatic Variants in the Phosphatidylinositol 3-Kinase/AKT/Mammalian Target of Rapamycin Pathway. *The Journal of molecular diagnostics : JMD* **19**, 487-497 (2017).

10. Ngeow, J., Sesock, K. & Eng, C. Clinical Implications for Germline PTEN Spectrum Disorders. *Endocrinology and metabolism clinics of North America* **46**, 503-517 (2017).

11. Laplante, M. & Sabatini, D.M. mTOR signaling in growth control and disease. *Cell* **149**, 274-293 (2012).

12. Laplante, M. & Sabatini, D.M. Regulation of mTORC1 and its impact on gene expression at a glance. *J Cell Sci* **126**, 1713-1719 (2013).

13. Liu, Z., Jahn, L.A., Wei, L., Long, W. & Barrett, E.J. Amino acids stimulate translation initiation and protein synthesis through an Akt-independent pathway in human skeletal muscle. *The Journal of clinical endocrinology and metabolism* **87**, 5553-5558 (2002).

14. Mora, A., Komander, D., van Aalten, D.M. & Alessi, D.R. PDK1, the master regulator of AGC kinase signal transduction. *Seminars in cell & developmental biology* **15**, 161-170 (2004).

15. Engelman, J.A., Luo, J. & Cantley, L.C. The evolution of phosphatidylinositol 3-kinases as regulators of growth and metabolism. *Nat Rev Genet* **7**, 606-619 (2006).

16. Paraskevopoulou, M.D. & Tsichlis, P.N. A perspective on AKT 25-plus years after its discovery. *Science signaling* **10**(2017).

17. Wang, Y., Zhu, L., Kuokkanen, S. & Pollard, J.W. Activation of protein synthesis in mouse uterine epithelial cells by estradiol-17beta is mediated by a PKC-ERK1/2-mTOR signaling pathway. *Proceedings of the National Academy of Sciences of the United States of America* **112**, E1382-1391 (2015).

18. Wolfe, R.R. Branched-chain amino acids and muscle protein synthesis in humans: myth or reality? *Journal of the International Society of Sports Nutrition* **14**, 30 (2017).

19. Kasukonis, B., *et al.* Codelivery of Infusion Decellularized Skeletal Muscle with Minced Muscle Autografts Improved Recovery from Volumetric Muscle Loss Injury in a Rat Model. *Tissue engineering. Part A* **22**, 1151-1163 (2016).

20. Chen, W.S., *et al.* Leptin deficiency and beta-cell dysfunction underlie type 2 diabetes in compound Akt knockout mice. *Molecular and cellular biology* **29**, 3151-3162 (2009).

21. Crouthamel, M.C., *et al.* Mechanism and management of AKT inhibitor-induced hyperglycemia. *Clinical cancer research : an official journal of the American Association for Cancer Research* **15**, 217-225 (2009).

22. Dummler, B., *et al.* Life with a single isoform of Akt: mice lacking Akt2 and Akt3 are viable but display impaired glucose homeostasis and growth deficiencies. *Molecular and cellular biology* **26**, 8042-8051 (2006).

23. DeQuach, J.A., *et al.* Injectable skeletal muscle matrix hydrogel promotes neovascularization and muscle cell infiltration in a hindlimb ischemia model. *European cells & materials* **23**, 400-412; discussion 412 (2012).

24. Rachdi, L., *et al.* Disruption of Tsc2 in pancreatic beta cells induces beta cell mass expansion and improved glucose tolerance in a TORC1-dependent manner. *Proceedings of the National Academy of Sciences of the United States of America* **105**, 9250-9255 (2008).

25. Crozier, S.J., Kimball, S.R., Emmert, S.W., Anthony, J.C. & Jefferson, L.S. Oral leucine administration stimulates protein synthesis in rat skeletal muscle. *J Nutr* **135**, 376-382 (2005).

26. Wang, L., *et al.* Conditional inactivation of Akt three isoforms causes tau hyperphosphorylation in the brain. *Molecular neurodegeneration* **10**, 33 (2015).

27. Dummler, B. & Hemmings, B.A. Physiological roles of PKB/Akt isoforms in development and disease. *Biochemical Society transactions* **35**, 231-235 (2007).

28. Hurd, S.A., Bhatti, N.M., Walker, A.M., Kasukonis, B.M. & Wolchok, J.C. Development of a biological scaffold engineered using the extracellular matrix secreted by skeletal muscle cells. *Biomaterials* **49**, 9-17 (2015).

29. Ungerleider, J.L., Johnson, T.D., Rao, N. & Christman, K.L. Fabrication and characterization of injectable hydrogels derived from decellularized skeletal and cardiac muscle. *Methods* **84**, 53-59 (2015).

30. Oh, J.H., Chung, S.W., Kim, S.H., Chung, J.Y. & Kim, J.Y. 2013 Neer Award: Effect of the adipose-derived stem cell for the improvement of fatty degeneration and rotator cuff healing in rabbit model. *Journal of shoulder and elbow surgery* **23**, 445-455 (2014).

31. Matsumoto, F., Uhthoff, H.K., Trudel, G. & Loehr, J.F. Delayed tendon reattachment does not reverse atrophy and fat accumulation of the supraspinatus--an experimental study in rabbits. *Journal of orthopaedic research : official publication of the Orthopaedic Research Society* **20**, 357-363 (2002).

32. Dobin, A., *et al.* STAR: ultrafast universal RNA-seq aligner. *Bioinformatics* **29**, 15-21 (2013).

33. Robinson, M.D., McCarthy, D.J. & Smyth, G.K. edgeR: a Bioconductor package for differential expression analysis of digital gene expression data. *Bioinformatics* **26**, 139-140 (2010).

34. Kramer, A., Green, J., Pollard, J., Jr. & Tugendreich, S. Causal analysis approaches in Ingenuity Pathway Analysis. *Bioinformatics* **30**, 523-530 (2014).

35. Drake, J.C., *et al.* Long-lived Snell dwarf mice display increased proteostatic mechanisms that are not dependent on decreased mTORC1 activity. *Aging cell* **14**, 474-482 (2015).

36. Busch, R., *et al.* Measurement of protein turnover rates by heavy water labeling of nonessential amino acids. *Biochimica et biophysica acta* **1760**, 730-744 (2006).

37. Kong, B.W., *et al.* Correction: Proteomics of Breast Muscle Tissue Associated with the Phenotypic Expression of Feed Efficiency within a Pedigree Male Broiler Line: I. Highlight on Mitochondria. *PloS one* **11**, e0159897 (2016).

38. Kong, B.W., *et al.* Proteomics of Breast Muscle Tissue Associated with the Phenotypic Expression of Feed Efficiency within a Pedigree Male Broiler Line: I. Highlight on Mitochondria. *PloS one* **11**, e0155679 (2016).

39. Newsom, S.A., *et al.* Long-term rates of mitochondrial protein synthesis are increased in mouse skeletal muscle with high-fat feeding regardless of insulin-sensitizing treatment. *American journal of physiology. Endocrinology and metabolism* **313**, E552-E562 (2017).

40. Shigeyama, Y., *et al.* Biphasic response of pancreatic beta-cell mass to ablation of tuberous sclerosis complex 2 in mice. *Molecular and cellular biology* **28**, 2971-2979 (2008).

41. Killian, M.L., *et al.* Chronic Degeneration Leads to Poor Healing of Repaired Massive Rotator Cuff Tears in Rats. *The American journal of sports medicine* **43**, 2401-2410 (2015).

42. Gerber, C., *et al.* Rotator cuff muscles lose responsiveness to anabolic steroids after tendon tear and musculotendinous retraction: an experimental study in sheep. *The American journal of sports medicine* **40**, 2454-2461 (2012).

43. Sandri, M. Signaling in muscle atrophy and hypertrophy. *Physiology* **23**, 160-170 (2008).

44. Lee, Y.S., Kim, J.Y., Kim, H.N., Lee, D.W. & Chung, S.W. Gene Expression Patterns Analysis in the Supraspinatus Muscle after a Rotator Cuff Tear in a Mouse Model. *BioMed research international* **2018**, 5859013 (2018).

45. Hotamisligil, G.S. & Bernlohr, D.A. Metabolic functions of FABPs--mechanisms and therapeutic implications. *Nature reviews. Endocrinology* **11**, 592-605 (2015).

46. Fischer, H., *et al.* Fatty acid binding protein 4 in human skeletal muscle. *Biochemical and biophysical research communications* **346**, 125-130 (2006).

47. Hoashi, S., *et al.* Association between fatty acid compositions and genotypes of FABP4 and LXR-alpha in Japanese black cattle. *BMC genetics* **9**, 84 (2008).

48. Chao, T., Burmeister, D.M., Corona, B.T. & Greising, S.M. Oxidative pathophysiology following volumetric muscle loss injury in a porcine model. *Journal of applied physiology* **126**, 1541-1549 (2019).

49. Southern, W.M., *et al.* PGC-1alpha overexpression partially rescues impaired oxidative and contractile pathophysiology following volumetric muscle loss injury. *Scientific reports* **9**, 4079 (2019).

50. Corona, B.T., Wenke, J.C. & Ward, C.L. Pathophysiology of Volumetric Muscle Loss Injury. *Cells, tissues, organs* **202**, 180-188 (2016).

51. Corona, B.T., *et al.* Impact of volumetric muscle loss injury on persistent motoneuron axotomy. *Muscle & nerve* **57**, 799-807 (2018).

52. Lowe, D.A., Warren, G.L., Ingalls, C.P., Boorstein, D.B. & Armstrong, R.B. Muscle function and protein metabolism after initiation of eccentric contraction-induced injury. *Journal of applied physiology* **79**, 1260-1270 (1995).

53. Albadawi, H., *et al.* Effect of DNase I treatment and neutrophil depletion on acute limb ischemia-reperfusion injury in mice. *Journal of vascular surgery* **64**, 484-493 (2016).

54. Aguilar, C.A., *et al.* Multiscale analysis of a regenerative therapy for treatment of volumetric muscle loss injury. *Cell death discovery* **4**, 33 (2018).

55. Lepper, C., Partridge, T.A. & Fan, C.M. An absolute requirement for Pax7-positive satellite cells in acute injury-induced skeletal muscle regeneration. *Development* **138**, 3639-3646 (2011).

56. Stratos, I., Graff, J., Rotter, R., Mittlmeier, T. & Vollmar, B. Open blunt crush injury of different severity determines nature and extent of local tissue regeneration and repair. *Journal of orthopaedic research : official publication of the Orthopaedic Research Society* **28**, 950-957 (2010).

CHAPTER 3: Delivery of a tissue derived extracellular matrix gel modulates early fibro-adipogenic cell behavior and improves recovery following both acute and chronic atrophy muscle injury.

Tai Huynh[1], Chris Slavin[1], Shahryar Ahmadi[2], and Jeff Wolchok[1,2]

[1]Department of Biomedical Engineering, University of Arkansas, Fayetteville, AR, USA

[2]Department of Orthopedics, University of Arkansas for Medical Sciences, Little Rock, AR, USA

3.1 Abstract

In this study we examined the potential of muscle derived extracellular matrix (ECM) gel prepared from skeletal muscle as a treatment strategy for acute and chronic degenerative atrophy. We conducted experiments to evaluate the gel's effectiveness in both a mouse hindlimb unloading (HU) model (disuse atrophy), and on a rabbit shoulder rotator cuff tear (RCT) model (diseased atrophy). In the HU mouse model, the gel enhanced *denovo* muscle regeneration (4000% higher in centralized nuclei myofiber density) and muscle mass (22% heavier) in the tibialis anterior muscle compared to PBS group. The transcriptomic and proteomic analysis using mouse tissues revealed that the gel elicited adult myogenesis programme. In the RCT rabbit model, the gel enhanced muscle mass (19% heavier), average myofiber cross-sectional area (29% larger), and lowered fatty infiltration (72% less fat) in the supraspinatus muscle compared to repair only. The transcriptomic and proteomic analysis using rabbit tissues revealed that the gel enhanced recovery through promoting a pro-myogenic muscle environment while lessening adipogenesis. The findings suggested that gel injection had a positive effect on the treatment of muscle atrophy and the therapeutic effect of the ECM gel was in part via its impact on fibro-

adipogenic progenitor cell behavior, a mechanistic finding that could be exploited for even greater impact.

3.2 Introduction

Long periods of muscle inactivity due to muscle injury or extended hospital bed rest are associated with a rapid loss of muscle mass (i.e., disuse atrophy) and function due to unloading and decreased neural activation of the muscle. Disuse atrophy can be challenging to overcome, and often persists even after physical rehabilitation treatments [1,2]. The resulting deficits in muscle mass and functional capacity can noticeably limit day to day life. Therefore, developing strategies to attenuate muscle atrophy and preserve muscle function with disuse is necessary to accelerate and optimize recovery following long periods reduced activity. Although, disuse-linked muscle atrophy using human and rodent models has been extensively studied to understand the mechanism of atrophy and the recovery afterward, there is still a lack of treatments that effectively aid the recovery process [3]. Regenerative therapy that can enhance the recovery of disused atrophied muscle will greatly increase the quality of life for those that are afflicted, while also shedding light on the muscle atrophy microenvironment, which could be of great interested to research in atrophy related diseases/injuries. The tail suspension murine model, which results in unloading of the hind limb muscles, has been used extensively to study this type of disuse-linked atrophy [4]. Disuse muscle atrophy in murine model results in a rapid loss of muscle mass as well as in fiber CSA with only 2 days of hind limb unloading (HU) [5]. In the adult murine model, while the hind limb muscles eventually regain their mass and strength given enough recovery period, therapies that can aid or enhance this recovery process can greatly add to the tool kit to treat other complicated disuse muscle atrophy [6].

Rotator cuff injuries, which are most commonly caused by tears in the associated tendons and result in over 4.5 million visits to physicians in the United States each year, often cause an even more problematic type of atrophy to occur [7]. After tendon injury, the rotator cuff muscles undergo a characteristically high amount of degeneration due to fatty infiltration alongside the usual atrophy of muscle fibers. Fatty infiltration has been shown to hamper proper healing after rotator cuff repair, and it's rare to see a reverse in fatty levels once the degeneration has already taken place [8]. Despite advances in techniques and assisting devices, rotator cuff surgery failure rates remain high. Currently, there are no effective means of dealing with the fatty degeneration that accompanies rotator cuff injuries, and it has stayed as a recognized problem without treatment for some time [8-12]. Our goal in this study is the development of an effective treatment for degenerative muscle atrophy that can also prevent and reverse the onset of fatty degeneration.

Based on results of some of our previous studies and the work of Dr. Christman's group at the University of California at San Diego, we decided to explore an injectable, water-based extracellular matrix (ECM) gel as a way of providing the necessary signaling ques to guide regeneration in two types of atrophy models. Similar gels used on infarcted cardiac muscle stimulated repair, possibly through the upregulation angiogenesis, myogenesis and immune cell infiltration, and we believe that they have the potential to do the same in skeletal muscle [13]. We examined the effect of ECM gel on two different models of atrophy, (1) a mouse hindlimb suspension model meant to simulate long periods of disuse due to bed rest or other similar causes of inactivity, and (2) a rabbit shoulder cuff tear model that looks at meant to simulate diseased muscle with the added complication of fatty infiltration.

3.3 Results

3.3.1 Mouse hindlimb suspension

Gel Injection promoted muscle regeneration.

At day 3 and day 7 following the hind-limb reloading and injection (DPI), H&E stains of TA from PBS group showed evidence of cells infiltration typically observed in HU injury while the same stain from gel group showed a much larger degree of cells infiltration that have been observed followed ECM injection in muscle (Fig 1a, 1b)[14,15]. At these 3DPI and 7DPI timepoints, the TA mass (g/kg BW) of PBS group and gel group were statistically indistinguishable from one another and uninjured control (1.76 + 0.21) (Fig. 1c). By day 14, the TA mass of PBS group (1.61+0.09) was significantly ($p=0.035$) lower than uninjured controls while the TA mass of gel group (2.05+0.09) was significantly ($p=0.011$) higher than uninjured and PBS groups. By day 28, the TA mass of PBS group (1.85+0.12) had recovered to similar level as uninjured controls while the TA mass of gel group (2.27+0.24) continued to significantly ($p<0.001$) increase to higher level than both uninjured and PBS groups. Quantitative assessment of tissue structure revealed varying levels of average myofiber cross sectional area (CSA) (μm2) between the gel injection and PBS controls groups across timepoints (Fig. 1d). At 3DPI, the CSA in PBS controls (1165+129) were statistically similar to uninjured controls (1226+193) while the CSA of gel group (950+52) was significantly ($p=0.046$) smaller than uninjured and PBS groups. By 7DPI, the CSA of gel group (1103+76) had increased to the same level as the other two controls groups, while no significant change in CSA were detected in PBS group (1127+134). By 14DPI, the CSA of gel group (1199+42) continued to rise, while the CSA of PBS controls (901+137) had significantly decreased to a lower level than uninjured controls ($p<0.001$) and gel groups ($p=0.011$). By day 28, although the CSA of gel group (1318+47) continued to increase, it did not reach statistically significant compared to the other two controls groups. Furthermore, the CSA of the PBS (1250+70) had recovered to the similar level compared to the uninjured controls

by the study endpoint. Histological assessment of the tissue near injection site of the two treatments also showed varying level (cells/field of view) of centralized nuclei myofiber (CNI) density with no detectable CNI in uninjured controls (Fig. 1e). At day 3, PBS (11.8+2.5) and gel (12.2+5.5) groups had similar level of CNI. At day 7, CNI density had decreased in PBS controls (7.8+2.2) but had increased in in gel group (70+16) making the CNI density gel group 9 times higher ($p<0.0001$) than PBS group. At day 14, the CNI density continued to decrease in PBS group (5+2.8) but increased in gel group (124+16), widening the gap between the two groups to 25 times ($p<0.0001$). At day 28, the CNI density further reduced in PBS group (1.7+0.6) leaving some samples with no CNI. Although the CNI density had also decreased in gel group (68+41) by this time, the difference between the two groups continued to widen to about 41 times ($p<0.0001$).

Gel injection produced transcriptomic signature of muscle repair and regeneration.

We next examined the 7DPI transcriptome using RNA-Seq to determine which molecular mechanisms may have led to the regeneration that occurred in response to gel delivery. Principal component analysis (PCA) revealed distinct transcriptome clustering within gel treated, PBS controls, and uninjured controls with clear separation between each group (Fig. 2a). Notably, the uninjured and PBS groups clustered in closer proximity to one another when compared to the gel treated, suggesting that the PBS group was approaching homeostasis while gel group was still in active repair/regeneration. When normalized to uninjured controls (cut off for differential expressed genes at FDR < 0.05 and $|\log2FC| > 1.5$), the two treatment groups shared 57 differentially expressed genes (DEGs), while the gel group had 729 unique DEGs, and PBS group had 36 unique DEGs (Fig. 2b). Examination of the GO: biological process annotation of

the shared DEGs reveals that these genes are highly clustered in the positive regulation of apoptotic process (e.g., Fas). This finding is consistent with the atrophy and reloading injury that are accompanied in an unloading and reloading model[16]. Analysis of unique DEGs from each treatment groups revealed that those in PBS group were clustered in cell differentiation (5 genes) and cell projection (4 genes), while those in gel group were clustered in a variety of processes including immune response process (75 genes), cell cycle (33 genes), and regulation of actin cytoskeleton organization (13 genes) (Fig. S1a and S1b).

Pathway analysis (normalized to uninjured controls) revealed that the most dominant pathways detected within the PBS group and gel group were osteoarthritis pathway and leukocytes extravasation signaling respectively (Fig. 2d and 2e). Direct comparison between transcriptomes of the gel group and PBS controls revealed that phagocytosis in macrophages and monocytes was the most dominant pathway (Fig. 2f). The top gel-induced regulators effects are involved in immune cells migration, recruitment, activations as well as cell migrations, viability, and survival. Beside the highly activated immune cell activity, and inflammation-related signaling pathways due to gel injection, the RAC signaling pathway, which has been implicated in cell growth and myoblast fusion, was notably activated[17]. In this context of myofusion, both essential myofiber fusion genes MYMK (Myomaker) and MYMX (Myomixer) were both upregulated due to gel injection (Fig. 2c)[18,19]. Many notable DEGs due to gel injection has been shown to be involved in SC activations (WNT4, CDCA3), myoblast differentiation (MYOG), cell-cell contact myogenesis (Notch2, CDH11), cell proliferation (GDF3, HGF) and cytokines enhanced myogenesis (IL-6, TNF, IGF1, IFNG, and MSTN) (Fig. 2c and Fig. S1a)[20]. Lastly, we found that fibro- adipogenic progenitors' (FAPs) markers (e.g., PDGFR) and pathways (e.g.,

PDGF signaling) were highly upregulated suggesting the coordination of myogenesis partly though this population of cell[21].

Gel injection produced the proteome that followed the stages of muscle repair and regeneration.

We then examined the proteome of the TA at 3 DPI and 14 DPI to identify the altered proteins that influenced the transcriptomic and phenotypic changes previously described in response to gel injection. At FDR < 0.05 and |log2FC| > 1.5 cutoff, we found 101 and 30 differentially expressed proteins (DEPs) between gel and PBS group at 3DPI and 14DPI respectively. At 3DPI, pathway analysis revealed the top pathways are actin cytoskeleton signaling, remodeling of epithelial adherence junction, and RHOA signaling (Fig. 3a). The top regulators effects are involved in leukocytes activations, endocytosis, and cytoskeletons formation. The top networks are similarly implicated in cell-to cell signaling and activation, tissue development, hematological system development & function. To produce a meaningful analysis of the proteomic changes at the 14 DPI, p <0.05 (instead of FDR) and |log2FC| > 1 (instead of 1.5) cutoff were used resulting in 177 DEPs. Pathway analysis at 14DPI showed a different top pathway, namely EIF2 signaling, regulation of eIF4 and p70SK6 signaling, calcium signaling (Fig. 3b). The top networks are involved with cell death and survival, cellular assembly and organization, and protein synthesis. Notably, at both 3 DPI and 14 DPI, we observed a gel-induced effect on mitochondrial oxidative metabolic proteins (SIRT5, SOD2, G6PD) (Fig. S1c) which play important roles in muscle hypertrophy and regrowth [22,23]. When compared with the DEGs (7DPI) of gel vs. PBS, there are 24 overlapped DEPs at 3DPI and 19 overlapped DEPs at 14 DPI. Examination of the GO: Biological Process annotation of the overlapped

proteins/transcripts revealed that these genes are clustered in immune system process (e.g., LGALS3), cell growth (e.g., RAB32), actin filament organization (e.g., CORO1A), energy metabolism (e.g., FABP5), cell projection (e.g., RAC2), and calcium signaling (e.g., ANAX4) (Fig. 3c). Most notable was the decrease in MAPK transcripts (e.g., MAPK14) and protein (e.g., MAPK12) abundances (Fig. S1a, S1c) which could affect in FAPs signaling in muscle regeneration[24]. The dynamic changes of these molecules and involved biological processes at different timepoints pointed toward a unique gel-elicited regeneration programme that was likely via FAPs signaling.

3.3.2 Rabbit shoulder cuff

Gel injection lowered the effects of atrophy and fatty infiltration.

At 16 weeks after shoulder cuff rotator repair, the most apparent differences were visible in the Oil RedO stains showing the fat content between groups (Fig. 4a). The tissue sections from the repair only group had a noticeably higher amount of fat than the ones that received a gel treatment, and the fat often formed large pockets inside the muscle the tissue. This phenomenon did not occur in the gel treatment group. The Masson's Trichrome stains were not as conclusive, with both treatment groups exhibiting higher collagen content than the uninjured control but with heavy variance within groups (Fig. 4b). Regarding the muscle fibers, the gel treated tissue had larger fibers and fewer gaps between fibers (Fig. 4c, 4d). The shoulder cuff muscle mass (g/kg BW) of the uninjured (2.77+0.09), repair (1.85+0.13) and repair+gel (2.19+0.15) groups were all statistically different from one another (Fig. 4e). Although the SSP mass of both treatment groups were significantly ($p<0.0001$) lower than that of the uninjured group, the repair+gel group had significantly ($p=0.015$) larger average mass than the repair only group. Similar relation between the three groups' average myofiber cross sectional area (μm2) was observed

(Fig. 4f). The repair only group (2406+324) had a significantly ($p=0.016$) lower average CSA than the repair+gel group (3112+138), which was closer to but still significantly ($p<0.001$) different from the uninjured group (3439+134). Fatty infiltration (% fat) was highest in the repair only group (25.0+4.8), whose average was close to twice ($p=0.004$) as high as the repair+gel group (14.5+4.1) (Fig. 4g). The uninjured muscles (0.6+0.2) had no noticeable fat buildup. The presence of collagen, which is used as a measure of non-contractile scar tissue (%NCT), followed similar trends to the other measurements (Fig. 4h). While muscles in the repair only group (3.77+2.8) trended to have more collagen accumulation overall than the ones in the repair+gel group (2.4+1.2), the results were not statistically significant ($p=0.18$) due to the large variance within groups.

Gel injection resulted in transcriptomic and proteomic changes which indicate differences in inflammatory response, angiogenesis and adipogenesis.

We examined the transcriptome and proteome to determine which molecular mechanisms may have led to the functional differences observed at 16 weeks after treatment. Principal component analysis showed that the 16-week repair and repair+gel samples clustered closely with the uninjured ones, and the 2-week treatment and no repair groups were more spread out but tended to cluster with each other (Fig. 5a). When the 2-week no repair, repair, and repair+gel groups were normalized to uninjured controls (cut off for differentially expressed genes was FDR < 0.05 and $|\log2FC| > 1.5$), the repair and repair+gel groups had a much higher number of DEGs than the no repair group (Fig. 5b). Out of those, we chose to focus on DEGs related to inflammation, angiogenesis and adipogenesis, as well as some common markers for myogenesis (Pax7, Myod1, Myog, Myf5) (Fig. 5c). Overall, there was no noticeable pattern in myogenesis

related genes. As for the selected DEGs, the no repair and repair only groups were more similar to each other than to the repair+gel group, which had tamped down activity in immune response (lower IL6, higher IL10), downregulated adipogenic genes (PPARγ, Dgat2), but upregulated angiogenic genes (VEGFA, ANG). Proteomic analysis revealed that uninjured and no repair samples clustered into distinct groups, while the differences between the repair only and gel groups were not as distinct (Fig. 6a). However, the repair only samples tended to have more similarity to the no treatment samples than the ones in the gel group. A cut off of $p < 0.05$ and $|\log2FC| > 1$ was used to determine differentially expressed proteins between repair and repair+gel groups identified 32 DEPs (Fig. 6b). Among those IDs, we found that there were significant differences in expression of Annexin A1 (ANXA1), Arachidonate 15-Lipoxygenase (ALOX15), and Alpha 2-macroglobulin 2 (A2M2), which have been shown to reduce inflammation (Fig. 6c).

Pathway analysis (normalized to uninjured) performed on the transcriptomic data showed that many of the same pathways were among the most active ones in each group (Fig. S2). The EIF2 signaling pathway, associated with proinflammatory cytokine expression, was highly activated in the repair and repair+gel groups, but was much more dominant in the no repair group. Along with this pathway, the repair only group showed upregulation in several other pathways associated with proinflammatory activity such as hepatic stellate cell activation, osteoarthritis, and leukocyte extravasation (Fig. S2a). Activity of these pathways was largely reduced in the repair+gel treatment group, and instead there was a higher presence of pathways related to a pro-regenerative wound healing and muscle hypertrophy (mTOR signaling, eIF4 and p70s6k signaling). The proteome pathway analysis revealed that the top two pathways for both the repair and repair+gel groups (when normalized to uninjured) were LXR/RXR activation and

acute phase response signaling (Fig. S2b). Acute phase response signaling is associated with pro-inflammatory activity during the early stages of wound healing, while LXR/RXR activation is tied to the regulation and tamping down of the inflammatory response [25,26]. Interestingly, the top pathway in the no repair group was LXR/RXR activation, but acute phase response signaling was not one of the top ten pathways. However, the level of activity of the LXR/RXR pathway, and the rest of the pathways in general, in the no repair group was much lower than the two treatment groups, perhaps indicating an insufficient immune response to counteract the effects of a shoulder cuff tear.

3.4 Discussion

In the mouse model, muscle environment from 3DPI H&E stains of PBS group demonstrated the typical reloading injury following hindlimb unloading with a some degree cell infiltration [14] (Fig. 1a). Multiple studies conducted in acute skeletal muscle injury in hindlimb unloading / reloading provided that a temporally regulated immune response produced the pro-inflammatory phase lasts up to 3-4 days post-injury, followed by the pro-regenerative phase that promotes tissue remodeling and repair [16,27] . This seemed to be the case in PBS controls with reduced infiltrating cells by 7 DPI compared to 3DPI and no visible infiltrating cells by 14 DPI and 28 DPI. Though, the wet muscle mass were not significantly reduced until 14 DPI compared injured group (Fig. 1c), it can be attributed to the interstitial fluid accumulation negating any myofiber mass loss during the first week of reloading period [28]. A similar response was also observed in CSA in PBS controls, as myofiber CSA of atrophied muscle was only significantly reduced at 14 DPI (Fig. 1d). By 28 DPI, both skeletal muscle mass and CSA returned to the preinjury state [29] (Fig. 1c, 1d). Gel injection, on the other hand, dramatically altered the course of recovery. Muscle environment from 3DPI H&E stains of gel treatment showed much higher

degree of cell filtration (Fig. 1b) consistent with other findings of injectable matrix gel promoting cellular infiltration to the injection site [15,30]. Histologically analysis across timepoints revealed that there were significant higher numbers of CNI myofibers throughout the recovery process in gel group (compared to PBS controls) suggesting de novo myofibers formation (Fig. 1e). Others have also confirmed that ECM gel injection enhanced muscle progenitors' infiltration and proliferation [15,30]. These new myofibers could have contributed to a smaller overall average fiber size in gel group at early timepoints. The gel also seemed to provide continuing regeneration by 28 DPI (study end point) evidenced by significantly higher muscle mass, trended higher CSA and sustained high numbers of CNI myofibers (Fig. 1c, 1d, 1e). Similar enhancement of muscle recovery by 28 DPI was also observed in an ischemic muscle injury/repair study [31]. This boost in muscle structural outcomes could be attributed the known myogenic property of ECM degradation fragments [32].

To further understand the molecular mechanism of this gel-induced regeneration, we investigated the dynamic changes in the muscle transcriptome at 7 DPI. At this time point, there were significantly less DEGs in PBS group than in gel group when normalized to uninjured controls demonstrating a unique programme produced by gel injection (Fig. 2b). Pathway analyses revealed that while some mild degree of inflammation was still ongoing in PBS group, the activation of fibroblast and cell death signaling indicated a transition into repair phase of muscle injury [33] (Fig. 2d). On the other hand, in gel group, the main responses indicated an early stage of inflammation with enhanced immune response, and cell recruitment/proliferation (Fig. 2e). Direct comparison between PBS and gel group also showed that gel injection enhanced cell survival, and cell motility – indicators of enhanced muscle regeneration (Fig. 2f). Genes associated with extracellular matrix were unaffected or downregulated in PBS group but were

upregulated in gel group (Fig. 2c). This correlates with other studies of transcriptomic profile during skeletal muscle regeneration with increased level of ECM, cell migration, and myogenic development transcripts [34]. Furthermore, we found that gene related to later stage of myogenesis (MYOG) were upregulated but not early stage ones (Pax7, MYOD, MYF5) corresponding with histological evidence of immature myofibers with defined basement membrane by 7 DPI[35] (Fig. 1b). Specifically, these myofibers were likely setting up for fusion and becoming mature fiber evidenced by the upregulated myofusion genes (Mymx, MYMK) (Fig. 2c). This finding was further corroborated by the upregulation of fibro-adipogenic progenitors (FAPs) markers (PDGFRα, Ly6a/SCA-1) as FAPs have been shown to play important roles in myoblast fusion through specific cocktail of cytokines (Fig. S1a). Many of those cytokine transcripts were significantly altered in gel group suggesting a stimulated regenerative environment coordinated, at least partially, by FAPs. Specifically, the upregulation of IL-1, IL-10, and IL-15 in gel groups are particularly associated with pro-myogenic activity of FAPs [34,36,37], while the combination of DEGs for cytokines such as IL-6, TNF, IGF1,IFNG, and MSTN has been shown to be essential in the later differentiation stages of myogenesis [38] (Fig. 2c, S1a).

The proteomic analysis of TA muscle at 3 DPI and 14 DPI between gel and PBS groups also highlighted the unique regeneration programme elicited by gel injection. At 3DPI, several pathways pointed to enhancement of muscle ECM remodeling and repair, cell motility, signal transduction and intracellular signaling in gel group (Fig. 3c). At 14 DPI, the pathways were evolving into enhancement energy metabolism, pro-regenerative immune environment, and mitochondrial metabolic activities. The time course changes in the pathway profiles in gel group closely followed the stages of muscle growth [39]. We then performed a global comparison of the omics data from TA muscles to provide insight into the program of transcription and translation

events governing the gel mediated muscle regeneration. Though a large number of significant transcriptomic changes (673 genes) when compared gel to pbs groups were not accompanied by a significant change in the proteome, several overlapping molecules (discussed in the next paragraph) were identified further providing evidence of regeneration in gel group (Fig. 3c). The level of LGALS3 which aids in the fusion and differentiation of myoblasts during muscle repair and regeneration increased in 7DPI transcript, 3 DPI and 14DPI protein abundance [40,41]. Similar increases were observed for RAC2 which is essential in myotube formation and hypertrophy [42,43]. Comparably, FABP5, regulating the insulin-mediated glucose uptake through activation of AKT and AMPK and promoting cell proliferation, also increased [44,45]. It is notable that these molecules have been shown to be upregulated or increased immediately following strenuous exercise [46-48]. Another notable finding is the reduction of Sirt5 (only in protein abundance but not transcripts) (Fig. S1c), presiding exclusively in mitochondria, which can further activate AMPK [49,50]. Although AMPK plays important roles in muscle hemostasis, the immediate effect of an increase in AMPK activation is still unresolved in the context of skeletal muscle regeneration and growth [51]. For example, studies have reported an increase or decrease in AMPK activation in HU-induced atrophy as well as exercised-induced hypertrophy [52-55]. In this context of muscle energy metabolism, pathway analysis also identified an activated Sirtuin pathways in gel group which identified the increased level of SOD2 and G6PD. Both of these molecules, primarily present in the mitochondria, are known muscle antioxidants and help the skeletal muscle combat ROS [56]. While most of the overlapped molecules were significantly enhanced at 3DPI, Periostin (POSTN)- a secreted extracellular matrix protein significantly increased at 14 DPI. Studies have found that POSTN played an important role in extracellular matrix remodeling during myofiber differentiation and maturation especially at later timepoints during hypertrophy and regeneration

[57,58]. Most notable among the uniquely overlapped molecules at 14 DPI is CYIFIP2 which stimulates apoptosis [59]. The decrease of this molecule indicated a gel-induced protection from cell apoptosis at this stage of regeneration. This anti-apoptosis process maybe the result of an MAPK signaling cascades since we also found that MAPK12 protein as well as many MAPKs transcripts were decreased throughout 14 DPI [60] (Fig. S1a, S1c). However, myoblast differentiation is often accompanied by an increase level of MAPKs, suggesting another cell population were proliferating while suppressing differentiation [61,62]. Furthermore, we found that TGFB transcripts were upregulated and that this class of cytokine that can induce FAPs proliferation through the MAPK signaling pathway [24,63]. The omics data taken together suggested that ECM gel injection seemed to induce adult myogenesis through a coordinated programme involving (at least by 14 DPI) FAPs [64].

In the rabbit model, at 12 weeks, there was a significant distinction in muscle structural outcome between the two treatment groups that were partly explained by the omics differences noticed at 2 weeks (Fig. 4a-4d). There was notable improvement in both mass and average myofiber cross-sectional area of the supraspinatus muscles in the gel injection group (Fig. 4e, 4f). Histological analysis also revealed that most of the difference in muscle mass was likely due to the increase in size of existing fibers. Along with that, muscles in the gel injection group experienced a much lower amount of fatty infiltration (Fig. 4g). These differences in gross histology were further explored with transcriptomic and proteomic analysis which revealed significant differences in factors regulating inflammation, angiogenesis, myogenesis and adipogenesis between gel injection and repair only groups 2 weeks post tendon repair.

The level of IL-6, a pro-inflammatory cytokine and indicator of M1 macrophage activity, was highly upregulated in the repair only group [37] (Fig. 5c). In contrast, the group that received

gel injections saw no significant changes in IL-6 transcript expression when compared to normal tissue and a greater concentration of ALOX15 and A2M2, which have anti-inflammatory properties (Fig. 6c). IL-10, which is linked with the repair phase of the wound healing process by promoting a M2 macrophage phenotype, was heavily upregulated in both repair only and gel groups [65-70] (Fig. 5c). However, the ratio between IL-6 and IL-10 seems to indicate that the repair only group is an inflammatory environment, and the gel group is in its repair phase. Interestingly, the presence of ANXA1, which is considered to have anti-inflammatory effects, was significantly lower in gel treatment group compared to the repair only group. One of the main ways it functions to bring about the end of inflammation is by inhibiting leukocyte infiltration[71]. In this immune cells context, while both treatment groups exhibited elevated expression of CCL2, a promoter of M2 macrophage polarization in certain context, it was present at significantly greater levels in the gel injection group [72]. Furthermore, CCL2 are involved in angiogenesis and the gel injection increased expression of several key angiogenic genes (Fgf1, Fgf2, VEGF, ANG)[73,74]. These findings suggested that a wound healing programme was elicited by the matrix gel injection. We also examined several key myogenic regulatory factors (MRFs) to determine the gel's effect on the dysregulated myogenic process accompanying the RCT injury. The most significant difference was in the expression of Myf5, a factor that is expressed early on during myogenesis and promotes the expression of all other MRFs as well as the activation and proliferation of satellite cells, and muscle hypertrophy [75,76]. The transcript level of factor was increased in the gel group while it was decreased in the repair only group. Interestingly, it was the opposite for MYOG, another key MRFs that signals terminal differentiation of myoblasts into new muscle fibers[35]. These findings suggested that the gel elicited a prolonged the proliferative stage of muscle wound healing.

When examining genes related to fatty infiltration, one of the key issue that results in poor outcomes for many shoulder cuff repairs, we noticed trends in gene expression that hint at the gel injections having an effect on fibro-adipogenic progenitors (FAPs), a cell type that has been gaining increased attention as a possible master regulator of the wound healing process in skeletal muscle [64]. Normally present in small numbers in the interstitial space between myofibers, where their main function is maintenance of muscle homeostasis, these cells quickly proliferate following injury and release cytokines that promote immune cell recruitment and myogenesis [77]. Throughout the repair process, the newly created FAPs have to ability to differentiate into either fibroblasts or adipocytes or go through apoptosis when they are no longer needed. As such, dysregulation of FAP activity can result in inefficient repair, atrophy, and a buildup of fat and fibrosis in muscle tissue [78,79]. Transcriptomic data showed that PDGFRα, a key marker of FAPs, was highly upregulated in the repair only group, but even more so in the gel injection group [78] (Fig. 5c). This higher upregulation of FAPs markers could possibly be partially responsible for the larger muscle fiber sizes observed in the rabbits that received a gel injection due to their capability to promote hypertrophy [64]. More importantly, we also found that the gel injection had a very large impact on the expression of IL-15 and GDF10, both of which act to prevent FAPs from differentiating into adipocytes [80-83]. The transcripts for these genes were present at much higher concentrations in the gel injection group, although they were still upregulated in the repair only group. Meanwhile, expression of Ppar-gamma, a key promoter of adipogenesis, was upregulated in the repair only animals when compared to the control, while it was downregulated in the gel group [84]. Dgat2, another pro-adipogenic gene which was significantly upregulated in animals that didn't receive any treatment for their torn tendon, was downregulated in the gel group while staying at baseline levels in the repair only group [85].

Overall, these findings lead us to believe that ECM gel injection promoted a pro regenerative environment and lowered fatty formation by blocking the differentiation of FAPs into adipocytes in our rabbit shoulder cuff tear model.

3.5 Conclusion

To sum, we observed an overall benefit of ECM gel delivery to reduce muscle atrophy and increase muscle mass in both an acute (hindlimb unloading) and chronic (rotator cuff injury) muscle injury model. In the acute model, muscle mass recovery was largely the result of new myofiber growth, while in the chronic setting mass recovery appeared to be driven more by hypertrophy of existing myofibers. For both models, the proteomic and transcriptomic data suggest that stimulation of fibro-adipogenic progenitor cells in response to ECM gel delivery may have played a role, a mechanistic finding that that could be exploited for even greater therapeutic impact.

3.6 Methods

ECM Gel Preparation

Matrix gel was prepared according to previously published protocols [86,87]. Briefly, human quadriceps muscle (Science Care) was thawed, trimmed to remove fat and connective tissue, and decellularized in the following steps: enzyme digestion solution (0.2% trypsin/0.1% EDTA) at RT for 3 hrs., in 0.5% Triton X-100 at 4°C overnight, and then in 1% Triton X-100/0.2% sodium deoxycholate at RT for 6–8 hrs. We then rinsed the product with deionized water and incubated in DNase/RNase solution overnight at 4°C with agitation. The remaining decellularized ECM (dECM) was rinsed, lyophilized, flash-frozen using liquid nitrogen, and ground into fine powder. We digested the dECM powder using a pepsin solution (1 mg/ml pepsin in 0.1 M HCl) at a ratio of 10mg dECM/1ml pepsin at a pH of 2.4 for 48h at room temperature. The solubilized dECM

solution was neutralized (pH=7.4), lyophilized, stored at -80°C. On the day of injection, the lyophilized dECM was solubilized to a concentration of 6 mg/ml in PBS, loaded into syringes, and stored at 4°C. All injectable dECM used in this proposal was made as indicated in the process above.

Rotator Cuff Tear Using Rabbit Model

Adult (24-weeks old) male New Zealand white rabbits (pre-surgery mass ~3.5 kg) purchased commercially (Charles River) (n=24) were used to examine the effect of ECM gel injection on recovery from torn rotator cuff repair. All animal procedures were approved by the Institutional Animal Care and Use Committee of the University of Arkansas for Medical Sciences. All experiments were performed in accordance with all guidelines and ARRIVE guidelines. The rotator cuff tear and delayed tendon repair surgeries were performed following published methods [88,89]. A trained orthopedic surgeon performed the surgeries. We used isoflurane for anesthesia with induction dosage of 5% and maintenance dosage of 3% in oxygen. The left shoulder was shaved and disinfected. A longitudinal incision was made over the shoulder, and dissection performed down to the deltoid. The deltoid was retracted to reveal the supraspinatus (SSP) tendon. The supraspinatus tendon was transected at its insertion onto the greater tuberosity. The cut end of the tendon was tagged with a non-resorbable No. 4-0 suture (Prolene, Ethicon, Somerville, NJ) for later identification. All attachments of the tendon to the surrounding tissues, including the infraspinatus, were released, allowing the tendon to retract freely away from its insertion site. The incisions were closed with interrupted, subcutaneous No. 3-0 Vicryl sutures (Ethicon), and the skin was closed with a running 4-0 monocryl suture

(Ethicon). The contralateral shoulder remained untreated to serve as a comparative control. All animals were housed for a 12-week recovery period to simulate chronic RCT.

After this period of recovery, six animals were selected for SSP muscles harvest to evaluate the conditions of torn muscles and the contralateral uninjured control while the rest of the animals underwent SSP tendon reattachment repair surgery. The free tendon edge was identified by use of the tag suture and double stitched to the humerus using a fiber wire suture. We randomly assigned half of the animals to receive 1 mL of muscle derived ECM gel injection into the SSP muscle at five locations along its length. Following repair, the surgeon closed surgical site with a suture as previously described. The animals will then be divided into 2 groups (n=12/group) where half (n=6) of each group are dECM-injected animals. Group 1 were allowed one-week (short-term) recovery, while group 2 were allowed 12-weeks (long-term) recovery. At the end of each recovery period, a veterinarian euthanized all animals via intracardiac injection of a commercial euthanasia solution. SSP muscles were harvested, weighed, imaged, and prepared for further evaluation.

Hind Limb Unloading and Reloading Mouse Model

All animal procedures were approved by the Institutional Animal Care and Use Committee of the University of Arkansas. All experiments were performed in accordance with all guidelines and ARRIVE guidelines. Adult (8 weeks) male C57BL/6J mice (n=25) were subjected to 5 days of hind limb unloading (HU) as previously described [90]. Briefly, an unanesthetized animal's tail was cleaned with rubbing alcohol and air dried, covered with a light coat of benzoin tincture and dried with a hair dryer until tacky. Strips of elastoplast (Biersdorf, Norwalk, CT) adhesive bandage were applied to the proximal 2/3rd of all sides of the tail and

looped through a swivel attachment. This provided a secure loop for line attachment connected to the top of the cage. Mice were attached to a HU apparatus designed to allow access to all areas of the cage with only their forelimbs able to contact the cage floor. At the time of reloading (day 0), animals were anesthetized; the body mass of each animal was weighed; the anterior crural compartment muscles were subjected to contractile force measurement (see section 2.4). Each animal received 50 µl of matrix gel (6 mg/ml) on the left TA, and 50 µl of vehicle control (PBS) on the right TA. At this time, a cohort of uninjured control animals (n=5) that were age-matched with the HU animals received 50 µl of PBS on the left TA. HU animals were then randomly assigned to five different recovery time points (3, 7, 14, 28 days, n =5/time point); uninjured animals were allowed 14 days recovery. At the end of each time point, animals were anesthetized; the body mass was weighed; the anterior crural compartment muscles were subjected to contractile force measurement. The TA muscles were dissected, weighed, and flash-frozen for further analysis. The animals were euthanized by CO_2 asphyxiation.

Histological Analysis

Muscle tissues was flash frozen in isopentane (2-methylbutane) chilled in liquid nitrogen. Tissue was sectioned (10µm for rabbit and 8µm for mouse) with the aid of a cryostat (Leica BioSystems) and mounted onto microscopic slides. Slides were immuno-stained using primary antibodies (1:300, Invitrogen) directed against Laminin (IgG). Additional tissue sections were stained using hematoxylin and eosin (H&E), Oil red-O (rabbit only), and Masson's trichrome following manufacturer's guidelines. The immuno-stained sections were digitally imaged (100X, Nikon CiL), while the dye-stained sections were scanned using a slide scanner (Nano Zoomer, Hamamatsu).

Representative tissue sections collected from four to five animals per group were used for all calculations. Three separate regions/section/animal of laminin-stained images (100X) were analyzed using in-house developed codes in ImageJ (NIH) to automatically isolate the borders of individual muscle fibers and compute muscle fiber cross-sectional area. Fiber cross sectional area (μm2) for all fibers within an individual image (typically 100+ fibers) were calculated. Centralized nuclei cells (CNI) were manually counted using H&E images (100x) to compute density of CNI per field of view. Oil red and Masson's Trichrome images were analyzed using an in-house color extract tool which determines the percentage each color occupies on the image. The percentages were then used to determine the fat (red) and collagen (blue) fraction present in the entire tissue cross section.

Transcriptome Analysis

Tissue biopsies (all timepoints (n=5/group) for rabbit and 7DPI for mouse) for RNA extraction and subsequent sequencing were sent out to a commercial lab (BGI Genomic Services) for RNA-Seq analysis using BGISeq-500 platform to a mean depth of 20,000,000 reads per library. RNA sequencing reads were mapped to either Mus musculus (mm39) or the Oryctolagus cuniculus genome (OryCun2.0) from NCBI using the 2-pass STAR protocol[91]. Reads were quantified using FeatureCounts[92], followed by analysis of differential expression and normalization in EdgeR[93]. Differential expression was selected using a maximum false discovery rate (FDR) of 0.05 and a minimum log fold change of 1.5. Pathway level analysis was also performed using Ingenuity Pathway Analysis (IPA) (Qiagen)[94].

Lysate Extraction and Proteomic Analysis

Tissue biopsies (2 weeks post injury for rabbit, 3DPI and 14DPI for mouse) were homogenized to extract protein lysate using RIPA Lysis Buffer System (sc-24948, Santa Cruz Biotechnology) as previously described [95]. Homogenates were centrifuged at 13,000g for 5 min at 4ºC, and the supernatant was collected. Protein concentration was determined using a bicinchoninic acid assay (BCA) (2322, Life Technologies). Protein lysates were sent out to a commercial lab (UMAS Proteomic Core) for proteomic analysis using Orbitrap Exploris Data-independent acquisition mass spectrometry.

Data Analysis

Statistical analyses for assessment of non-omics data were performed on JMP software, using Student's t-test or ANOVA with Tukey's test post-hoc. Assessment of significance for differential gene expression was performed using EdgeR with TMM normalization of read counts and adjustment of p-values (FDR) for multiple comparisons by the Benjamini-Hochberg procedure. Assessment of significance for differential protein expression was performed by the same proteomic commercial lab. Significance was accepted at $P \leq 0.05$ (*) $P \leq 0.01$ (**), $P \leq 0.001$ (***), and $P \leq 0.0001$ (****). Quantitative data are displayed as mean + standard deviation.

Data Availability

The datasets generated during and/or analyzed in this study are available from the corresponding author on reasonable request. The mouse and rabbit RNA-seq data generated in this study have been deposited in the National Center for Biotechnology Information (NCBI) Gene Expression Omnibus (GEO) database under the accession codes GSE220641 and GSE220641.

Acknowledgements

This project was supported by the National Institute of Arthritis and Musculoskeletal and Skin Diseases of the National Institutes of Health (Award Number 1R15 AR073492-01) as well as the Arkansas Bioscience Institute.

Author Contributions

T.H and J.W designed the study. T.H ran most of the experiments and led the overall data analyses. C.S helped with rabbit histological work and ran the rabbit omics data analyses. S.A performed the rabbit rotator cuff tendon tear surgery. All authors edited the manuscript.

3.7 Figure

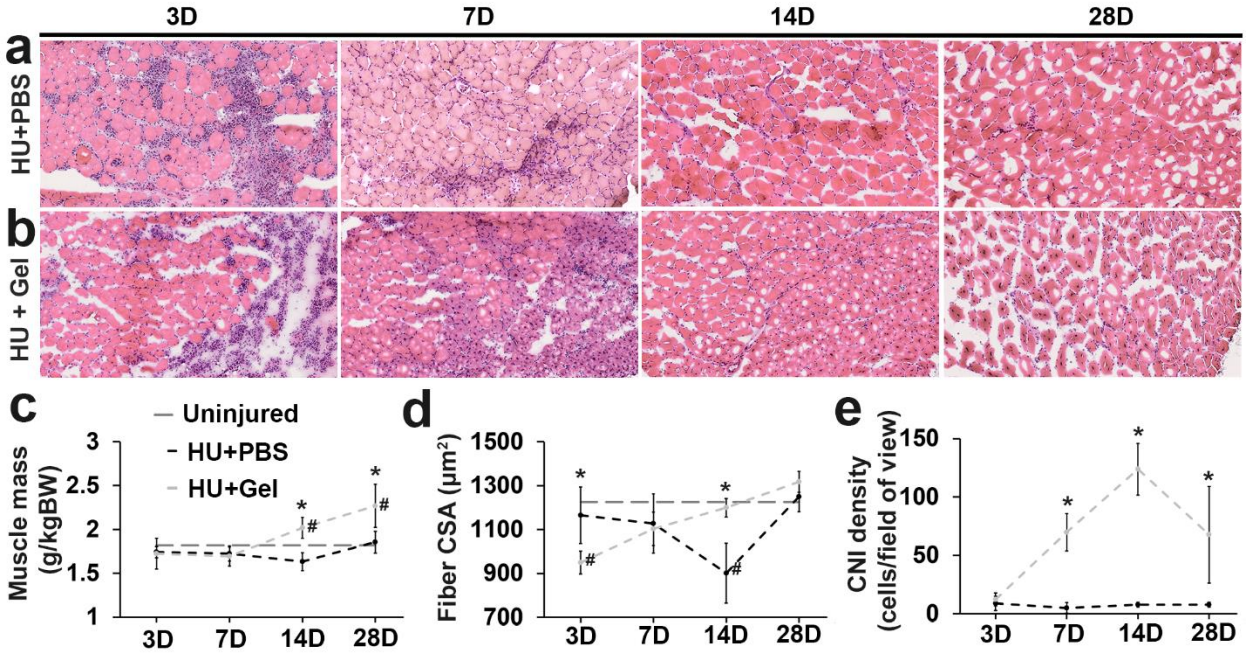

Figure 1. Mouse Muscle Environment and Functional Outcome. Representative H&E stained Tibialis anterior muscle (TA) cross-sections collected at 3,7,14, and 28 DPI from (a) PBS and (b) gel groups at 200X show injection areas and cell infiltrations. Scale bar = 250μm. (c) TA mass (g/kg mouse body weight) for gel treated and PBS controls groups were assessed at 3,7,14, and 28 DPI. Cross-sections were quantified for (d) average muscle fiber cross-sectional area (μm^2) and (e) centralized nuclei density (cells/mm^2) for gel treated and PBS control groups were assessed at 3,7,14, and 28 DPI. The values of uninjured controls are represented as straight line

in (c) and (d). The * indicates significant difference of p<0.05 between treatment groups, while the # indicates significant difference of p<0.05 from uninjured controls.

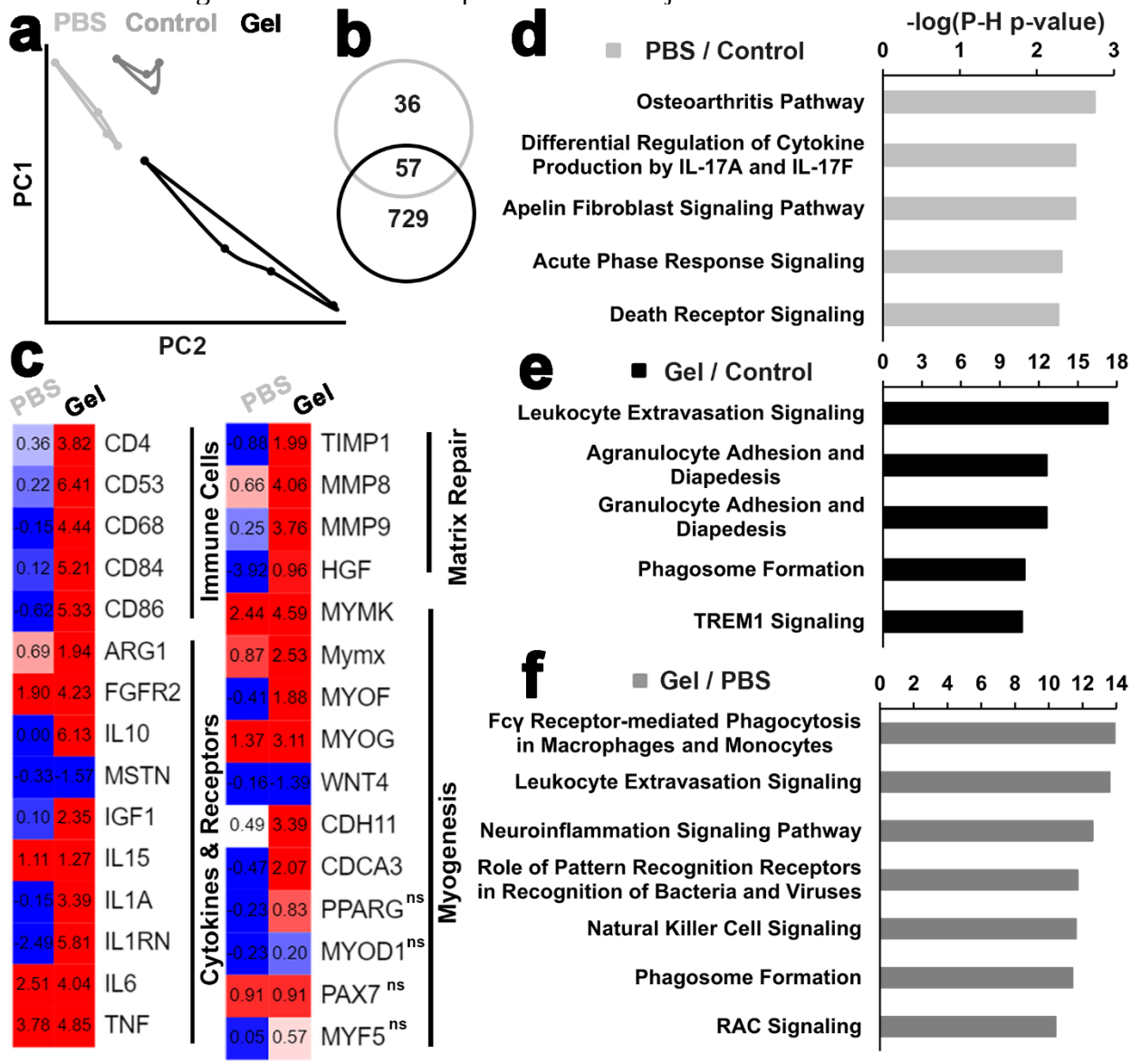

Figure 2. Mouse Transcriptomic Analysis. (a) Principal component analysis graph of TA skeletal muscle transcriptomes from uninjured, PBS, and gel groups normalized CPM using all transcripts. (b) Venn diagram illustrates differentially expressed genes counts for gel treatment and PBS controls groups with respect to uninjured controls. (c) Gene expression for gel treatment group and PBS controls selected genes with respect to uninjured controls are presented as log ratio (log_2FC). Top canonical pathways based on the Ingenuity Pathway Analysis (IPA) assessment of differentially expressed genes (FDR < 0.05 and $|log_2FC| > 1.5$) within (d) PBS controls and (e) gel treatment with respect to uninjured controls. (e) Top canonical pathways based on IPA assessment of differentially expressed genes of gel treatment with respect to PBS controls.

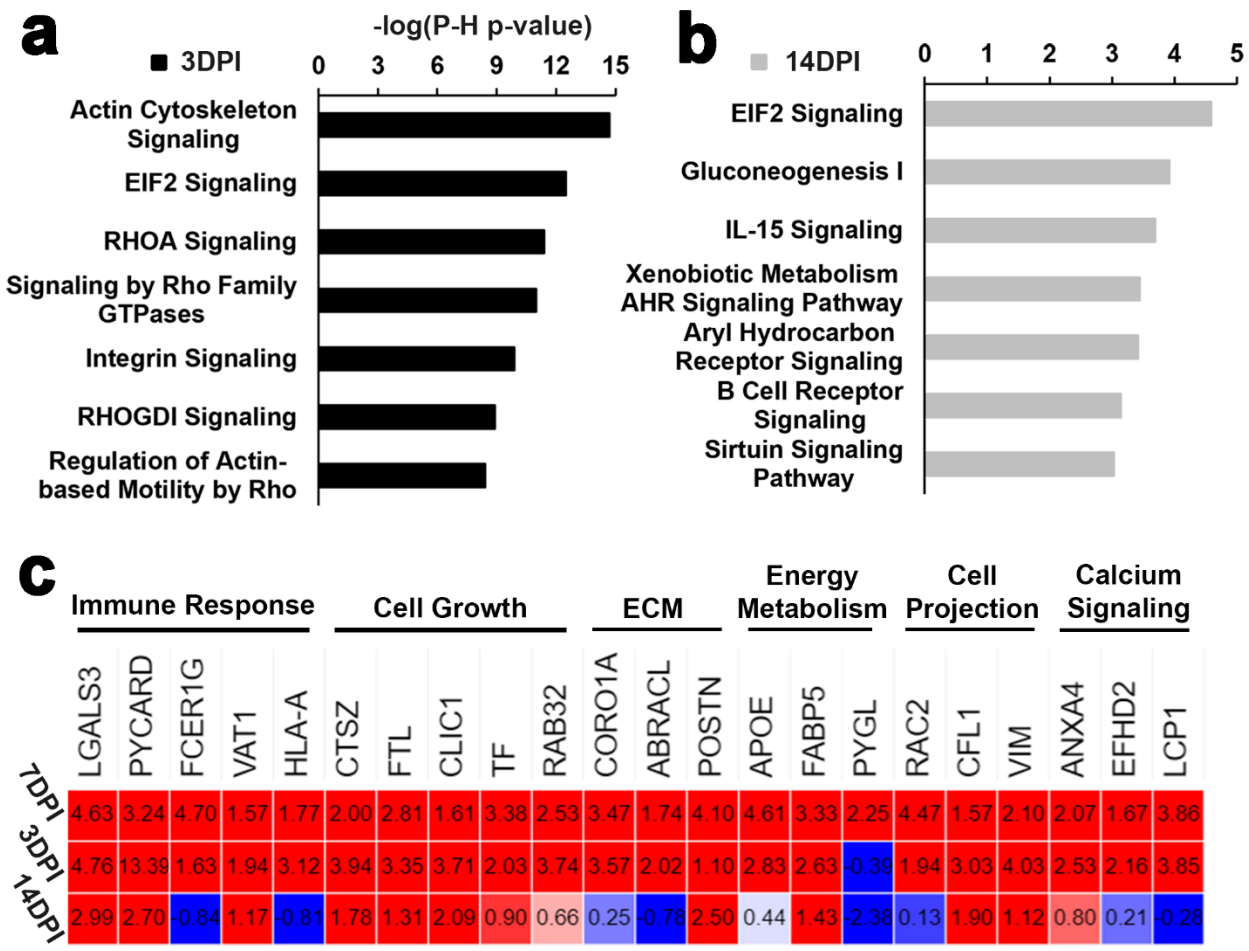

Figure 3. Mouse Proteomic Analysis. Top canonical pathways based on the Ingenuity Pathway Analysis (IPA) assessment of differentially expressed proteins at (a) 3DPI (FDR < 0.05 and $|\log_2 FC| > 1.5$) and (b) 14 DPI ($p<0.05$ and $|\log_2 FC| > 1$) within gel treatment with respect PBS controls. (c) The levels of overlapped IDs between DEGs (7DPI) and DEPs (3DPI and 14DPI) when compare gel treatment group to PBS controls are presented as log ratio ($\log_2 FC$).

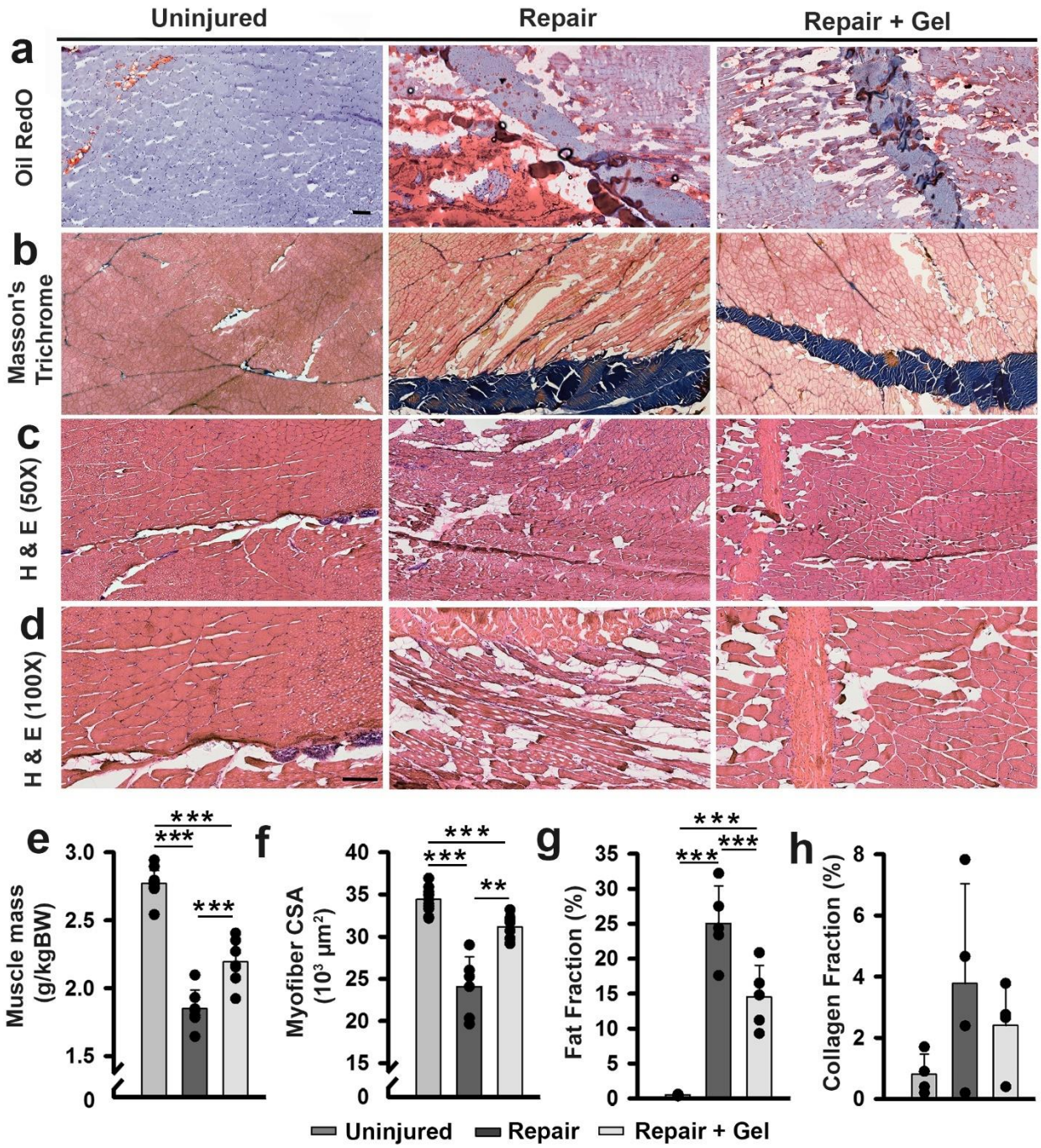

Figure 4. Rabbit Muscle Environment and Functional Outcome. TA muscle cross-sections were stained with (a) oil red o, (b) Masson's Trichrome, and hematoxylin and eosin (H&E) at (c) 50x and (d) 100x. Representative 16-week post treatment rabbit shoulder cuff muscle cross-sections are presented. Magnification is 50x unless stated otherwise. (e) muscles were weighed, and cross-sections were quantified for (f) myofiber cross-sectional area, (g) fat-fraction % and (h) collagen fraction %. Group means + Standard Deviation are presented; n = 4/group. The *, **, and *** indicate statistically significant difference of $p<0.05$, $p<0.01$, and $p<0.001$ between groups.

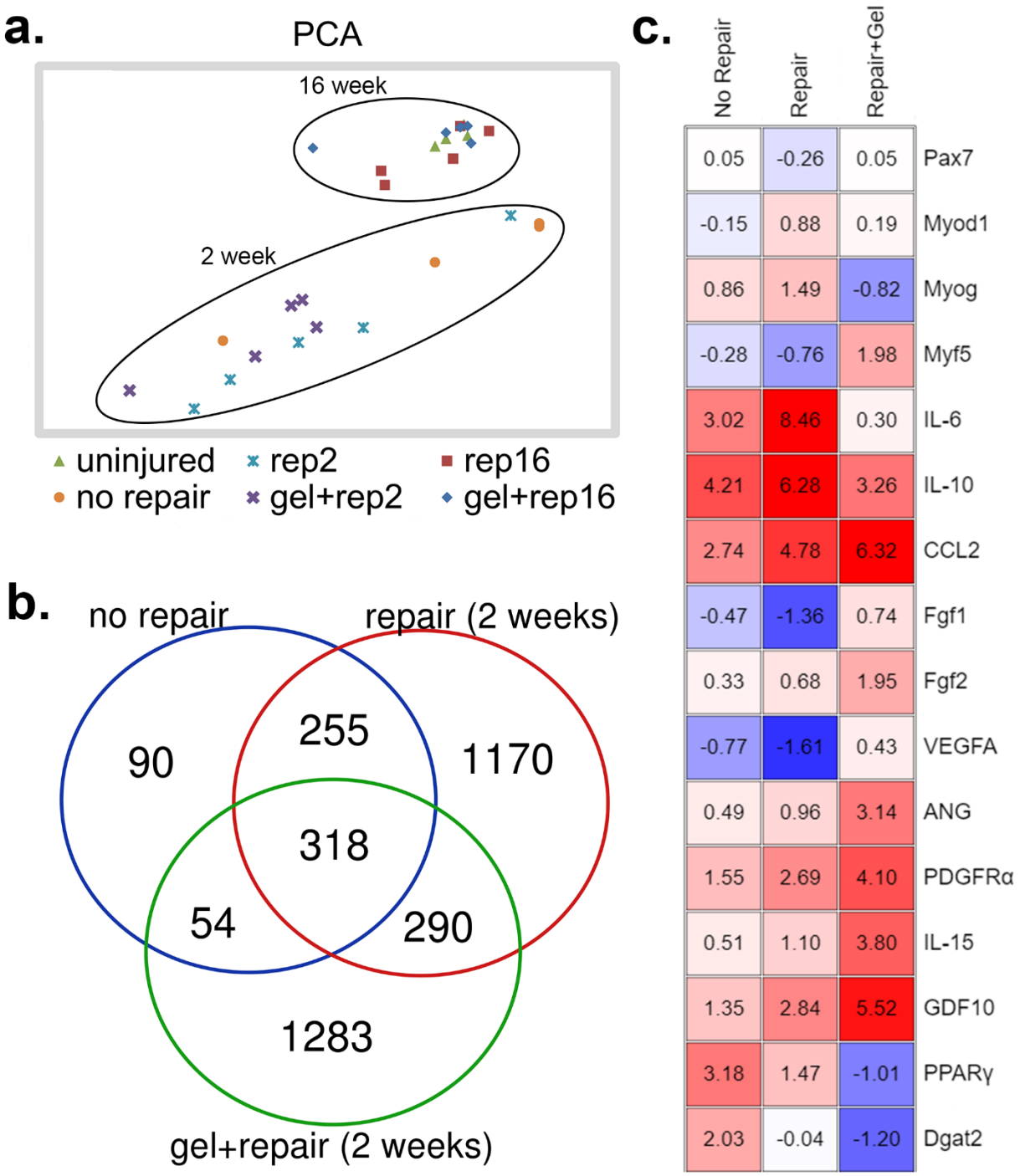

Figure 5. Rabbit Transcriptomic Analysis (a) Principal component analysis graph of supraspinatus muscle transcriptomes from all groups (2 weeks and 16 weeks post rotator cuff tendon tear surgery) normalized CPM using all transcripts. (b) Venn diagram illustrates differentially expressed genes (FDR < 0.05 and $|\log_2 FC| > 1.5$) counts for injured (no repair), repair only and repair+gel groups with respect to uninjured controls. (c) Gene expression (compared to uninjured controls) are presented as log ratio ($\log_2 FC$) at 2 weeks post treatment; positive numbers indicate upregulated genes and vice versa for negative numbers

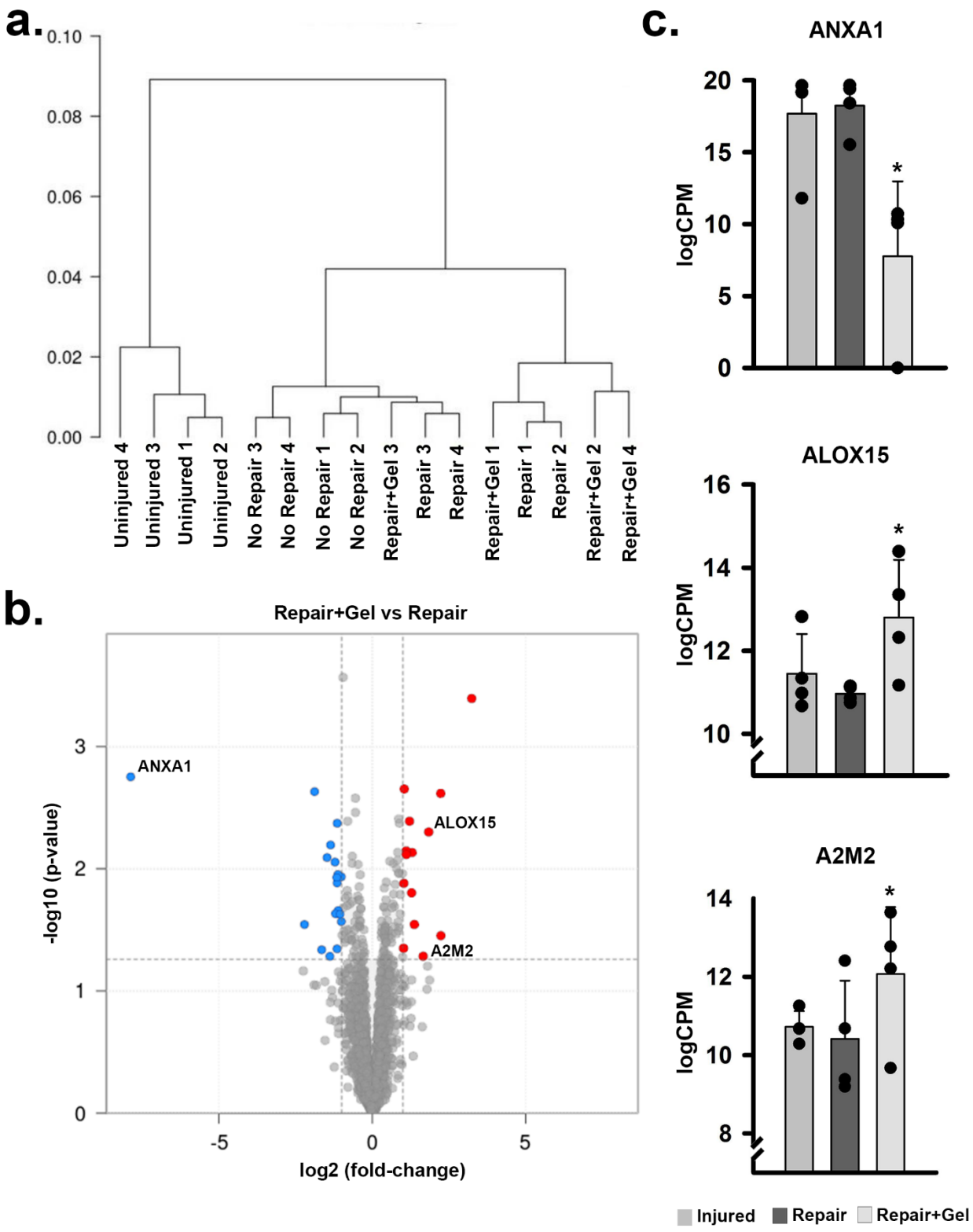

Figure 6. Rabbit Proteomic Analysis (a) Cluster dendrogram created using the hierarchical clustering method to determine distance between samples (b) Volcano plot of all protein identified in samples when compared the proteomes of repair and repair+gel groups.

Differentially expressed protein ($p < 0.05$ and $|\log_2 FC| > 1.5$) are colored either red (upregulated) or blue (downregulated). (c) The levels of selected proteins from injured, repair and repair+gel are presented as log counts per million (logCPM). Group means + SD are presented; n=4/group. The * indicate statistically significant difference of $p<0.05$ between groups.

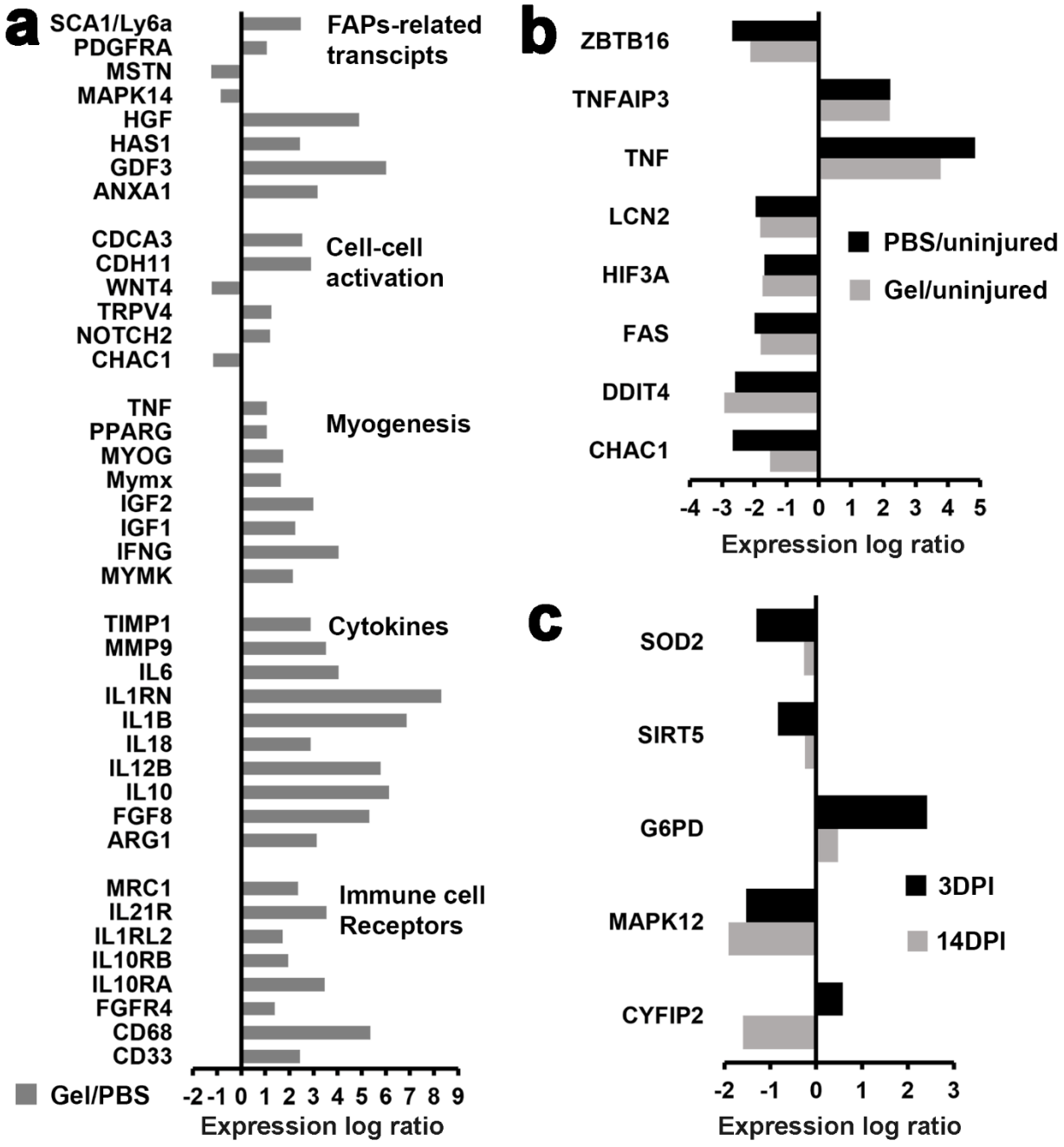

Supplementary figure 1: (a) Expression of selected differentially expressed genes (DEGs) for ECM gel treatment with respect to PBS controls genes are presented as log ratio ($\log_2 FC$). (b) Expression of selected shared genes (apoptosis process) between ECM gel treatment and PBS controls with respect to uninjured controls are presented as log ratio ($\log_2 FC$). (c) Selected

shared differentially expressed proteins (mitochondrial oxidative metabolism, apoptosis process) for ECM gel treatment with respect to PBS controls genes (3DPI and 14 DPI) are presented as log ratio (log_2FC).

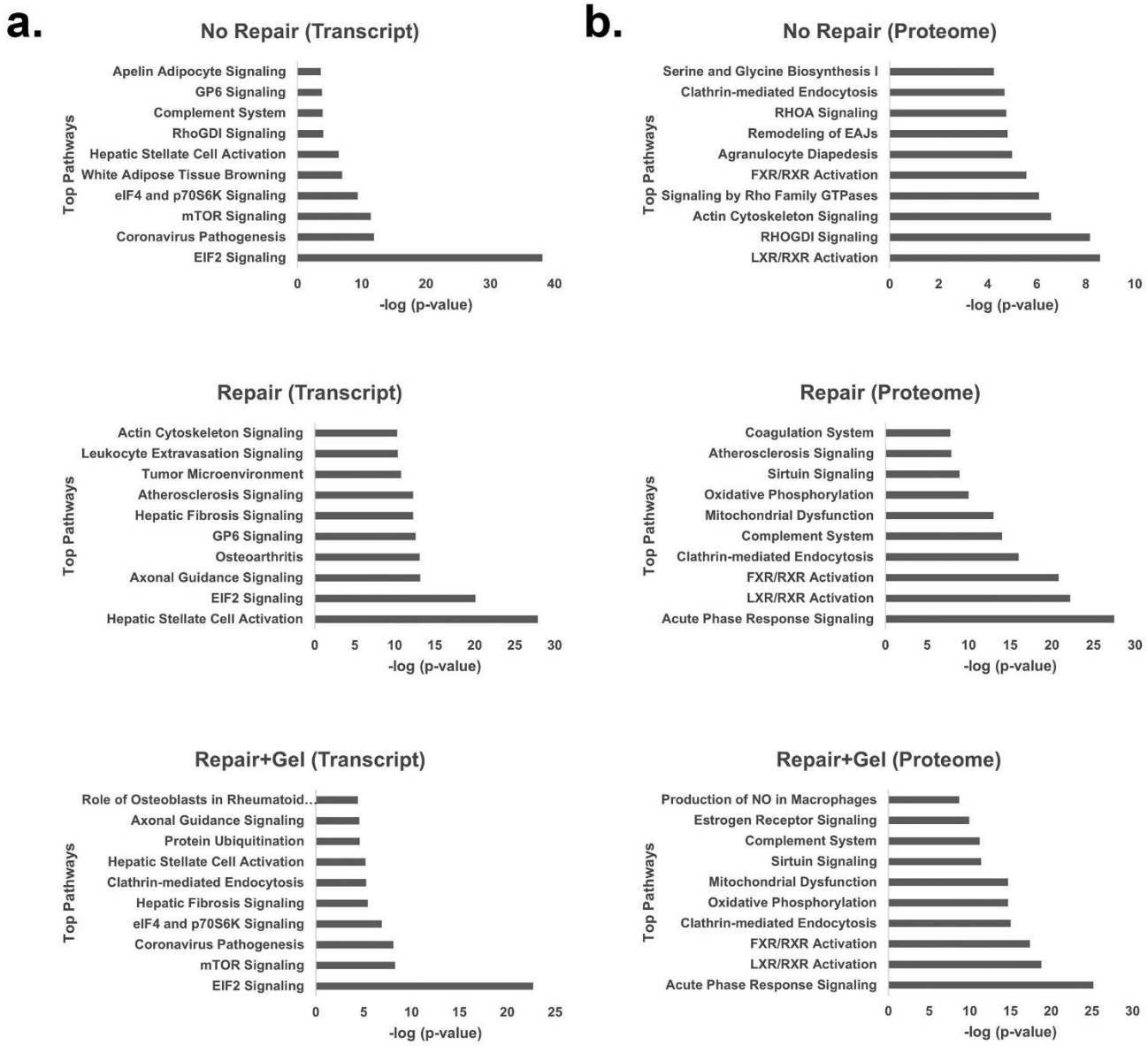

Supplementary figure 2: (a) Top pathways given by Ingenuity Pathway Analysis (IPA) based on differentially expressed genes (cut off for DEGs was FDR < 0.05 and |log2FC| > 1.5) compared to uninjured muscle. (b) Top pathways given by IPA based on differentially expressed proteins (cut off for DEPs was $p < 0.05$ and |log2FC| > 1) compared to uninjured muscle (EAJs = epithelial adherent junctions).

3.8 Reference

1. Parry, S.M. & Puthucheary, Z.A. The impact of extended bed rest on the musculoskeletal system in the critical care environment. *Extrem Physiol Med* **4**, 16 (2015).

2. Thomas, A.C., Wojtys, E.M., Brandon, C. & Palmieri-Smith, R.M. Muscle atrophy contributes to quadriceps weakness after anterior cruciate ligament reconstruction. *J Sci Med Sport* **19**, 7-11 (2016).

3. Chopard, A., Hillock, S. & Jasmin, B.J. Molecular events and signalling pathways involved in skeletal muscle disuse-induced atrophy and the impact of countermeasures. *Journal of cellular and molecular medicine* **13**, 3032-3050 (2009).

4. Gao, Y., Arfat, Y., Wang, H. & Goswami, N. Muscle Atrophy Induced by Mechanical Unloading: Mechanisms and Potential Countermeasures. *Frontiers in physiology* **9**, 235 (2018).

5. Cros, N., *et al.* Upregulation of M-creatine kinase and glyceraldehyde3-phosphate dehydrogenase: two markers of muscle disuse. *The American journal of physiology* **276**, R308-316 (1999).

6. Machida, S. & Booth, F.W. Regrowth of skeletal muscle atrophied from inactivity. *Medicine and science in sports and exercise* **36**, 52-59 (2004).

7. Rahman, H., *et al.* Primary and Secondary Consequences of Rotator Cuff Injury on Joint Stabilizing Tissues in the Shoulder. *J Biomech Eng* **139**(2017).

8. Goutallier, D., Postel, J.M., Bernageau, J., Lavau, L. & Voisin, M.C. Fatty muscle degeneration in cuff ruptures. Pre- and postoperative evaluation by CT scan. *Clinical orthopaedics and related research*, 78-83 (1994).

9. Aagaard, K.E., Lunsjo, K. & Frobell, R. Early repair of trauma-related full-thickness rotator cuff tears does not eliminate the problem of healing failure. *The bone & joint journal* **101-B**, 603-609 (2019).

10. Consigliere, P., *et al.* Preliminary Results of a Consecutive Series of Large & Massive Rotator Cuff Tears Treated with Arthroscopic Rotator Cuff Repairs Augmented with Extracellular Matrix. *The archives of bone and joint surgery* **5**, 14-21 (2017).

11. Hamano, N., *et al.* Does successful rotator cuff repair improve muscle atrophy and fatty infiltration of the rotator cuff? A retrospective magnetic resonance imaging study performed shortly after surgery as a reference. *Journal of shoulder and elbow surgery* **26**, 967-974 (2017).

12. Namdari, S., *et al.* Factors affecting outcome after structural failure of repaired rotator cuff tears. *The Journal of bone and joint surgery. American volume* **96**, 99-105 (2014).

13. Spang, M.T. & Christman, K.L. Extracellular matrix hydrogel therapies: In vivo applications and development. *Acta biomaterialia* **68**, 1-14 (2018).

14. Dumont, N., Bouchard, P. & Frenette, J. Neutrophil-induced skeletal muscle damage: a calculated and controlled response following hindlimb unloading and reloading. *American journal of physiology. Regulatory, integrative and comparative physiology* **295**, R1831-1838 (2008).

15. DeQuach, J.A., *et al.* Injectable skeletal muscle matrix hydrogel promotes neovascularization and muscle cell infiltration in a hindlimb ischemia model. *European cells & materials* **23**, 400-412; discussion 412 (2012).

16. Riley, D.A., Thompson, J.L., Krippendorf, B.B. & Slocum, G.R. Review of spaceflight and hindlimb suspension unloading induced sarcomere damage and repair. *Basic Appl Myol* **5**, 139-145 (1995).

17. Kim, S.K. Cell polarity: new PARtners for Cdc42 and Rac. *Nature cell biology* **2**, E143-145 (2000).

18. Millay, D.P., *et al.* Myomaker is a membrane activator of myoblast fusion and muscle formation. *Nature* **499**, 301-305 (2013).

19. Bi, P., *et al.* Control of muscle formation by the fusogenic micropeptide myomixer. *Science* **356**, 323-327 (2017).

20. Schmidt, M., Schuler, S.C., Huttner, S.S., von Eyss, B. & von Maltzahn, J. Adult stem cells at work: regenerating skeletal muscle. *Cellular and molecular life sciences : CMLS* **76**, 2559-2570 (2019).

21. Giuliani, G., Rosina, M. & Reggio, A. Signaling pathways regulating the fate of fibro/adipogenic progenitors (FAPs) in skeletal muscle regeneration and disease. *The FEBS journal* **289**, 6484-6517 (2022).

22. Tsuchiya, Y., Kitajima, Y., Masumoto, H. & Ono, Y. Damaged Myofiber-Derived Metabolic Enzymes Act as Activators of Muscle Satellite Cells. *Stem cell reports* **15**, 926-940 (2020).

23. Karvinen, S., *et al.* Effects of intrinsic aerobic capacity, aging and voluntary running on skeletal muscle sirtuins and heat shock proteins. *Experimental gerontology* **79**, 46-54 (2016).

24. Contreras, O., *et al.* Cross-talk between TGF-beta and PDGFRalpha signaling pathways regulates the fate of stromal fibro-adipogenic progenitors. *J Cell Sci* **132**(2019).

25. Gruys, E., Toussaint, M.J., Niewold, T.A. & Koopmans, S.J. Acute phase reaction and acute phase proteins. *J Zhejiang Univ Sci B* **6**, 1045-1056 (2005).

26. Thomas, D.G., *et al.* LXR Suppresses Inflammatory Gene Expression and Neutrophil Migration through cis-Repression and Cholesterol Efflux. *Cell reports* **25**, 3774-3785 e3774 (2018).

27. Mirzoev, T.M. Skeletal Muscle Recovery from Disuse Atrophy: Protein Turnover Signaling and Strategies for Accelerating Muscle Regrowth. *International journal of molecular sciences* **21**(2020).

28. Andrianjafiniony, T., Dupre-Aucouturier, S., Letexier, D., Couchoux, H. & Desplanches, D. Oxidative stress, apoptosis, and proteolysis in skeletal muscle repair after unloading. *American journal of physiology. Cell physiology* **299**, C307-315 (2010).

29. Zhang, B.T., Yeung, S.S., Cheung, K.K., Chai, Z.Y. & Yeung, E.W. Adaptive responses of TRPC1 and TRPC3 during skeletal muscle atrophy and regrowth. *Muscle & nerve* **49**, 691-699 (2014).

30. Ungerleider, J.L., *et al.* Extracellular Matrix Hydrogel Promotes Tissue Remodeling, Arteriogenesis, and Perfusion in a Rat Hindlimb Ischemia Model. *JACC. Basic to translational science* **1**, 32-44 (2016).

31. Hernandez, M.J., Zelus, E.I., Spang, M.T., Braden, R.L. & Christman, K.L. Dose optimization of decellularized skeletal muscle extracellular matrix hydrogels for improving perfusion and subsequent validation in an aged hindlimb ischemia model. *Biomaterials science* **8**, 3511-3521 (2020).

32. Reing, J.E., *et al.* Degradation products of extracellular matrix affect cell migration and proliferation. *Tissue engineering. Part A* **15**, 605-614 (2009).

33. Buckley, C.D., *et al.* Fibroblasts regulate the switch from acute resolving to chronic persistent inflammation. *Trends in immunology* **22**, 199-204 (2001).

34. Goetsch, S.C., Hawke, T.J., Gallardo, T.D., Richardson, J.A. & Garry, D.J. Transcriptional profiling and regulation of the extracellular matrix during muscle regeneration. *Physiological genomics* **14**, 261-271 (2003).

35. Ganassi, M., Badodi, S., Wanders, K., Zammit, P.S. & Hughes, S.M. Myogenin is an essential regulator of adult myofibre growth and muscle stem cell homeostasis. *eLife* **9**(2020).

36. Quinn, L.S., Haugk, K.L. & Grabstein, K.H. Interleukin-15: a novel anabolic cytokine for skeletal muscle. *Endocrinology* **136**, 3669-3672 (1995).

37. Yang, W. & Hu, P. Skeletal muscle regeneration is modulated by inflammation. *Journal of orthopaedic translation* **13**, 25-32 (2018).

38. Waldemer-Streyer, R.J., Kim, D. & Chen, J. Muscle cell-derived cytokines in skeletal muscle regeneration. *The FEBS journal* (2022).

39. Chaillou, T., Lee, J.D., England, J.H., Esser, K.A. & McCarthy, J.J. Time course of gene expression during mouse skeletal muscle hypertrophy. *Journal of applied physiology* **115**, 1065-1074 (2013).

40. Cerri, D.G., *et al.* Endogenous galectin-3 is required for skeletal muscle repair. *Glycobiology* **31**, 1295-1307 (2021).

41. Rancourt, A., *et al.* Galectin-3 and N-acetylglucosamine promote myogenesis and improve skeletal muscle function in the mdx model of Duchenne muscular dystrophy. *FASEB journal : official publication of the Federation of American Societies for Experimental Biology*, fj201701151RRR (2018).

42. Gildor, B., Massarwa, R., Shilo, B.Z. & Schejter, E.D. The SCAR and WASp nucleation-promoting factors act sequentially to mediate Drosophila myoblast fusion. *EMBO Rep* **10**, 1043-1050 (2009).

43. Zhang, G., *et al.* Study on the transcriptome for breast muscle of chickens and the function of key gene RAC2 on fibroblasts proliferation. *BMC genomics* **22**, 157 (2021).

44. Iso, T., *et al.* Capillary endothelial fatty acid binding proteins 4 and 5 play a critical role in fatty acid uptake in heart and skeletal muscle. *Arteriosclerosis, thrombosis, and vascular biology* **33**, 2549-2557 (2013).

45. Fang, L.Y., Wong, T.Y., Chiang, W.F. & Chen, Y.L. Fatty-acid-binding protein 5 promotes cell proliferation and invasion in oral squamous cell carcinoma. *J Oral Pathol Med* **39**, 342-348 (2010).

46. Khajeian, N. & Moghadasi, M. Effect of 8 weeks regular endurance training on galectin-3 changes after a strenuous aerobic exercise. (2017).

47. Feng, M., Ji, J., Li, X. & Ye, X. Identification of the Exercise and Time Effects on Human Skeletal Muscle through Bioinformatics Methods. *Genetics Research* **2022**, 9582363 (2022).

48. Keller, P., *et al.* A transcriptional map of the impact of endurance exercise training on skeletal muscle phenotype. *Journal of applied physiology* **110**, 46-59 (2011).

49. Zhang, M., *et al.* SIRT5 deficiency suppresses mitochondrial ATP production and promotes AMPK activation in response to energy stress. *PloS one* **14**, e0211796 (2019).

50. Michishita, E., Park, J.Y., Burneskis, J.M., Barrett, J.C. & Horikawa, I. Evolutionarily conserved and nonconserved cellular localizations and functions of human SIRT proteins. *Mol Biol Cell* **16**, 4623-4635 (2005).

51. Thomson, D.M. The Role of AMPK in the Regulation of Skeletal Muscle Size, Hypertrophy, and Regeneration. *International journal of molecular sciences* **19**(2018).

52. Hilder, T.L., *et al.* Insulin-independent pathways mediating glucose uptake in hindlimb-suspended skeletal muscle. *Journal of applied physiology* **99**, 2181-2188 (2005).

53. Han, B., Zhu, M.J., Ma, C. & Du, M. Rat hindlimb unloading down-regulates insulin like growth factor-1 signaling and AMP-activated protein kinase, and leads to severe atrophy of the soleus muscle. *Applied physiology, nutrition, and metabolism = Physiologie appliquee, nutrition et metabolisme* **32**, 1115-1123 (2007).

54. Tarini, V.A., *et al.* Effect of exhaustive ultra-endurance exercise in muscular glycogen and both Alpha1 and Alpha2 Ampk protein expression in trained rats. *Journal of physiology and biochemistry* **69**, 429-440 (2013).

55. McConell, G.K., *et al.* Short-term exercise training in humans reduces AMPK signalling during prolonged exercise independent of muscle glycogen. *The Journal of physiology* **568**, 665-676 (2005).

56. Ji, L.L. Antioxidant enzyme response to exercise and training in the skeletal muscle. in *Oxidative Stress in Skeletal Muscle* (eds. Reznick, A.Z., Packer, L., Sen, C.K., Holloszy, J.O. & Jackson, M.J.) 103-125 (Birkhäuser Basel, Basel, 1998).

57. Ozdemir, C., *et al.* Periostin is temporally expressed as an extracellular matrix component in skeletal muscle regeneration and differentiation. *Gene* **553**, 130-139 (2014).

58. Chaillou, T., *et al.* Identification of a conserved set of upregulated genes in mouse skeletal muscle hypertrophy and regrowth. *Journal of applied physiology* **118**, 86-97 (2015).

59. Saller, E., *et al.* Increased apoptosis induction by 121F mutant p53. *EMBO J* **18**, 4424-4437 (1999).

60. Yue, J. & Lopez, J.M. Understanding MAPK Signaling Pathways in Apoptosis. *International journal of molecular sciences* **21**(2020).

61. Gillespie, M.A., *et al.* p38-gamma-dependent gene silencing restricts entry into the myogenic differentiation program. *The Journal of cell biology* **187**, 991-1005 (2009).

62. Uezumi, A., Ikemoto-Uezumi, M. & Tsuchida, K. Roles of nonmyogenic mesenchymal progenitors in pathogenesis and regeneration of skeletal muscle. *Frontiers in physiology* **5**, 68 (2014).

63. Contreras, O., Rossi, F.M. & Brandan, E. Adherent muscle connective tissue fibroblasts are phenotypically and biochemically equivalent to stromal fibro/adipogenic progenitors. *Matrix Biol Plus* **2**, 100006 (2019).

64. Molina, T., Fabre, P. & Dumont, N.A. Fibro-adipogenic progenitors in skeletal muscle homeostasis, regeneration and diseases. *Open biology* **11**, 210110 (2021).

65. Liu, X., *et al.* Evaluation of Akt/mTOR activity in muscle atrophy after rotator cuff tears in a rat model. *Journal of orthopaedic research : official publication of the Orthopaedic Research Society* **30**, 1440-1446 (2012).

66. Leoni, G., *et al.* Annexin A1-containing extracellular vesicles and polymeric nanoparticles promote epithelial wound repair. *The Journal of clinical investigation* **125**, 1215-1227 (2015).

67. Leoni, G. & Nusrat, A. Annexin A1: shifting the balance towards resolution and repair. *Biol Chem* **397**, 971-979 (2016).

68. Laberge, A., *et al.* α-2-Macroglobulin induces the shedding of microvesicles from cutaneous wound myofibroblasts. *Journal of cellular physiology* **234**, 11369-11379 (2019).

69. Gronert, K., *et al.* A role for the mouse 12/15-lipoxygenase pathway in promoting epithelial wound healing and host defense. *The Journal of biological chemistry* **280**, 15267-15278 (2005).

70. Kim, S.-N., *et al.* Anti-inflammatory role of 15-lipoxygenase contributes to the maintenance of skin integrity in mice. *Scientific reports* **8**, 8856 (2018).

71. Sugimoto, M.A., Vago, J.P., Teixeira, M.M. & Sousa, L.P. Annexin A1 and the Resolution of Inflammation: Modulation of Neutrophil Recruitment, Apoptosis, and Clearance. *J Immunol Res* **2016**, 8239258 (2016).

72. Gschwandtner, M., Derler, R. & Midwood, K.S. More Than Just Attractive: How CCL2 Influences Myeloid Cell Behavior Beyond Chemotaxis. *Frontiers in immunology* **10**, 2759 (2019).

73. Prudovsky, I. Cellular Mechanisms of FGF-Stimulated Tissue Repair. *Cells* **10**(2021).

74. Frey, S.P., Jansen, H., Raschke, M.J., Meffert, R.H. & Ochman, S. VEGF improves skeletal muscle regeneration after acute trauma and reconstruction of the limb in a rabbit model. *Clinical orthopaedics and related research* **470**, 3607-3614 (2012).

75. Asfour, H.A., Allouh, M.Z. & Said, R.S. Myogenic regulatory factors: The orchestrators of myogenesis after 30 years of discovery. *Experimental biology and medicine* **243**, 118-128 (2018).

76. Ustanina, S., Carvajal, J., Rigby, P. & Braun, T. The Myogenic Factor Myf5 Supports Efficient Skeletal Muscle Regeneration by Enabling Transient Myoblast Amplification. *Stem cells* **25**, 2006-2016 (2007).

77. Petrilli, L.L., *et al.* High-Dimensional Single-Cell Quantitative Profiling of Skeletal Muscle Cell Population Dynamics during Regeneration. *Cells* **9**(2020).

78. Joe, A.W.B., *et al.* Muscle injury activates resident fibro/adipogenic progenitors that facilitate myogenesis. *Nature cell biology* **12**, 153-163 (2010).

79. Uezumi, A., Fukada, S.-i., Yamamoto, N., Takeda, S.i. & Tsuchida, K. Mesenchymal progenitors distinct from satellite cells contribute to ectopic fat cell formation in skeletal muscle. *Nature cell biology* **12**, 143-152 (2010).

80. Kang, X., *et al.* Interleukin-15 facilitates muscle regeneration through modulation of fibro/adipogenic progenitors. *Cell Commun Signal* **16**, 42 (2018).

81. Quinn, L.S., Strait-Bodey, L., Anderson, B.G., Argilés, J.M. & Havel, P.J. Interleukin-15 stimulates adiponectin secretion by 3T3-L1 adipocytes: evidence for a skeletal muscle-to-fat signaling pathway. *Cell biology international* **29**, 449-457 (2005).

82. Li, Y., *et al.* Myokine IL-15 regulates the crosstalk of co-cultured porcine skeletal muscle satellite cells and preadipocytes. *Mol Biol Rep* **41**, 7543-7553 (2014).

83. Camps, J., *et al.* Interstitial Cell Remodeling Promotes Aberrant Adipogenesis in Dystrophic Muscles. *Cell reports* **31**, 107597 (2020).

84. Joshi, S.K., *et al.* mTOR regulates fatty infiltration through SREBP-1 and PPARgamma after a combined massive rotator cuff tear and suprascapular nerve injury in rats. *Journal of orthopaedic research : official publication of the Orthopaedic Research Society* **31**, 724-730 (2013).

85. Heredia, J.E., *et al.* Type 2 innate signals stimulate fibro/adipogenic progenitors to facilitate muscle regeneration. *Cell* **153**, 376-388 (2013).

86. Ungerleider, J.L., Johnson, T.D., Rao, N. & Christman, K.L. Fabrication and characterization of injectable hydrogels derived from decellularized skeletal and cardiac muscle. *Methods* **84**, 53-59 (2015).

87. Fu, Y., *et al.* Decellularization of porcine skeletal muscle extracellular matrix for the formulation of a matrix hydrogel: a preliminary study. *Journal of cellular and molecular medicine* **20**, 740-749 (2016).

88. Oh, J.H., Chung, S.W., Kim, S.H., Chung, J.Y. & Kim, J.Y. 2013 Neer Award: Effect of the adipose-derived stem cell for the improvement of fatty degeneration and rotator cuff healing in rabbit model. *Journal of shoulder and elbow surgery* **23**, 445-455 (2014).

89. Matsumoto, F., Uhthoff, H.K., Trudel, G. & Loehr, J.F. Delayed tendon reattachment does not reverse atrophy and fat accumulation of the supraspinatus--an experimental study in rabbits. *Journal of orthopaedic research : official publication of the Orthopaedic Research Society* **20**, 357-363 (2002).

90. Washington, T.A., *et al.* Skeletal muscle mass recovery from atrophy in IL-6 knockout mice. *Acta physiologica* **202**, 657-669 (2011).

91. Dobin, A., *et al.* STAR: ultrafast universal RNA-seq aligner. *Bioinformatics* **29**, 15-21 (2013).

92. Liao, Y., Smyth, G.K. & Shi, W. featureCounts: an efficient general purpose program for assigning sequence reads to genomic features. *Bioinformatics* **30**, 923-930 (2014).

93. Robinson, M.D., McCarthy, D.J. & Smyth, G.K. edgeR: a Bioconductor package for differential expression analysis of digital gene expression data. *Bioinformatics* **26**, 139-140 (2010).

94. Kramer, A., Green, J., Pollard, J., Jr. & Tugendreich, S. Causal analysis approaches in Ingenuity Pathway Analysis. *Bioinformatics* **30**, 523-530 (2014).

95. Ngoka, L.C. Sample prep for proteomics of breast cancer: proteomics and gene ontology reveal dramatic differences in protein solubilization preferences of radioimmunoprecipitation assay and urea lysis buffers. *Proteome Sci* **6**, 30 (2008).

CHAPTER 4: Local IL-10 delivery modulates the immune response and enhances repair of volumetric muscle loss muscle injury

Submitted as an original article by:

Tai Huynh[1], Cassandra Reed[1], Zain Blackwell[1], Payton Phelps[1], Luis C. Pinzon Herrera[2], Jorge Almodovar[2], David A. Zaharoff[3], and Jeffrey Wolchok[1]

[1]Department of Biomedical Engineering, College of Engineering, University of Arkansas, Fayetteville, AR, USA

[2]Ralph E. Martin Department of Chemical Engineering, College of Engineering, University of Arkansas, Fayetteville, AR, USA

[3]Joint Department of Biomedical Engineering, University of North Carolina-Chapel Hill & North Carolina State University, Raleigh, NC, USA

4.1 Abstract

This study was designed to test the hypothesis that in addition to repairing the architectural and cellular cues via regenerative medicine, the delivery of immune cues (immunotherapy) may be needed to enhance regeneration following volumetric muscle loss (VML) injury. We identified IL-10 signaling as a promising immunotherapeutic target. To explore the impact of targeting IL-10 signaling, tibialis anterior (TA) VML injuries were created and then treated in rats using autologous minced muscle (MM). Animals received either

recombinant rat IL-10 or phosphate buffered saline (PBS) controls injections at the site of VML repair beginning 7 days post injury (DPI) and continuing every other day (4 injections total) until 14 DPI. At 56 DPI (study endpoint), significant improvements to TA contractile torque (82% of uninjured values & 170% of PBS values), TA mass, and myofiber size in response to IL-10 treatment were detected. Whole transcriptome analysis at 14 DPI revealed activation of IL-10 signaling, muscle hypertrophy, and lymphocytes signaling pathways. Expression of ST2, a regulatory T (T_{reg}) cell receptor, was dramatically increased at the VML repair site in response to IL-10 treatment when compared to PBS controls. The findings suggest that the positive effect of delayed IL-10 delivery might be due to immuno-suppressive T_{reg} cell recruitment.

4.2 Background

When provided the appropriate cues, skeletal muscle has a strong capacity for self-repair. Following mild muscle damage (ex. strains, contusions, and lacerations), cells are damaged but the underlying extracellular matrix (ECM) is largely intact and regeneration at the injury site is robust[1,2]. However, when significant muscle volume is lost (trauma, infection, surgical resection), or volumetric muscle loss (VML), the cues provided by the injured tissue are missing and the endogenous repair mechanisms of skeletal muscle are overwhelmed, often leading to overt fibrosis and chronic inflammation at the site of injury regeneration [3-6]. Current soft tissue repair techniques and traditional rehabilitation have not been able to reverse the pathological changes that occur following VML injury. To maximize recovery from VML injury, our group and others are exploring the use of regenerative medicine strategies as a means of restoring these lost cues. The vast majority of VML regenerative medicine research, including our own[7-12], has focused on the development of scaffolds and muscle progenitor cells as a means to re-establish the architectural and pro-myogenic cues lost to injury. Although regenerative medicine strategies

have shown tantalizing promise and warrant continued research**,** the results across several strategies appear to suggest that regenerative medicine alone may have a ceiling; typically restoring no more than half of the contractile force lost to VML injury [7,13-17]. What has been overlooked by us and others may be the importance of reestablishing a pro-myogenic immune environment as part of the regenerative medicine repair strategy.

The immune system coordinates muscle regeneration following injury, making it an attractive therapeutic target. What we know about muscle regeneration has been largely elucidated through the use of acute injury models (toxin, unloading/reloading, etc.)**.** Following this type of acute injury, muscle regeneration is robust and characterized by spatially and temporally coordinated responses by leukocytes (macrophages), lymphocytes (T cells), and muscle progenitor cells (also termed satellite cells). Evidence suggests that coordination between these cells in the muscle-immune micro-environment (MIME) is mediated by soluble cytokines [18]. Recovery from acute injury begins with the activation of satellite cells that reside at the periphery of individual muscle fibers**.** Within hours of injury, muscle tissue is invaded by neutrophils, then later by macrophages and T-cells that are polarized toward the pro-inflammatory M1 and Th1 phenotypes, respectively. The early immune response is characterized by increased levels of pro-inflammatory cytokines, including IFN-γ, TNF-α, and IL-6, which stimulate the proliferation of satellite cells and initiate their differentiation into myoblasts [19].

Following the initial inflammatory phase, the immune response transitions to a pro-regenerative phase, during which the available stockpile of myoblasts is recruited and further differentiated to build new muscle tissue. During this transition there is a dramatic shift in intramuscular cytokine levels from pro-inflammatory (IL-6, TNF-α, IFN-γ) to anti-inflammatory (IL-10, IL-4, IGF) cytokines [18,20]. The transition is coupled with a shift from an M1/Th1 immune

cell population to one that is dominated by M2 macrophages and regulatory T cells (T_{regs})[21]. While the biology of immune cell polarization is complex and polarization is not binary, the preponderance of evidence suggests that the presence of M2 biased macrophages and Th2/T_{reg} biased T-cells within the wound site is essential for optimal muscle regeneration[18,22-24]. To be clear, the robust and well-coordinated regenerative paradigm described above was deciphered from acute injury models. While similar dynamics are expected to enhance recovery from VML repair, a detailed picture of the immune response and the MIME following VML injury is incomplete but the limited information that does exist suggests that VML injury dysregulates the regenerative response[4]. Restoring the coordinated communication between immune cells (macrophage and T cell polarization) and muscle progenitor cells (satellite cell dynamics) provides a strong rationale for the development of immunotherapeutic approaches capable of recapitulating the pro-regenerative acute injury wound healing response in order to achieve ideal clinical outcomes following VML repair. Evidence from our preliminary efforts as well as published evidence from others suggest that VML injury decreases endogenous IL-10 which is a critical cytokine produced by immune cells driving tissue repair and regeneration as well as promoting the transition from the pro-inflammatory/proliferative to the anti-inflammatory/regenerative stage of muscle healing [25-27]. The objective of this study was to determine whether exogenous delivery of IL-10 can improve the performance of a regenerative medicine strategy for the repair of VML injury.

4.3 Results

The IL-10 signaling node appears to be a particularly promising immunotherapeutic target for the treatment of VML injury.

We first examined and paired the early *in vivo* functional response induced by differing VML tissue engineering repair strategies that are broadly representative of those explored by the field (scaffold alone, cells alone, or scaffold + cells) to the transcriptomic response induced by each intervention in order to elucidate potential immunotherapeutic targets (**Fig. 1a**). Muscle tissue was collected from the VML repair site at 3 and 14 days post VML injury (DPI) across the differing regenerative medicine repair strategies (n=4-5 / group) and the transcriptome was examined with the aid of RNA Sequencing (RNA-Seq). Unrepaired VML injuries and uninjured normal muscle served as comparative controls. At 3 DPI, a broadly similar pattern of gene expression, dominated by upregulation of genes related to acute inflammation, was observed across all groups. However, by 14 DPI the muscle transcriptome began to vary across the differing repair strategies. Of particular interest, we observed that while expression of the IL-10 gene remained low across all groups (often undetectable) at 14 DPI, the expression of the IL-10R receptor gene was elevated in response to VML repair (**Fig. 1b**). The elevated expression of the IL10R gene in the VML repair groups is likely the result of an increase in the population of immune cells carrying the receptor, which as described previously are known to infiltrate muscle following injury. Furthermore, the expression of the IL10R gene was moderately correlated (R=0.51) with early (14 DPI) muscle torque values (**Fig. 1c**) suggesting a link to improved functional recovery. When viewed together, the IL-10 / IL10R findings point to a potential responsiveness to IL-10 signaling at the VML repair site, however the absence of significant endogenous IL-10 production at 14 DPI following regenerative medicine intervention suggests that modulation of IL-10 cytokine levels through exogenous delivery could be a promising adjunct immunotherapeutic approach. Lastly, when compared directly VML, both MM and DSM+MM groups elicited significantly higher level of IL10R transcripts (**Fig. 1d**). Because

IL10R transcripts level from DSM+MM group were not statistically different from MM group, we decided to employ MM as the repair strategy in our IL-10 delivery experiment to reduce variability between subjects which increase our ability to detect the effect of the exogenous IL10 delivery strategy.

Delayed IL-10 delivery improved functional and structural recovery following VML repair.

To exploit IL-10 signaling sensitivity and counteract insufficient endogenous production, we next examined the impact of supplementing IL-10 cytokine at a VML repair site through exogenous delivery (200ng/injection) delayed until one week after VML injury + repair and sustained for one week (**Fig. 2a**). VML injuries (removal of approximately 20% the muscle mass) were repaired using minced muscle (MM) autografts (**Fig. 2b)**. Immediately following the IL-10 delivery period (14 DPI), mean TA muscle peak contractile torque values were similar for both the IL-10 treated (3.75+1.49 Nmm/kg) and PBS controls groups (4.11+1.22 Nmm/kg); these torques were approximately 40% of uninjured contralateral limb values (10.18+ 3.02 Nmm/kg), a statistically significant reduction in torque. However, by 56 DPI, a significant main effect of IL-10 treatment to increase peak contractile torque ($p<0.001$) when compared to PBS controls was detected (**Fig. 2c)**. Mean torque values for the IL-10 treated group (8.34+2.13 Nmm/kg) had returned to approximately 82% of uninjured contralateral contractile torque values (10.78+ 3.16), while 56 DPI PBS controls group values (4.90+ 1.17) had not improved from 14 DPI values. Similar to the response detected within the peak torque data, the main effect of IL-10 treatment on TA mass was at first not significant at 14 DPI but did reach significance ($p=0.002$) at 56 DPI when compared to PBS controls (**Fig. 2d**). Specifically, IL-10 treated TA mass increased from 1.50+0.28 mg/g at 14 DPI post repair to 1.71+0.12 mg/g at 56 DPI, a recovery of

55%. At 56 DPI, IL-10 treated TA muscle mass was on average 16% larger than PBS controls group samples. Alternatively, TA mass recovery (-21%) between 14 DPI (1.55+0.25 mg/g) and 56 DPI (1.48+0.22 mg/g) was not significant for the PBS group.

The gross morphology of whole TA muscles collected from both the IL-10 treated and PBS controls groups at 56 DPI showed evidence of repair site healing (**Fig. 2e)**. When viewed in cross section, IL-10 treated and PBS controls repair site tissue samples (56 DPI) contained numerous muscle fibers, which were surrounded by dense connective tissue that extended proximally into the belly of the TA muscle (**Fig. 2f**). PBS controls repair site tissue sections were characterized by a notable presence of infiltrated cells within the connective tissue suggestive of continued inflammation in PBS group, which was not observed in IL-10 treated sections (**Fig. 2f**). Quantitative assessment of tissue structure revealed a significant increase ($p= 0.047$) in myofiber cross sectional area (CSA) of IL-10 treatment when compared to PBS controls (1695±434 μm^2 vs. 859.92±176 μm^2) (**Fig. 2g**), though no significant difference was detected when compared the CSA distributions of the two treatment groups (**Fig. S2c**). While CSA recovery was improved following IL-10 treatment, repair site fibrosis was not affected. Specifically, collagen I+ area fraction (% tissue area) was statistically indistinguishable between the IL-10 treatment (18.7±3.1%) and PBS controls (22.9±4.4%) groups (**Fig. 2h**). Although not different from each other, the %NCT for both the IL-10 treated and PBS controls groups was significantly elevated when compared to uninjured contralateral controls. To summarize, while recovery was similar between the groups immediately following the 7 day delivery period (14 DPI), the delayed and sustained delivery of IL-10 significantly improved peak contractile torque (81.1±17.6% vs. 45.7±9.3% of uninjured controls), muscle mass (85.8+6.1 vs. 75+9.7 % of

uninjured controls) as well as myofiber CSA (61.2±12.4% vs. 31.1±2.1% of uninjured controls) recovery when compared to the PBS group at 56 DPI.

Delayed IL-10 delivery enhanced key muscle wound healing transcripts and signaling pathways.

We next examined the early (14 DPI) transcriptome using RNA-Seq to determine which molecular mechanisms may have led to the functional and structural improvements that occurred in response to IL-10 delivery. Principal component analysis (PCA) revealed distinct transcriptome clustering within IL-10 treated, PBS controls, and uninjured contralateral with clear separation between each group. Notably, the IL-10 treated and PBS controls groups clustered in closer proximity to one another when compared to the uninjured controls, suggesting transcriptome commonalities resulting from VML injury independent of IL-10 treatment (**Fig. 3a**). When normalized to uninjured controls (cut off for differential expressed genes at FDR < 0.05 and $|\log_2 FC| > 1.5$), the two treatment groups shared 1653 differentially expressed genes (DEGs), while IL-10 had 1865 unique DEGs, and PBS had 198 unique DEGs (**Fig. 3b**).

Pathway analysis (normalized to uninjured controls) revealed that most of the top pathways (five pathways) were related to fibroblast / immune cell infiltration, immune cells/fibrosis signaling, and inflammation-related pathways (**Fig. 3c**) suggesting the delivery of exogenous IL-10 had a significant impact on immune system dynamics. It is also notable that the PBS controls group was characterized by less activation in all of the top IL-10 treatment group pathways with the exception of fibroblast cell activation. Direct comparison of the IL-10 treatment group transcriptome to PBS controls revealed that, IL-10 signaling was the most dominant pathway, as expected. Other top pathways involved enhanced muscle hypertrophy signaling, immune cell activity, and inflammation-related signaling pathways (**Fig. 3d**). Notably,

IL-10 uniquely upregulated cell marker (CD53) present on both macrophages and myoblasts that is critical to myofiber regeneration[28] as well as many pro and anti-inflammatory cytokines (ARG1, IL6, HGF) that were not affected in PBS controls (**Fig. 3e and Fig. S1**). Furthermore, IL-10 treatment enhanced expression of several chemotactic transcripts (Ccl2, Cxcl13) (**Fig. 3e**). These transcriptomic findings suggested that delayed IL-10 treatment broadly altered the post VML repair wound healing environment at 14 DPI which potentially enhanced muscle repair/regeneration via recruitment and activation of critical immune cell populations.

IL-10 delivery boosted the infiltration of pro-regenerative regulatory T cells at the site of VML repair.

We then examined infiltration of immune cells, using the transcriptomic data, immunohistochemistry (IHC), western blot, and multiplexed ELISA in order to narrow in on the types of immune cells present at the repair site following IL-10 treatment. At 14 DPI, immunoreactivity to the pan-T cell marker CD3e (**Fig. 4a and 4d**) was markedly increased within IL-10 treated repair site tissue, resulting in significantly ($p=0.029$) higher (128% compared to PBS) T cell counts in IL10 group (242 ± 87 cells/mm^2) tissue sections when compared to PBS controls (106 ± 15 cells/mm^2), suggesting IL-10 treatment increased VML repair site T cell infiltration during the early post treatment phase of muscle healing. To determine if exogenous IL-10 delivery also influenced the concentration of T cell related cytokines that had previously demonstrated upregulated expression, we measured the concentration (pg/mg protein) of IL-4 & IFN-γ using the tissue lysate extracted from the defect site. We found that IL-10 treatment significantly increased the tissue concentration of IL-4 ($p=0.01$), but did not affect IFN-γ. Specifically, the concentration of anti-inflammatory cytokine IL-4 measured within IL-10 treatment group tissue (2.62 ± 1.06 pg/mg) increased by 207% when

compared to PBS group concentration (0.85±0.09 pg/mg) (**Fig. 4e**). The increased IL-4 concentration and T-cell infiltration at the IL-10 treated VML repair site prompted us to examine the RNA-Seq data for unique T cell related markers. We found that IL-10 significantly upregulated the expression of several key T cell related markers (BTLA, CD4, CD8E, CD25), when compared to PBS controls, most notably IL33R/ST2, a surface receptor protein highly expressed in T_{regs} (**Fig. 4c**). The increased expression of ST2 within the repair site was also validated through IHC. Expression of ST2 was qualitatively increased within IL-10 treated tissue sections at 14 DPI when compared to PBS controls (**Fig. 4b**). Lastly, we measured the relative protein level of ST2 in all groups using western blots against ST2 (**Fig. 4f**). We found that while VML repair alone trended ($p=0.07$) toward higher ST2 proteins level (1.65±0.35) compared to uninjured controls (1±0.35), IL-10 treatment significantly doubled ($p=0.047$) this response (2.38±0.43) (**Fig. 4g**). When taken together, the RNA-Seq, ELISA, western blot, and histology results provide strong evidence that IL-10 treatment had a dramatic effect on T-cell accumulation and activation, specifically coaxing the muscle environment toward an anti-inflammatory/pro-regenerative state with an elevated presence of muscle T_{regs}-like cells. This finding points to a potential therapeutic mechanism responsible for the enhanced functional muscle recovery that was observed in response to delayed IL-10 treatment.

IL-10 delivery prolonged *de novo* myofiber regeneration and shortened macrophage residency.

To decipher the impact of IL-10 treatment on VML repair site myogenesis and macrophage dynamics we examined the repair site using immuno-stains directed against embryonic myosin heavy chain (eMHC), a marker protein present in de-novo myofibers, as well as the macrophage markers (CD68 and CD163) at both 14 and 56 DPI (**Fig. 5a, 5b, 5c**). VML

repair site immuno-reactivity to eMHC was more widespread within the repair site following IL-10 treatment as compared to PBS controls. Although quantitative assessment of eMHC+ de-novo myofiber count differences between IL-10 treatment (554±116 cells/mm^2) and PBS controls (352±141 cells/mm^2) showed some elevation in the IL-10 treatment groups, the difference approached ($p=0.058$) but did not reach statistical significance (**Fig. 5a and 5d**). However, eMHC expression was sustained in the IL-10 delivery group at 56 DPI, but not in PBS controls group, suggesting that while IL-10 may not have increased de-novo regeneration immediately following the treatment period (14 DPI), it appears to prolong de-novo muscle fiber regeneration within the VML repair site tissue (**Fig. 5c**). Similarly, we did not detect significant differences in either pan macrophage ($CD68^+$) density or activated M2c macrophage (CD163+) density in response to IL-10 treatment at 14 DPI (**Fig. 5b and 5e**). Yet, by 56 DPI, there were significantly ($p<0.005$) fewer macrophages ($CD68^+$) within the IL-10 treatment group tissue sections when compared to PBS controls (**Fig. 5f**), suggesting that IL-10 delivery may have modulated the immune environment in the longer term, resulting in accelerated macrophage clearance.

IL-10 delivery increased VEGF concentration and promoted repair site arteriole formation.

Lastly, to assess re-vascularization at the repair site, we measured capillary and arteriole density at 56 DPI using immunofluorescent antibodies directed against CD31 and α-SMA (**Fig. 6a and 6b**). Although, we did not detect a significant difference in $CD31^+$ capillary counts between groups, we did detect a dramatic ($p<0.0005$) increase (150%) in arteriole density (α-SMA^+) in response to IL-10 treatment when compared to PBS controls (**Fig. 6c and 6d**). Enhanced vascularization at the repair site via increased arteriole density could be a contributor to the sustained myofiber regeneration that was observed at 56 DPI in response to IL-10 treatment. To

identify a potential trigger for the increase in arteriole density we also measured (multiplexed ELISA) the concentration (pg/mg protein) of IL-6 and VEGF, cytokines with known angiogenic signaling functions[29,30], as well as the endothelial cell surface protein ICAM-1 using 14 DPI tissue lysate extracted from the defect site. We found that IL-10 injection significantly increased the levels of IL-6 ($p=0.001$) and VEGF ($p=0.039$), but did not affect ICAM-1. Specifically, the concentrations of IL-6 and VEGF collected from repair site tissue of IL-10 treatment group (0.84±1.14 pg/mg IL-6, 19.87±3.58 pg/mg VEGF) increased by 52% and 34% compared to PBS group (7.13±0.64 pg/mg IL-6, 14.82±3.16 pg/mg VEGF) respectively (**Fig. 6e and 6f)**. The increase in VEGF in the absence of ICAM-1 at 14 DPI might suggest that immediately following IL-10 treatment, a nascent pro-angiogenic environment was developing that had not yet stimulated increased endothelial cell infiltration.

4.4 Discussion

The results from this study suggest that delayed (1 week) and sustained (1 week) delivery of exogenous IL-10 can have a positive effect on muscle recovery when used in combination with regenerative medicine for the repair of VML injury. Study findings provide significant *in vivo* insights regarding the therapeutic potential of using immunotherapeutics to establish a pro-myogenic wound healing environment, which can in turn improve post VML repair muscle mass and contractile torque recovery. Our data are the first to show such an effect for muscle injury, and in fact, others have shown that delivery of IL-10 to injured muscle during the first week following muscle injury (days 2 and 4) slows regeneration [31]. While these prior findings contradict ours and would appear to discourage IL-10 delivery, our data underscore the importance of immunotherapy timing as well as differences in the immune response between muscle injury types (i.e. acute myotoxin injury versus VML). A full appreciation of endogenous

IL-10 production would suggest that early post injury delivery is unlikely to produce much benefit and may in fact suppress the necessary pro-inflammatory phase. As we described previously, the increase in endogenous IL-10 production during tissue healing from acute non-VML injury is delayed and timed to coordinate the transition from a pro-inflammatory to an anti-inflammatory muscle microenvironment[32]. In muscle, the timing corresponds to transition from the early proliferative to the later differentiation and growth stage of myogenesis, and as such, elevated IL-10 levels may be detrimental when delivered too early or ineffective when too late. Thus, we suspect that the delayed delivery was a critical factor responsible for the enhanced recovery we observed when exogenous IL-10 delivery was paired with a VML regenerative medicine strategy. Our encouraging preliminary efforts using a delayed IL-10 delivery scheme support this hypothesis and underscore the importance of immuno-modulator delivery timing as well as the need to consider the design of injury specific immuno-modulatory strategies.

The results suggest that exogenous delivery of IL-10 enhanced VML repair/recovery, in part via its anti-inflammatory effect on both macrophage and T-cell dynamics. In particular, delayed IL-10 treatment appeared to polarize the muscle environment toward a pro-regenerative/anti-inflammatory stage of wound healing that we suspect helped sustain the formation of *de novo* myofibers (**Fig. 5c**). Alternatively, the PBS controls group was characterized by a prolonged pro-inflammatory muscle immune environment that may have inhibited the survival and maturation of *de novo* myofibers. Specifically, IL-10 treatment doubled T-cell counts at the VML repair site during the early post treatment period (14 DPI) and decreased macrophage counts by half at later stages (56 DPI). As such, enhancing the level of pro-regenerative cytokines like IL-10 at the site of injury is a potential two-pronged immuno-modulatory strategy as it not only plays a well recognized role in the polarization of

macrophages towards the M2 phenotype [33], but our results suggest that it also has a positive effect on T-cell recruitment. In the context of VML, this is a novel finding that indicates a potentially powerful targeting mechanism for exogenous IL-10 during muscle regeneration, and also suggests the delivery of exogenous T-cells as a complementary immuno-modulatory strategy for VML. While the endogenous delivery of single cytokines like IL-10 enables tighter control of dosage and timing, it comes with a potentially narrowed immuno-modulatory impact. Alternatively, endogenous release of numerous cytokines by T cells is temporally regulated through cellular feedback mechanisms that would be impossible to reverse engineer. As such, exogenous T-cell delivery could provide a means to modulate the production of IL-10 as well as other key immuno-modulatory factors at the wound site through manipulation of cell delivery numbers. At this stage, neither the results of this study nor literature precedents, provide a strong exclusionary rationale for the delivery of either IL-10 or T-cells, and we suggest that future head-to-head examination of both cellular and protein-based strategies could provide unique insights into performance differences between immunomodulation modalities.

The results indicate that IL-10 treatment not only increased total T-cell ($CD3e^+$) numbers, but also doubled the immuno-reactivity against the ST2 protein compared to PBS[34] (**Fig. 4d** and **4g**). ST2 is a regulatory T cell (T_{reg}) marker, commonly expressed by activated T_{regs} in inflammatory environments, including on T_{regs} isolated from injured muscle[35]. Recent literature suggests that the presence of T_{regs} within the wound site is beneficial to muscle regeneration (reviewed in [24]). This distinct population of $ST2^+$ T_{reg} cells in skeletal muscle potentiates regeneration through direct signaling on progenitor cells and other immune cells at the injury site[36]. Specifically, the T_{reg} phenotype is known to promote muscle regeneration via the secretion of immuno-modulatory factors, including IL-4 and IL-33, that suppress pro-inflammatory M1 macrophages

and Th1 cells in combination with growth factors like AREG that promote the continued expansion and maintenance of muscle satellite cells [36]. Genes for all three of these key T_{reg} products (IL-4, IL-33, AREG) were significantly upregulated in response to IL-10 treatment (**Fig. 3d** and **4c**). Given that VML injury is known to impair the muscle's regenerative capacity due to a prolonged and dysregulated inflammatory feedback loop that persists even following regenerative repair, the broad immunosuppressive influence of T_{reg} cells would be expected to benefit recovery. T_{regs} can further enhance wound healing through the secretion of angiogenic (VEGF) and neuro-protective (IL-35) factors that our data suggests were also upregulated in response to IL-10 treatment [37,38]. As such, increasing T_{regs} recruitment at the repair site represents an attractive mean to enhance endogenous delivery of pro-regenerative signals to the repair site that enhance the repair of multiple tissues (vessel, nerve, myofiber). To definitely establish the role of T_{regs} during recovery from VML repair, future studies by others or us could take the logical next step and probe whether the elevated T_{reg} numbers were truly beneficial using T_{reg} depleted animal models[39]. If they are, the delivery of exogenous T_{reg} cells could be exploited to enhance the performance of VML regenerative medicine.

The enhanced functional recovery in response to IL-10 treatment may also be attributed in part to improved maintenance and repair of the residual injured muscle fibers that surround the VML repair site. We found that IL-10 injections significantly increased (2 fold increase) the expression of myoferlin (MYOF) (**Fig. 3d**). Myoferlin is highly expressed within multinucleated myofibers and surrounding mononuclear cells during muscle regeneration following injury and within myoblasts undergoing fusion during muscle development[40,41]. It has also been implicated in aiding fusion to reseal membrane disruption as well as endocytic recycling[42]. Furthermore, myoferlin can regulate growth-factor signaling, namely, promoting IL-4 production by myotubes

which in turn recruit myoblasts and enhance muscle repair/regeneration[43]. Multiplexed ELISA analysis revealed that IL-10 injections more than tripled the IL-4 concentration at the muscle injury site compared to PBS controls (**Fig. 4e**). Because T-cells and recovering myotubes can both produce IL-4, it is difficult to determine which cell type was responsible for the increase, but we suspect that IL-10 targeted both cell populations, creating a pro-regenerative myogenic and immunogenic muscle environment. If true, our data would indicate, and the known effects of IL-10 would support [18,23], a broad finding suggesting that IL-10 can enhance recovery from VML repair via its impact on overlapping feedback loops the modulate signaling molecules and receptors that direct the behavior of not just injury site cells, but also progenitor cells, damaged myotubes and T_{reg} cells in the surrounding muscle tissue.

We also detected an increase to both the expression (**Fig. 3d**) and concentration of vascular endothelial growth factor (VEGF) and IL-6 (**Fig. 6e and 6f**) at the VML repair site in response to IL-10 treatment. In the context of muscle injury, increased levels of VEGF during wound healing have been shown to enhance angiogenesis, via its effect on endothelial cell proliferation and migration[30]. As such, the increased level of VEGF in response to IL-10 treatment likely contributed to the increased arteriole density that was observed within the VML repair site at 56 DPI (**Fig. 6b**). The enhanced vascularization could also contribute to the prolonged *de novo* myofiber regeneration observed in IL-10 group. Increased VEGF concentration also plays a less recognized yet important role during axonogenesis and has been shown to accelerate neuromuscular junction regeneration, outcomes that would likely improve contractile signal transduction and in turn contractile torque recovery following VML injury and repair[44,45]. In addition to VEGF, the prolonged *de novo* myofiber survival observed in the IL-10 treatment group may in part be attributed to the significant increase to both the expression and

concentration of IL-6 within tissues collected from the site of repair. Generally considered a pro-inflammatory cytokine[46], the increased presence of IL-6 in response to IL-10 treatment could be viewed as paradoxical. However, IL-6 is a functionally pleiotropic growth and differentiation cytokine with context-dependent inflammatory and anti-inflammatory properties[47]. In that context, IL-6 can stimulate increased VEGF expression and production by myocytes and immune cells[48]. IL-6 can also enhance the secretion of IL-4 and IL-10 in immune cells and accelerate muscle regeneration via their effect on satellite cells[49,50]. Furthermore, studies have shown that IL-6 can enhance T cell survival and proliferation, especially under wound healing conditions, which corresponds well to our findings[51]. Although this increased IL-6 level may be responsible for the board upregulation of several chemotactic transcripts (Cxcl13, Ccl2), it was not complemented by other signs of increased pro-inflammatory cells within the IL-10 treatment group. Namely, at 14 DPI, both the IL-10 treatment and PBS controls groups had similarly high macrophage density (qualitatively), and by 56 DPI macrophage density had significantly decreased in the IL-10 treatment group (**Fig. 5f)**. Additionally, when compared to PBS group, IL-10 did not significantly change the level of neutrophil and M1 macrophage transcripts (LY6G6D, iNOS/NOS2), but significantly increased CD206/MRC1 (pan M2 macrophage marker) HGF, and IGF1 growth factor expression (**Fig. 3d**), findings consistent with reduced inflammation and polarization of the muscle wound healing environment towards growth and regeneration[52,53].

Lastly, the regenerative medicine test bed used to examine IL-10 immuno-modulatory performance deserves some discussion. We evaluated the effectiveness of a delayed IL-10 delivery strategy using autogenic minced muscle as the VML regenerative medicine strategy. Patient sourced minced muscle is a clinically attractive repair strategy that has shown

regenerative potential for the repair of VML injuries by our group and others [13,54,55]. However, while we employed the minced muscle approach as the test bed, the broader goal is development of an immunotherapeutic strategy that could be widely adopted to enhance VML regenerative medicine outcomes. With that broader use in mind, we see no reason why the main finding of this study, enhancement of muscle regeneration with delayed IL-10 treatment, could not be extended to other VML strategies, including those that employ implantable scaffolds, muscle stem cells, and/or pro-myogenic rehabilitation strategies[56-59]. In order to effectively translate this strategy for broader usage, it is important to also consider that the incorporation of exogenous cytokines into a regenerative medicine strategy is not trivial as cytokines are short-lived and require exquisite spatiotemporal control for appropriate function. In the case of Il-10, I.M injection of supraphysiological concetration of this cytokine in rodent was easily cleared within a day[60,61]. The maximum IL-10 concentration used in this study was determined using previous rodent research to simulate the highest concentration range of IL-10 after muscle injury [62-65]. As for the delivery window of exogenous IL-10, there are evidence that enhanced IL-10 level as early as 3 DPI and as late as 14 DPI can be beneficial to VML recovery. Although, we delivered IL-10 at 7 DPI out to 14 DPI to establish preliminary data on IL-10 as an adjunct treatment for VML repair, future studies should expand on the optimal delivery window for this type of therapy[26,66]. Lastly, the application of IL-10 as an immunotherapeutic need not be limited to use as an adjunct in combination with regenerative medicine. In order to sustain IL-10 in this study, it was injected at the repair site every other day for one week, an apparently effective, but potentially clinically cumbersome delivery approach. Alternatively, in order to maintain exogenous cytokines at the injury/repair site, it may be more efffective to employ a sustained release approach. For example, because collagen is a major component of muscle ECM as well

as many of the VML repair scaffolds being examined, it may be possible to anchor IL-10 to a scaffold and repair site using a collagen binding strategy to improve its residency. Using this technique, released IL-10 concentration can also be controlled in place of concentration spike. The indications for IL-10 delivery could include accelerated regeneration of surgical muscle trauma (ex. internal fixation placement or joint replacement) for even greater clinical impact.

4.5 Methods

Animal Model

Adult Sprague Dawley rats (n=20) weighing ~350 g, were subjected to an established VML injury model [67]. VML defects were created in the middle third of the Tibialis anterior (TA) muscle in the left leg by excising about 20% of the TA weight using an 8 mm biopsy punch. VML defect plugs were minced using a scalpel blade into 1 mm^3 fragments and used to repair the VML injuries. Fascia and skin were closed using interrupted stiches with 5-0 Vicryl sutures (J463G, Ethicon). The contralateral limb was not injured and served as an uninjured control. Buprenorphine (0.1 mL at 0.3 mg/mL) (LIST 7571, Buprenex) was administered to all rats subcutaneously for postoperative analgesia and access to Rimadyl (MD150-2, Bio-Serv) was provided at up to 1 mg per day for seven days post-injury + repair (DPI). Food and water were provided ad libitum. All animal procedures were approved by the Institutional Animal Care and Use Committee of the University of Arkansas. All experiments were performed in accordance with all guidelines and ARRIVE guidelines. Animals were randomly assigned to one of two treatment groups (n=10/treatment group): either rat recombinant IL-10 (400-19, PeproTech) in sterile phosphate buffered solution (PBS) (2000 ng/ml) or PBS injection (IM at site of repair) beginning 7 days after the initial surgery and continuing until day 14 (100µl every other day = 4

injections total) (**Fig. 1a-1b**). Animals (n=5/treatment/time point) from each treatment group were allowed either 14 or 56 days of recovery.

Electrophysiology

At 14 and 56 DPI, peak tetanic contractile torque of IL-10 treatment, PBS controls, and contralateral uninjured limbs was measured *in vivo* using techniques familiar to our groups and common to the field. To eliminate force contributions from the synergist muscle, distal tenotomies were performed on the extensor digitorum longus (EDL) and extensor halluces longus (EHL) after rats were anesthetized (2–2.5% isoflurane). Percutaneous needle electrodes were inserted into the anterior compartment of the TA to stimulate the peroneal nerve (150 Hz, 0.1 ms pulse width, 400 ms pulse train) by a S88 pulse stimulator (Grass Technologies, West Warwick) to induce contraction of the tibialis anterior muscle. Measurement of isometric torque (Nmm) was enabled by securing the foot of the limb to a force transducer system (Aurora Scientific) with surgical tape. To minimize muscle fatigue, 1-minute rest periods were taken between contraction cycles. The mean isometric torque value for each limb was calculated by averaging three contractions then normalizing to total animal mass (Nmm/kg body weight). The TA and EDL muscles were then harvested, weighed, and processed for further assessments. Tissue biopsies were collected (~30mg each) from the site of injury/treatment, snap frozen in liquid nitrogen, and stored at -80°C pending RNA isolation or protein lysate extraction. The rest of the muscle was flash frozen in isopentane (2-methylbutane) chilled in liquid nitrogen, and stored at -80°C. All animals were then euthanized by carbon dioxide inhalation in accordance with guidelines provided by the AVMA Panel on Euthanasia of Animals.

Histological Analysis

Tissue cross-sections (8μm) of the repair site were obtained via cryostat (Leica BioSystems) maintained at a temperature between -25 and -20°C. Prior to immunostaining, slides were permeabilized in 0.1% 100X triton and then rinsed in PBS. Sections were blocked in PBS containing 4% goat serum and 0.05% sodium azide for 1h at room temperature. Slides were immuno-stained using primary antibodies (1:300) directed against: laminin (PA116730, Invitrogen) , embryonic myosin heavy chain (eMHC) (F1.652, Hybridoma Bank), CD68 (MA6-13324, Invitrogen), CD163 (MCA342R, Bio-rad), CD3e (MA1-90582, Invitrogen), collagen I (Col I) (NB600-450, Novus Biologicals), CD31(Pa5-32321, Invitrogen), and α-smooth muscle actin (α-SMA) (ab7817,abcam) followed by incubation of appropriate fluorescently labeled secondary antibodies (Alexa Flour, Invitrogen). Additional tissue sections were stained using hematoxylin and eosin (VWR) following manufacturer's guidelines. All sections were digitally imaged (Nikon CiL).

Representative tissue sections collected from four to five animals per group were used for all calculations. Three separate regions/section/stain/animal were imaged (40X and 100X) at the site of injury or repair. Laminin stained images (100X) (**Fig. S2b**) were analyzed using in-house developed codes in ImageJ (NIH) to automatically isolate the borders of individual muscle fibers and compute muscle fiber cross-sectional area[68]. Fiber cross sectional area (μm^2) for all fibers within an individual image (typically 100+ fibers) were calculated. Col I stained images (100X) (**Fig. S2a**) were analyzed using ImageJ code to isolate Col I positive tissue regions within each section and calculate the percentage of total tissue area (% Col I)[68]. Laminin co-stained with eMHC images (100X) were superimposed and to identify de-novo myofibers (fibers with clear laminin boundary and also immuno-reactive to eMHC). The total numbers of these fibers were

manually counted for each imaged section and presented as de-novo myofiber density (myofibers/mm^2). CD68, CD163 and CD3e stained images (100x) were analyzed using ImageJ code to automatically count the density of total macrophage, M2 macrophage and T-cell, respectively, presented as cells/mm^2. CD31 and α-SMA images (100x) were manually counted to compute the density of capillary and arteriole (per mm^2), respectively.

Transcriptome analysis

Tissue biopsies for RNA extraction and subsequent sequencing were sent out to a commercial lab (BGI Genomic Services) for RNA-Seq analysis using BGISeq-500 platform to a mean depth of 20,000,000 reads per library. RNA sequencing reads were mapped to the Rattus norvegicus genome (RGSC build 6.0) from USCS using the 2-pass STAR protocol[69]. Reads were quantified using FeatureCounts[70], followed by analysis of differential expression and normalization in EdgeR[71]. Differential expression was selected using a maximum false discovery rate (FDR) of 0.05 and a minimum log fold change of 1.5. Pathway level analysis was also performed using Ingenuity Pathway Analysis (IPA) (Qiagen)[72].

Lysate extraction

Tissue biopsies were homogenized to extract protein lysate using RIPA Lysis Buffer System (sc-24948, Santa Cruz Biotechnology)[73]. Homogenates were centrifuged at 13,000g for 5 min at 4ºC, and the supernatant was collected. Protein concentration was determined using a bicinchoninic acid assay (BCA) (2322, Life Technologies).

Multiplexed Immunoassay

Magnetic Luminex Multiplex Immunoassay performed on a MAGPIX Luminex instrument and with the aid of Millipore Luminex software was used to measure the levels of various cytokines in protein lysate extracted from TA muscle tissue as previously described[74]. The Rat Premixed Multi-Analyte Kit (LXSARM-10, R&D Systems) including IL-4, IL-6, VEGF, and IL-10, ICAM-1, IFN-γ were used to create the standard curve. All reagents were prepared according to the manufacturer's protocol provided. Each standard and sample was added in duplicate. The analysis software was set to acquire data using 50 μL of sample per well, to collect a total of 1000 beads with an average of 50 events/bead. The raw data was collected as median fluorescence intensity (MFI). The lower limit of quantification was determined using the lowest standard that was at least 3 times above background. The concentrations of each cytokine were calculated using the MFI and from the standard curve obtained. The concentrations were then normalized to the total protein in each sample, presented as pg/mg of total protein.

Immunoblotting

Immunoblotting of proteins related to muscle protein synthesis and T-regulatory cell marker was measured as previously described[75]. Muscle homogenate (40 μg) was fractionated in 10% SDS-polyacrylamide gels. Gels were transferred to polyvinylidene difluoride (PVDF) membranes. Membranes were stained with Ponceau S before blotting to verify equal loading of the gels. Membranes were blocked in 5% milk, in Tris-buffered saline with 0.1% Tween-20 (TBST), for 2 h. Primary antibodies for 4E-BP1, Phospho-4E-BP1 (9644, 2855, Cell Signaling), and ST2 (11920-1-AP, Invitrogen) were diluted 1:1000 to 1:2000 in TBST and incubated at 4 °C overnight. Anti-rabbit and Anti-mouse monoclonal secondary antibodies (Cell Signaling Technologies) were diluted 1:2,000 in 5% milk, in TBST, and then incubated at room

temperature for one hour. The Ponceau-stained membranes were digitally scanned, and the 45-kDa actin bands were quantified by densitometry and used as a protein loading correction factor for each lane. Immunoblots were imaged with the Li-Cor Odyssey Fc System and quantified with Image Studio Software (Li-Cor).

Data Analysis

Statistical analyses for assessment of non-omics data were performed on JMP software, using Student's t-test or ANOVA with Tukey's test post-hoc. Assessment of significance for differential gene expression was performed using adjustment of p-values (FDR) for multiple comparisons by the Benjamini-Hochberg procedure. Significance was accepted at $P \leq 0.05$ (*) $P \leq 0.01$ (**), $P \leq 0.001$ (***), and $P \leq 0.0001$ (****). Quantitative data are displayed as mean + standard deviation.

Data Availability

The datasets generated during and/or analyzed in this study are available from the corresponding author on reasonable request. All RNA-seq data generated in this study have been deposited in the National Center for Biotechnology Information (NCBI) Gene Expression Omnibus (GEO) database under the accession codes GSE206823.

4.6 Figure

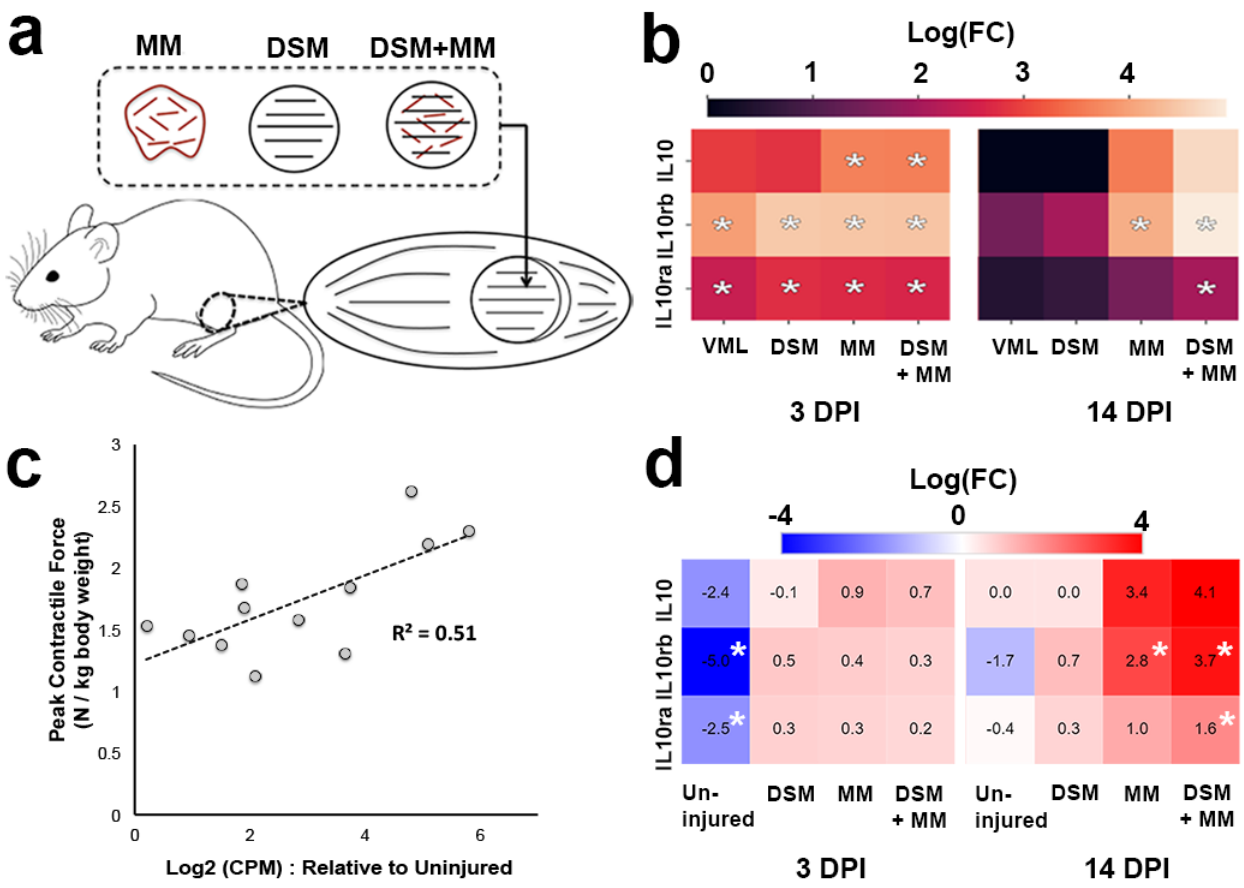

Figure 1: The IL-10 signaling node appears to be a promising immunotherapeutic target for the treatment of VML injury. **(a)** Rat tibialis anterior muscles were ablated with an 8 mm diameter biopsy punch to create a VML defect removing approximately 20% of muscle mass. VML defects were immediately subjected to implant repair strategies including minced muscle (MM), decellularized skeletal muscle (DSM), and a combination of the two (DSM+MM). (**b**) Heatmap of gene expression (log_2FC) for all treatment groups relative to uninjured muscle for key IL-10 signaling related genes. (**c**) IL10R expression correlated moderately with animal limb torque outcomes at 14 DPI, indicated through linear regression with $R^2 = 0.51$. (**d**) Heatmap of gene expression (log_2FC) for all groups relative to VML no repair injured muscle for key IL-10 signaling related genes. Asterisks (*) indicate measurements meeting differential gene expression criteria; $|log_2FC| > 1.5$) and $p < 0.05$.

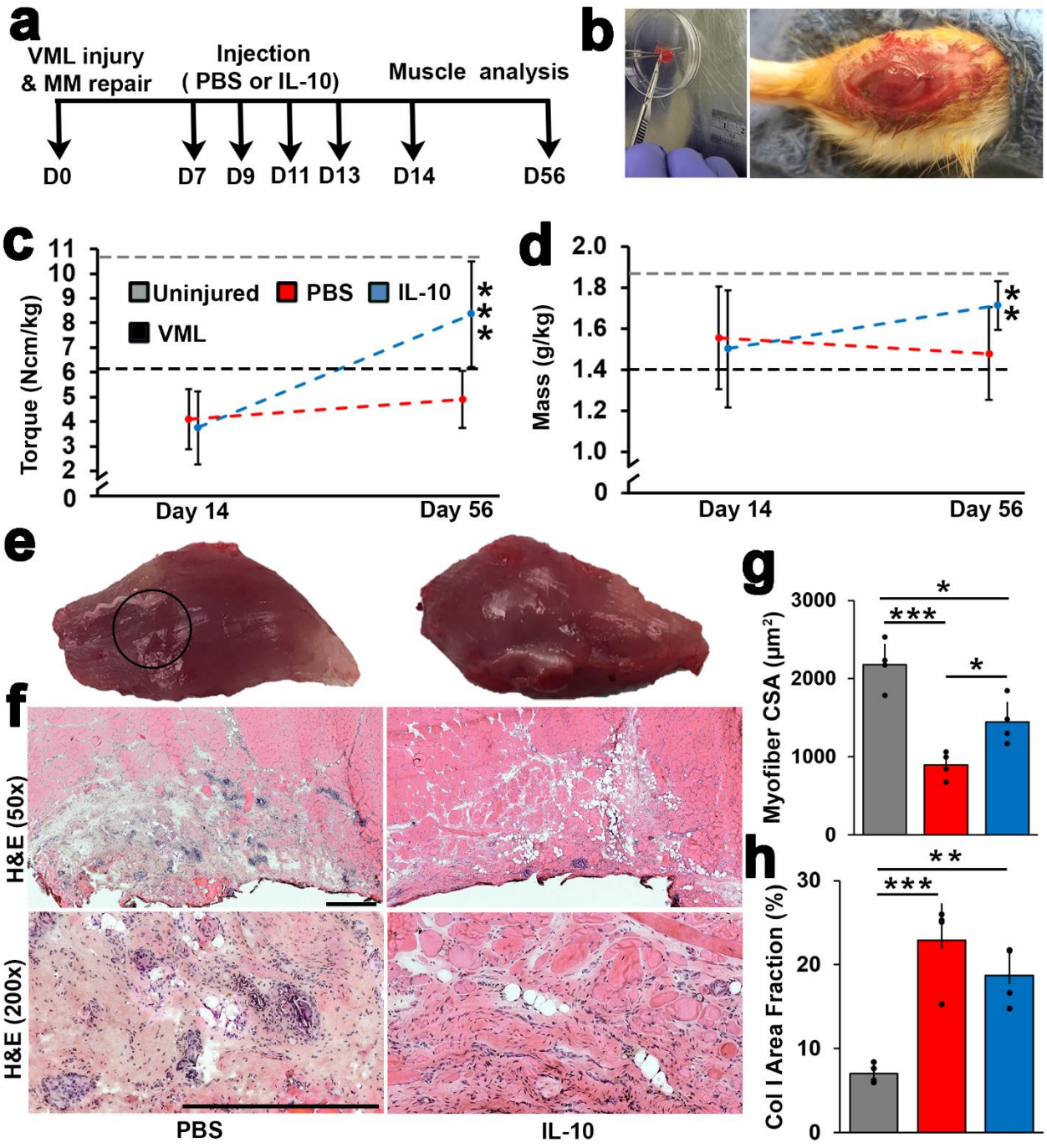

Figure 2: Delayed IL-10 delivery improved functional and structural recovery following VML repair. **a**) VML injuries were created and repaired using autologous MM. One week following repair, recombinant rat IL-10 was injected at the repair site every other day for one week. (**b**) Autologous MM grafts were prepared by mincing all of the removed muscle plug using a scalpel and scissors. The resulting MM paste was packed into the defect site; the fascia at the defect site was sutured to secure the MM paste in place. (**c**) Tibialis anterior (TA) electrophysiological measurement of mean peak contractile torque (Ncm/kg rat body weight) and (**d**) mass (g/kg rat

body weight) for IL-10 treated and PBS controls groups were assessed at 14 and 56 DPI. Average torque and mass from uninjured controls (accessed in this study) and VML with no repair groups at 56 DPI (accessed in previously published study[76]) were presented as 2 parallel dashed lines. Error bars are presented as ± standard deviation, with n = 5 animals per treatment group and timepoint. (**e)** Representative image of gross appearance of TA for PBS (left) and IL-10 (right) at 56 DPI are presented. Black circle indicates VML injury and repair site. (**f**) Representative H&E stained TA muscle cross-sections collected at 56 DPI from PBS and IL-10 groups at 50x and 200x show regions of tissue healing, cell infiltrations and the anterior TA surface. Scale bar = 250µm. Cross-sections were quantified for (**g**) collagen I area fraction (% Col I) and (**h**) muscle fiber cross-sectional area (µm^2). Group means + SD are presented; n=4/group. The * ,**, and *** indicate statistically significant difference of p<0.05, p<0.01, and p<0.001 between groups.

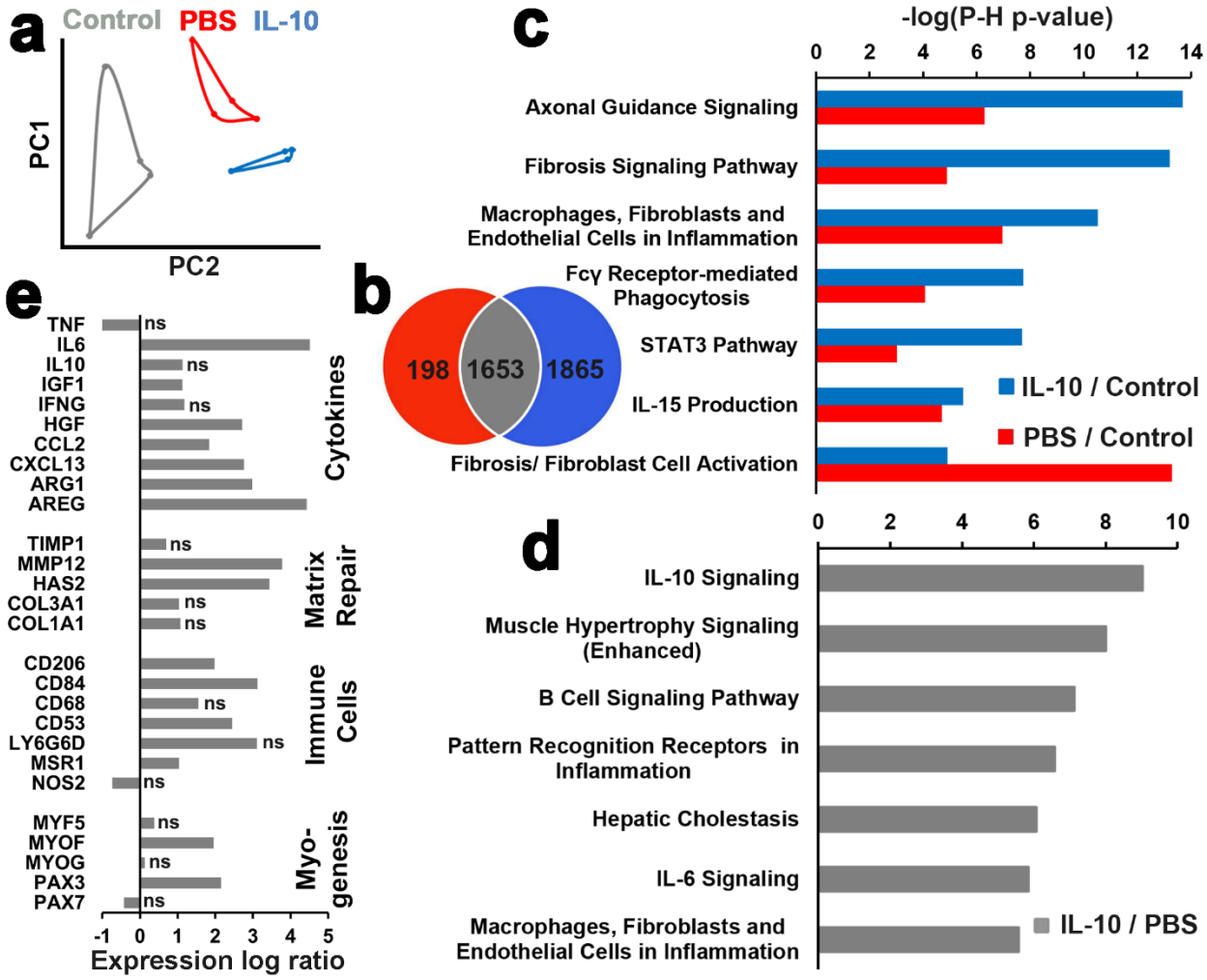

Figure 3: Delayed IL-10 delivery enhanced key muscle wound healing transcripts and signaling pathways. (**a**) PCA of TA skeletal muscle transcriptomes from uninjured, PBS, and IL-10 groups

normalized CPM using all transcripts. (**b**) Venn diagram illustrates differentially expressed gene counts for IL-10 treatment and PBS controls groups with respect to uninjured controls. (**c**) Top canonical pathways based on the Ingenuity Pathway Analysis (IPA) assessment of differentially expressed genes (FDR < 0.05 and $|\log_2 FC| > 1.5$) within IL-10 treatment and PBS controls with respect to uninjured controls. (**d**) Top canonical pathways based on IPA assessment of differentially expressed genes of IL-10 with respect to PBS. "ns" indicates no significant difference (FDR > 0.05). (**e**) Selected gene expression for key IL-10 treatment group genes with respect to PBS controls are presented as log ratio ($\log_2 FC$)

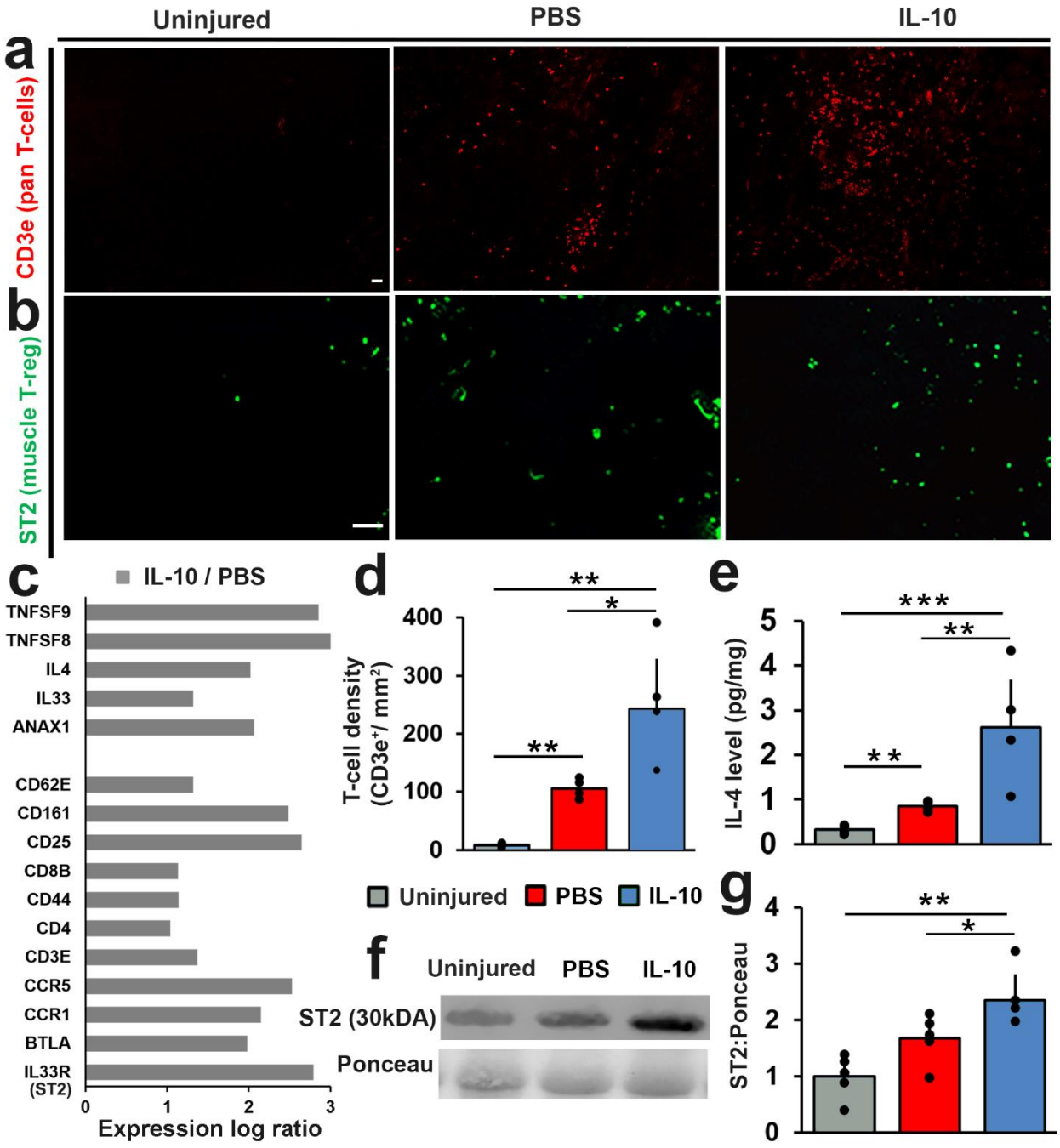

Figure 4: IL-10 delivery boosted the infiltration of pro-regenerative T-regulatory cells at the site of VML repair. TA muscle cross-sections were stained for (**a**) CD3e (red) and (**b**) ST2 (green). Representative TA cross-sections from uninjured, PBS, and IL-10 are presented. Scale bar = 100μm. (**c**) Key differentially expressed (FDR < 0.05) T-cell related genes are presented as log ratio (log_2FC) by comparing the transcriptome of IL-10 treatment to PBS controls. (**d**) CD3e immunostained tissue cross-sections were used to quantify T-cells density ($CD3e^+/mm^2$). (**e**) IL-4 concentration (pg/mg) was determined from protein lysate using multiplexed ELISA. (**f**) Representative immunoblots stained with ST2 and Ponceau (original blot images shown in **Fig. S3**). (**g**) The relative (to Ponceau) ST2 protein contents for both IL-10 treatment and PBS controls were quantified from Western blots. ST2 protein concentration values were normalized to uninjured controls. Group means + SD are presented; n=4-5/group. The *, **, and *** indicate statistically significant difference of $p<0.05$, $p<0.01$, and $p<0.001$ between groups.

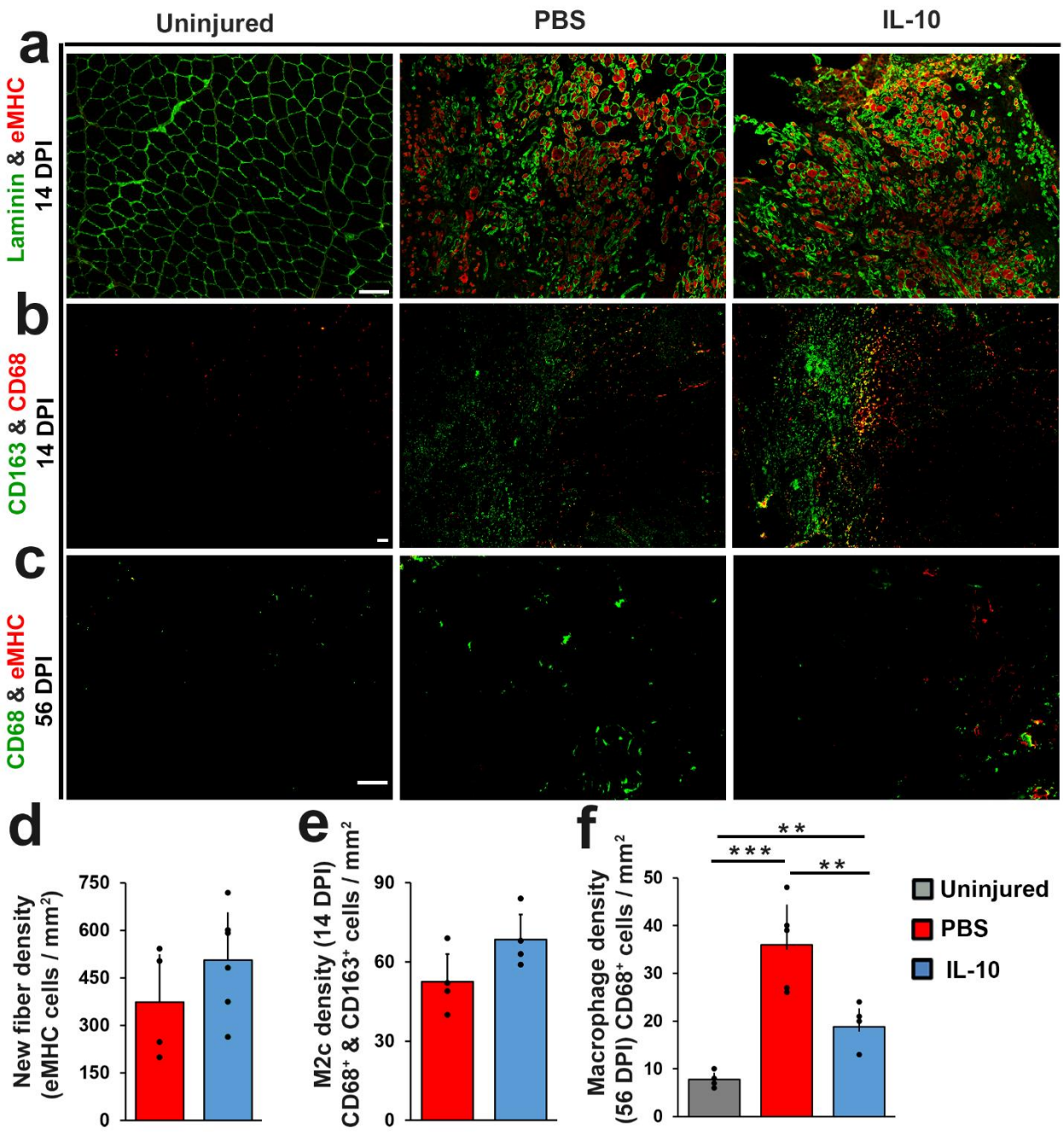

Figure 5: IL-10 delivery prolonged *de novo* myofiber regeneration and shortened macrophage residency delivery. TA muscle cross-sections prepared from 14 DPI tissue samples were co-stained for (**a**) CD68 (red) with CD163 (green) or (**b**) Laminin (green) with eMHC (red). (**c**) TA muscle cross-sections prepared from 56 DPI tissue samples were co-stained for CD68 (green) with eMHC (red). Scale bar = 100µm. Immuno-stained tissue cross sections prepared from 14 DPI tissue samples were quantified to determine (**d**) *de novo* myofiber density ($eMHC^+$ cells/mm^2), (**e**) M2c density ($CD68^+$ & $CD163^+$ cells/mm^2). (**f**) Immuno-stained tissue cross

sections prepared from 56 DPI tissue samples were quantified to determine macrophage density ($CD68^+$ cells /mm^2). Group means + SD are presented; n=4-5/group. The * ,**, and *** indicate statistically significant difference of $p<0.05$, $p<0.01$, and $p<0.001$ between groups.

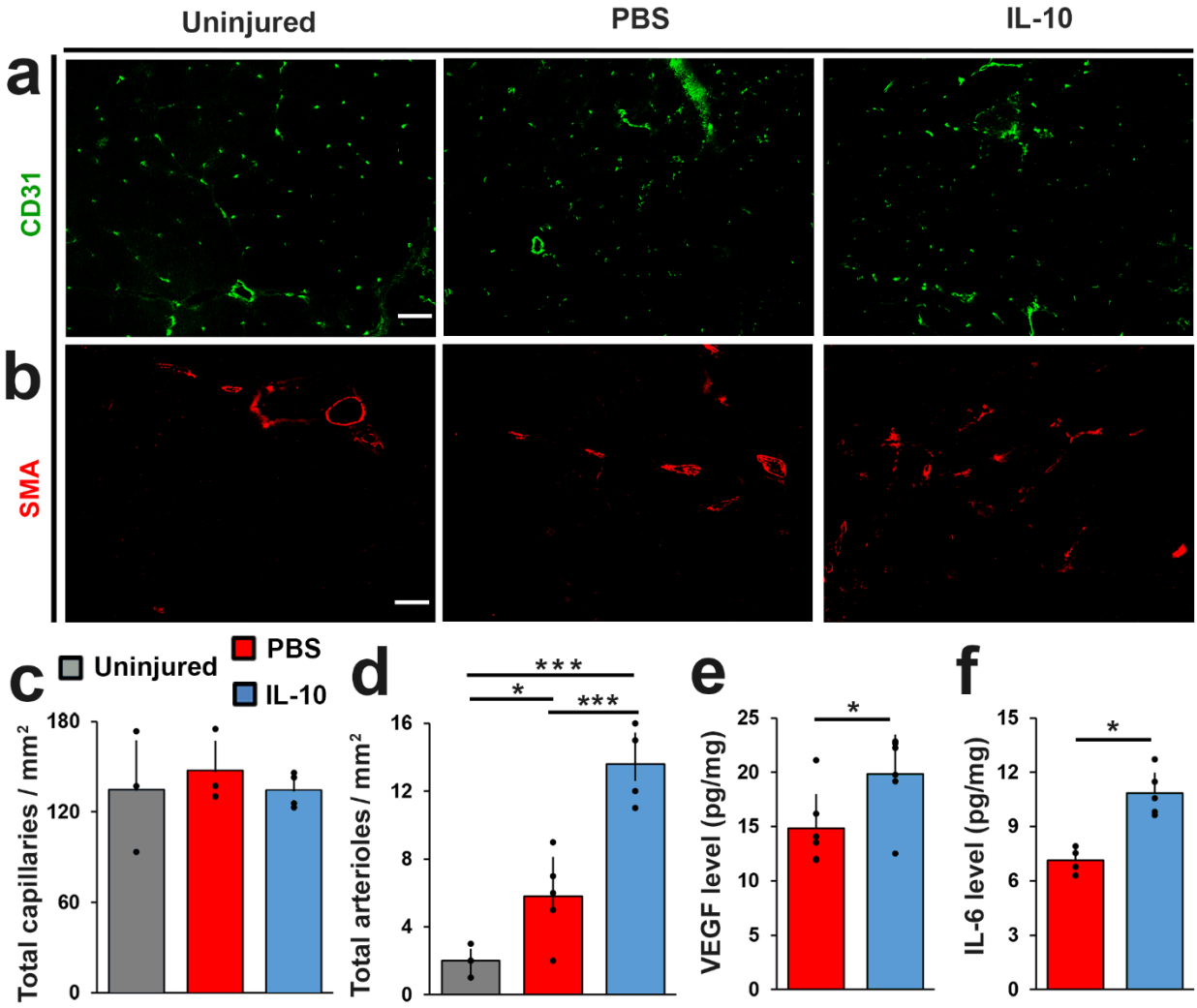

Figure 6: IL-10 promoted repair site arteriole formation. TA muscle cross-sections prepared from 56 DPI were individually stained for (**a**) CD31 (green) or (**b**) α-SMA (red). Scale bar = 100μm. Immuno-stained tissue cross sections prepared from 56 DPI tissue samples were quantified to determine (**c**) capillary density (capillaries/mm^2), and (**d**) arteriole density (arterioles/mm^2). (**e**) VEGF and (**f**) IL-6 concentrations (pg/mg) were measured from 14 DPI tissue samples using multiplex ELISA. Group means + SD are presented; n=4-5/group. The * ,**, and *** indicate statistically significant difference of $p<0.05$, $p<0.01$, and $p<0.001$ between groups.

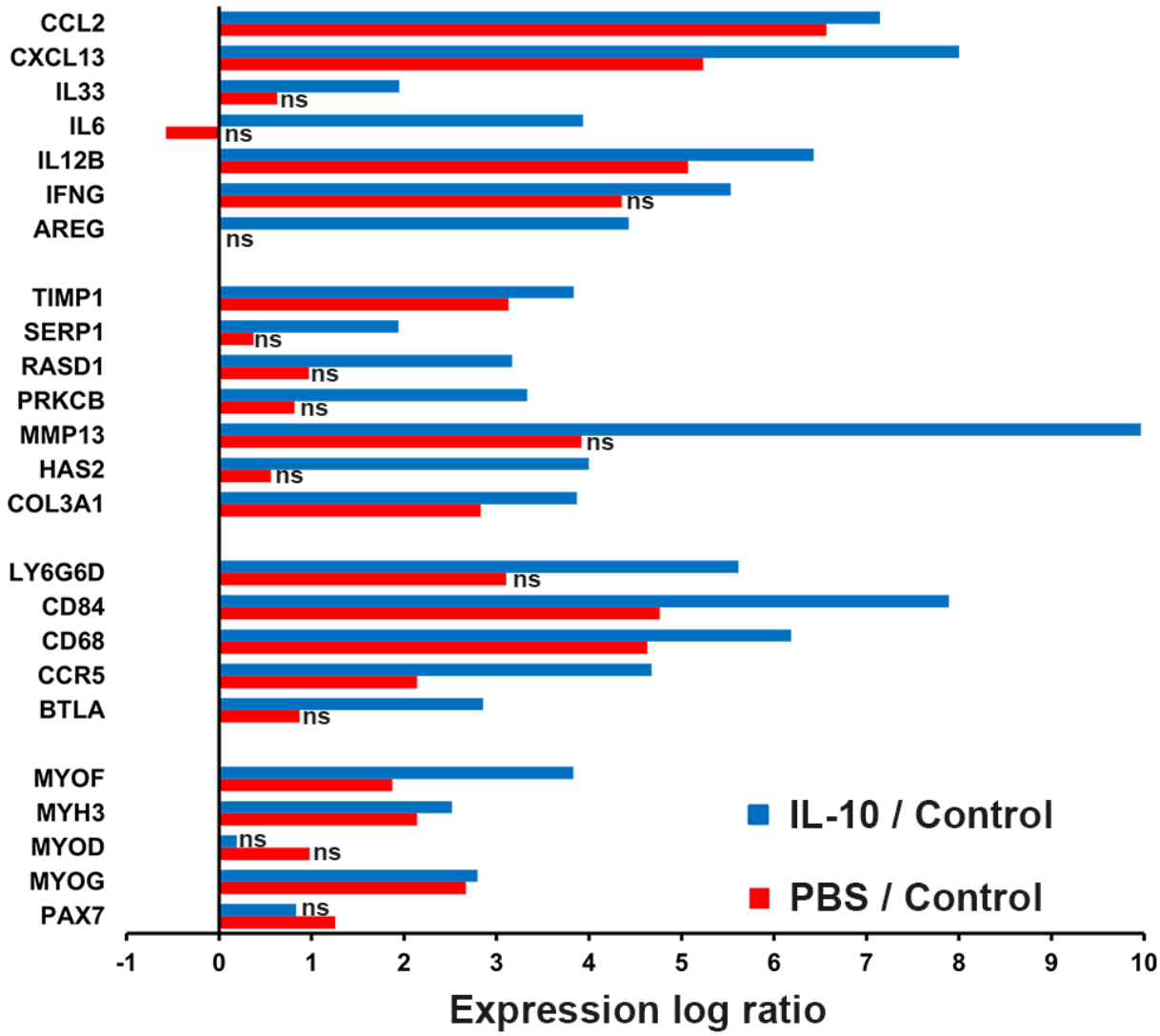

Supplementary figure 1: Selected gene expression for key IL-10 treatment and PBS controls genes with respect to uninjured controls are presented as log ratio (log_2FC). "ns" indicates no significant difference (FDR > 0.05).

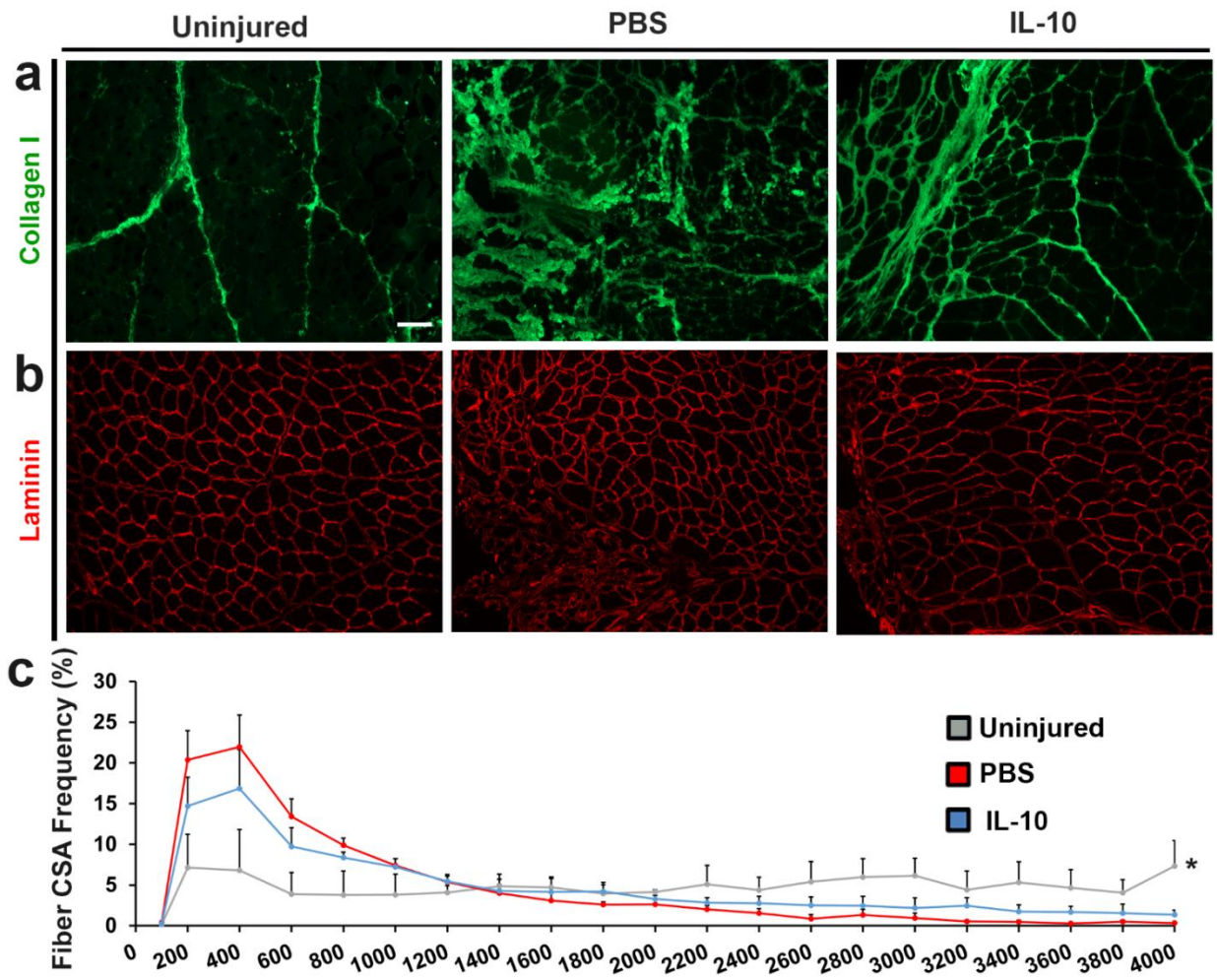

Supplementary figure 2: TA muscle cross-sections were stained for (a) collagen I (green), b) Laminin (red). Representative uninjured (left), 56 days post PBS injection (middle), and IL-10 injection (right) TA cross-sections are presented. Scale bar = 100µm. Lamin cross-sections were used to quantified for (c) muscle fiber cross-sectional area frequency distribution curve. About 600 fibers from and nearby to injury sites were included per animal, with 4 animals per groups. PBS and IL-10 curves displays a similar range of CSA values but are statistically different from injured control (Chi-squared analysis with $\alpha < 0.05$). Group means + SD are presented; n=4/bin/group. The * indicates statistically significant difference between uninjured controls and treatment groups.

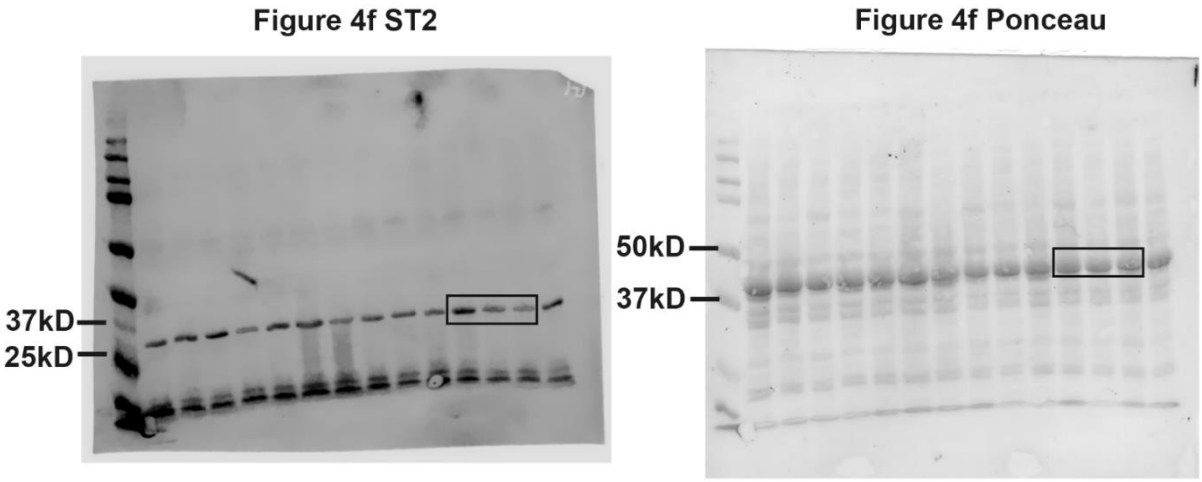

Supplementary figure 3: Original images of Western blots in **Fig. 4f**.

4.7 References

1. Hill, M., Wernig, A. & Goldspink, G. Muscle satellite (stem) cell activation during local tissue injury and repair. *J Anat* **203**, 89-99 (2003).

2. Mauro, A. Satellite cell of skeletal muscle fibers. *The Journal of biophysical and biochemical cytology* **9**, 493-495 (1961).

3. Corona, B.T., Rivera, J.C., Owens, J.G., Wenke, J.C. & Rathbone, C.R. Volumetric muscle loss leads to permanent disability following extremity trauma. *Journal of rehabilitation research and development* **52**, 785-792 (2015).

4. Corona, B.T., Wenke, J.C. & Ward, C.L. Pathophysiology of Volumetric Muscle Loss Injury. *Cells, tissues, organs* **202**, 180-188 (2016).

5. Hurtgen, B.J., *et al.* Severe muscle trauma triggers heightened and prolonged local musculoskeletal inflammation and impairs adjacent tibia fracture healing. *J Musculoskelet Neuronal Interact* **16**, 122-134 (2016).

6. Terada, N., Takayama, S., Yamada, H. & Seki, T. Muscle repair after a transsection injury with development of a gap: an experimental study in rats. *Scand J Plast Reconstr Surg Hand Surg* **35**, 233-238 (2001).

7. Kasukonis, B., *et al.* Codelivery of Infusion Decellularized Skeletal Muscle with Minced Muscle Autografts Improved Recovery from Volumetric Muscle Loss Injury in a Rat Model. *Tissue Eng Part A* (2016).

8. Hurd, S.A., Bhatti, N.M., Walker, A.M., Kasukonis, B.M. & Wolchok, J.C. Development of a biological scaffold engineered using the extracellular matrix secreted by skeletal muscle cells. *Biomaterials* **49**, 9-17 (2015).

9. Kasukonis, B., Kim, J., Washington, T. & Wolchok, J. Development of an infusion bioreactor for the accelerated preparation of decellularized skeletal muscle scaffolds. *Biotechnology progress* (2016).

10. Wilson, K., Terlouw, A., Roberts, K. & Wolchok, J.C. The characterization of decellularized human skeletal muscle as a blueprint for mimetic scaffolds. *Journal of materials science. Materials in medicine* **27**, 125 (2016).

11. Kim, J., *et al.* Graft alignment impacts the regenerative response of skeletal muscle after volumetric muscle loss in a rat model. *Acta biomaterialia* (2020).

12. Kim, J.T., *et al.* Regenerative Repair of Volumetric Muscle Loss Injury is Sensitive to Age. *Tissue engineering. Part A* **26**, 3-14 (2020).

13. Corona, B.T., *et al.* Autologous minced muscle grafts: a tissue engineering therapy for the volumetric loss of skeletal muscle. *American journal of physiology. Cell physiology* **305**, C761-775 (2013).

14. Corona, B.T., *et al.* Further development of a tissue engineered muscle repair construct in vitro for enhanced functional recovery following implantation in vivo in a murine model of volumetric muscle loss injury. *Tissue engineering. Part A* **18**, 1213-1228 (2012).

15. Corona, B.T., Ward, C.L., Baker, H.B., Walters, T.J. & Christ, G.J. Implantation of in vitro tissue engineered muscle repair constructs and bladder acellular matrices partially restore in vivo skeletal muscle function in a rat model of volumetric muscle loss injury. *Tissue engineering. Part A* **20**, 705-715 (2014).

16. Machingal, M.A., *et al.* A tissue-engineered muscle repair construct for functional restoration of an irrecoverable muscle injury in a murine model. *Tissue engineering. Part A* **17**, 2291-2303 (2011).

17. Merritt, E.K., *et al.* Repair of traumatic skeletal muscle injury with bone-marrow-derived mesenchymal stem cells seeded on extracellular matrix. *Tissue engineering. Part A* **16**, 2871-2881 (2010).

18. Tidball, J.G. Regulation of muscle growth and regeneration by the immune system. *Nature reviews. Immunology* **17**, 165-178 (2017).

19. Tidball, J.G. Inflammatory processes in muscle injury and repair. *American journal of physiology. Regulatory, integrative and comparative physiology* **288**, R345-353 (2005).

20. Brunelli, S. & Rovere-Querini, P. The immune system and the repair of skeletal muscle. *Pharmacological research* **58**, 117-121 (2008).

21. Deyhle, M.R. & Hyldahl, R.D. The Role of T Lymphocytes in Skeletal Muscle Repair From Traumatic and Contraction-Induced Injury. *Frontiers in physiology* **9**, 768 (2018).

22. Tidball, J.G. Mechanisms of muscle injury, repair, and regeneration. *Comprehensive Physiology* **1**, 2029-2062 (2011).

23. Tidball, J.G. & Villalta, S.A. Regulatory interactions between muscle and the immune system during muscle regeneration. *American journal of physiology. Regulatory, integrative and comparative physiology* **298**, R1173-1187 (2010).

24. Bonomo, A., *et al.* Crosstalk Between Inate and T Cell Adaptive Immunity With(in) the Muscle. *Frontiers in physiology* **11**, 1-11 (2020).

25. Wynn, T.A. & Vannella, K.M. Macrophages in Tissue Repair, Regeneration, and Fibrosis. *Immunity* **44**, 450-462 (2016).

26. Hurtgen, B.J., *et al.* Autologous minced muscle grafts improve endogenous fracture healing and muscle strength after musculoskeletal trauma. *Physiological reports* **5**(2017).

27. Crum, R.J., *et al.* Transcriptomic, Proteomic, and Morphologic Characterization of Healing in Volumetric Muscle Loss. *Tissue engineering. Part A* (2022).

28. Simpson, R.J., Florida-James, G.D., Whyte, G.P. & Guy, K. The effects of intensive, moderate and downhill treadmill running on human blood lymphocytes expressing the adhesion/activation molecules CD54 (ICAM-1), CD18 (beta2 integrin) and CD53. *European journal of applied physiology* **97**, 109-121 (2006).

29. Gopinathan, G., *et al.* Interleukin-6 Stimulates Defective Angiogenesis. *Cancer research* **75**, 3098-3107 (2015).

30. Hoeben, A., *et al.* Vascular endothelial growth factor and angiogenesis. *Pharmacological reviews* **56**, 549-580 (2004).

31. Perdiguero, E., *et al.* p38/MKP-1-regulated AKT coordinates macrophage transitions and resolution of inflammation during tissue repair. *The Journal of cell biology* **195**, 307-322 (2011).

32. Sag, D., Carling, D., Stout, R.D. & Suttles, J. Adenosine 5'-monophosphate-activated protein kinase promotes macrophage polarization to an anti-inflammatory functional phenotype. *Journal of immunology* **181**, 8633-8641 (2008).

33. Deng, B., Wehling-Henricks, M., Villalta, S.A., Wang, Y. & Tidball, J.G. IL-10 triggers changes in macrophage phenotype that promote muscle growth and regeneration. *Journal of immunology* **189**, 3669-3680 (2012).

34. Schmitz, J., *et al.* IL-33, an interleukin-1-like cytokine that signals via the IL-1 receptor-related protein ST2 and induces T helper type 2-associated cytokines. *Immunity* **23**, 479-490 (2005).

35. Kuswanto, W., *et al.* Poor Repair of Skeletal Muscle in Aging Mice Reflects a Defect in Local, Interleukin-33-Dependent Accumulation of Regulatory T Cells. *Immunity* **44**, 355-367 (2016).

36. Burzyn, D., *et al.* A special population of regulatory T cells potentiates muscle repair. *Cell* **155**, 1282-1295 (2013).

37. Lužnik, Z., Anchouche, S. & Dana, R. Regulatory T Cells in Angiogenesis. **205**, 2557-2565 (2020).

38. Machhi, J., *et al.* Harnessing regulatory T cell neuroprotective activities for treatment of neurodegenerative disorders. **15**, 32 (2020).

39. Weirather, J., *et al.* Foxp3+ CD4+ T cells improve healing after myocardial infarction by modulating monocyte/macrophage differentiation. *Circulation research* **115**, 55-67 (2014).

40. Doherty, K.R., *et al.* Normal myoblast fusion requires myoferlin. *Development* **132**, 5565-5575 (2005).

41. Demonbreun, A.R., *et al.* Myoferlin regulation by NFAT in muscle injury, regeneration and repair. *J Cell Sci* **123**, 2413-2422 (2010).

42. Doherty, K.R., *et al.* The endocytic recycling protein EHD2 interacts with myoferlin to regulate myoblast fusion. *Journal of Biological Chemistry* **283**, 20252-20260 (2008).

43. Horsley, V., Jansen, K.M., Mills, S.T. & Pavlath, G.K. IL-4 acts as a myoblast recruitment factor during mammalian muscle growth. *Cell* **113**, 483-494 (2003).

44. Borselli, C., *et al.* Functional muscle regeneration with combined delivery of angiogenesis and myogenesis factors. *Proceedings of the National Academy of Sciences of the United States of America* **107**, 3287-3292 (2010).

45. Borselli, C., Cezar, C.A., Shvartsman, D., Vandenburgh, H.H. & Mooney, D.J. The role of multifunctional delivery scaffold in the ability of cultured myoblasts to promote muscle regeneration. *Biomaterials* **32**, 8905-8914 (2011).

46. Uciechowski, P. & Dempke, W.C.M. Interleukin-6: A Masterplayer in the Cytokine Network. *Oncology* **98**, 131-137 (2020).

47. Akdis, M., *et al.* Interleukins, from 1 to 37, and interferon-gamma: Receptors, functions, and roles in diseases. *J Allergy Clin Immun* **127**, 701-U317 (2011).

48. Huey, K.A. Potential Roles of Vascular Endothelial Growth Factor During Skeletal Muscle Hypertrophy. *Exercise and sport sciences reviews* **46**, 195-202 (2018).

49. Meng, J., *et al.* Accelerated regeneration of the skeletal muscle in RNF13-knockout mice is mediated by macrophage-secreted IL-4/IL-6. *Protein & cell* **5**, 235-247 (2014).

50. Growth Factors and Cytokines in Skeletal Muscle Development, Growth, Regeneration and Disease Introduction. *Growth Factors and Cytokines in Skeletal Muscle Development, Growth, Regeneration and Disease* **900**, V-Vii (2016).

51. Rochman, I., Paul, W.E. & Ben-Sasson, S.Z. IL-6 increases primed cell expansion and survival. *Journal of immunology* **174**, 4761-4767 (2005).

52. Sawano, S., *et al.* Supplementary immunocytochemistry of hepatocyte growth factor production in activated macrophages early in muscle regeneration. *Animal science journal = Nihon chikusan Gakkaiho* **85**, 994-1000 (2014).

53. Tonkin, J., *et al.* Monocyte/Macrophage-derived IGF-1 Orchestrates Murine Skeletal Muscle Regeneration and Modulates Autocrine Polarization. *Molecular therapy : the journal of the American Society of Gene Therapy* **23**, 1189-1200 (2015).

54. Kasukonis, B., *et al.* Codelivery of Infusion Decellularized Skeletal Muscle with Minced Muscle Autografts Improved Recovery from Volumetric Muscle Loss Injury in a Rat Model. *Tissue engineering. Part A* **22**, 1151-1163 (2016).

55. Ward, C.L., *et al.* Autologous Minced Muscle Grafts Improve Muscle Strength in a Porcine Model of Volumetric Muscle Loss Injury. *Journal of orthopaedic trauma* **30**, e396-e403 (2016).

56. Aurora, A., Garg, K., Corona, B.T. & Walters, T.J. Physical rehabilitation improves muscle function following volumetric muscle loss injury. *BMC sports science, medicine and rehabilitation* **6**, 41-1847-1846-1841. eCollection 2014 (2014).

57. Mintz, E.L., *et al.* Long-Term Evaluation of Functional Outcomes Following Rat Volumetric Muscle Loss Injury and Repair. *Tissue engineering. Part A* **26**, 140-156 (2020).

58. Nakayama, K.H., *et al.* Rehabilitative exercise and spatially patterned nanofibrillar scaffolds enhance vascularization and innervation following volumetric muscle loss. *NPJ Regenerative medicine* **3**, 16 (2018).

59. Quarta, M., *et al.* Bioengineered constructs combined with exercise enhance stem cell-mediated treatment of volumetric muscle loss. *Nature communications* **8**, 15613 (2017).

60. Montravers, P., Maulin, L., Mohler, J. & Carbon, C. Microbiological and inflammatory effects of murine recombinant interleukin-10 in two models of polymicrobial peritonitis in rats. *Infection and immunity* **67**, 1579-1584 (1999).

61. Alvarez, H.M., *et al.* Effects of PEGylation and immune complex formation on the pharmacokinetics and biodistribution of recombinant interleukin 10 in mice. *Drug metabolism and disposition: the biological fate of chemicals* **40**, 360-373 (2012).

62. Szelenyi, E.R. & Urso, M.L. Time-course analysis of injured skeletal muscle suggests a critical involvement of ERK1/2 signaling in the acute inflammatory response. *Muscle & nerve* **45**, 552-561 (2012).

63. Ramos, L., *et al.* Characterization of Skeletal Muscle Strain Lesion Induced by Stretching in Rats: Effects of Laser Photobiomodulation. *Photomedicine and laser surgery* **36**, 460-467 (2018).

64. Beiting, D.P., Bliss, S.K., Schlafer, D.H., Roberts, V.L. & Appleton, J.A. Interleukin-10 limits local and body cavity inflammation during infection with muscle-stage Trichinella spiralis. *Infection and immunity* **72**, 3129-3137 (2004).

65. Barbe, M.F., *et al.* Key indicators of repetitive overuse-induced neuromuscular inflammation and fibrosis are prevented by manual therapy in a rat model. *BMC musculoskeletal disorders* **22**, 417 (2021).

66. Garg, K., Ward, C.L., Rathbone, C.R. & Corona, B.T. Transplantation of devitalized muscle scaffolds is insufficient for appreciable de novo muscle fiber regeneration after volumetric muscle loss injury. *Cell and tissue research* **358**, 857-873 (2014).

67. Wu, X., Corona, B.T., Chen, X. & Walters, T.J. A standardized rat model of volumetric muscle loss injury for the development of tissue engineering therapies. *BioResearch open access* **1**, 280-290 (2012).

68. Kim, J.T., Kasukonis, B.M., Brown, L.A., Washington, T.A. & Wolchok, J.C. Recovery from volumetric muscle loss injury: A comparison between young and aged rats. *Experimental gerontology* **83**, 37-46 (2016).

69. Dobin, A., *et al.* STAR: ultrafast universal RNA-seq aligner. *Bioinformatics* **29**, 15-21 (2013).

70. Liao, Y., Smyth, G.K. & Shi, W. featureCounts: an efficient general purpose program for assigning sequence reads to genomic features. *Bioinformatics* **30**, 923-930 (2014).

71. Robinson, M.D., McCarthy, D.J. & Smyth, G.K. edgeR: a Bioconductor package for differential expression analysis of digital gene expression data. *Bioinformatics* **26**, 139-140 (2010).

72. Kramer, A., Green, J., Pollard, J., Jr. & Tugendreich, S. Causal analysis approaches in Ingenuity Pathway Analysis. *Bioinformatics* **30**, 523-530 (2014).

73. Dunn, C., *et al.* Blood-Brain Barrier Breakdown and Astrocyte Reactivity Evident in the Absence of Behavioral Changes after Repeated Traumatic Brain Injury. *Neurotrauma reports* **2**, 399-410 (2021).

74. Castilla-Casadiego, D.A., *et al.* Methods for the Assembly and Characterization of Polyelectrolyte Multilayers as Microenvironments to Modulate Human Mesenchymal Stromal Cell Response. *ACS biomaterials science & engineering* **6**, 6626-6651 (2020).

75. Brown, L.A., *et al.* Moderators of skeletal muscle maintenance are compromised in sarcopenic obese mice. *Mechanisms of ageing and development* **194**, 111404 (2021).

76. Reed, C. University of Arkansas (2021).

Acknowledgements

This project was supported by the National Institute of Arthritis and Musculoskeletal and Skin Diseases of the National Institutes of Health (Award Number 1R15 AR073492-01) as well as the Arkansas Bioscience Institute.

Author Contributions

T.H and J.W designed the study. T.H ran most of the experiments and led the overall data analyses. C.R helped with animal work. Z.B and P.P helped with histological work. L.C.P.H helped with the Luminex Multiplex Immunoassay experiment. J.A and D.Z advised on this project. All authors edited the manuscript.

CHAPTER 5: Conclusion and future directions

5.1 Conclusion

In this dissertation, we have shown that injectable therapies that directly modulate the immune muscle microenvironment can enhance muscle regeneration and recovery. The findings also underlined that each injury model has a unique immune response in a sequential fashion. Additionally, when using similar therapeutics strategy (dECM), different models produced distinct regenerative and recovery mechanism in response to the dECM. Further, we also produced transcriptomic and proteomic profiles associated with the injuries, and the recovery responses to the repair strategies. As these omics data can be reanalyzed and reused in combination with old and new studies, integration of data from omics methods can produce a more comprehensive screening of relevant tissue environment than classic methods (qPCR, western blot, etc.). Further, the continually decreasing financial cost of these techniques is anticipated to lead to their application in personalized medicine, and applying omics technologies to regenerative research will provide datasets that would undoubtedly inform the development of future therapies. As demonstrated in this study, transcriptomic analysis at the early timepoints of the VML injury and repair strategies led to the hypothesis of using delayed delivery of IL-10 as a mean to boost repair and recovery. Though, this study only investigated the effect of IL-10 delivery, there are a variety of cytokines and soluble factors that could also be employed to enhance recovery based on the omics data. For example, our transcriptomic analysis in the VML study revealed that the delivery of IL-10 upregulated IL-4 and IL-33. They are not only important regulators of Treg cells which were found to contribute to the enhanced recovery following our VML injury and repair, but also affect other important cells populations that participate in the recovery process[1,2]. Therapeutics that incorporate these specific cytokines and

other targets identified by the omics data would provide us with novel approaches to tailor therapeutics depending on the types and the stages of investigated muscle injuries/diseases. Our study and others also showed that enhancement in muscle mass may not translate directly into enhanced force[3]. This recovery shortcoming has been attributed to the lack of regeneration in blood vessels, and NMJs[4]. In an ideal scenario, the biochemical cues from next generation biomaterial can be leveraged to promote muscle regeneration in conjunction with blood vessel infiltration, and NMJ formation.

Although skeletal muscle engineering was started with synthetic polymer systems, the future of skeletal muscle engineering may increasingly rely on combining ECM-derived and synthetic biomaterials with scaffold fabrication techniques to create tunable physicochemical therapeutic systems. Our studies have shown that dECM provide biological cues that is crucial in modulating the muscle microenvironment. Though not a scope of this study, our lab and others have shown that dECM and ECM-derived material also promoted implanted cell survival and allowed them to enhance the functional recovery [5,6]. For severe and chronic muscle injuries/diseases, the addition of cell delivery to many repair strategies appeared to produce an enhanced functional recovery in pre-clinical models[7-9], and has been used in the clinic with mixed outcomes[10]. Myogenic progenitors appear to be the most promising cell source owing to their ability to improve the development/survival of newborn myofibers thru paracrine signaling and to directly form new myofibers[11]. MSCs are another source for muscle regeneration given their positive outcomes in preclinical and clinical trials[12]. Unlike skeletal muscle-derived cells, MSCs present low immunogenicity, are well characterized, and are closer to clinical translation. In the case of MMGs repair, since they are freshly excised from muscle, they would be comprised of all muscle cell populations (discussed in chapter 1) including myogenic progenitors

and MSCs. This method of repair, though unable to translate directly into the clinic, has provided tremendous insight into the importance of cell delivery in tissue repair. For example, preclinical trials using MMGs or implanted cells with myogenic potential have only seen improved *de novo* myofiber generation at early time-points or enhanced myotube formation when GFs were co-delivered[13]. This limitation can be attributed to responses of immune cells and the muscle microenvironment to the implanted cells.

In this study, we demonstrated that delayed (7 DPI) IL-10 delivery that was sustained for 1 week would enhance muscle regeneration, but it remained uncertain how and what other physical and chemical signals can be added to this strategy to create a better environment for repair. As our timepoints are limited to 3DPI (before IL-10 delivery), 14 DPI (1 day after the last IL-10 delivery), there are unknown changes in the MIME during the delivery window or during the recovery window. Further work must be done to determine the pathological immune response to muscle injury and how therapeutic strategies that alter this response benefit the repair process. Lastly, though not classified as immune cells, FAPs can crosstalk and directly modulate the MIME (and vice versa) to influence recovery process[14]. In this study, we demonstrated that FAPs behaved differently to promote tissue regeneration in the two injury models (e.g., HU, RCT), and likely modulate the two MIMEs using distinctive mechanisms given the different starting MIMEs. In the case of RCT, as different tear size can produce different MIMEs, the FAPs from full thickness tears displayed greater fibrogenic and adipogenic differentiation capacity *in vitro* than those harvested from partial tears, suggestive of FAP epigenetic changes across tear states[15]. Furthermore, FAP production of fibrosis and FI can significantly alter the composition of the ECM in the affected muscle, which may negatively impact the regenerative capacity of MuSCs. Beyond indirectly influencing the SC activity via ECM modification, FAPs in injured muscle

may directly facilitate anti-myogenic signaling in different cells population in the MIME . During normal regeneration, FAP expansion is transient and supports myoblast differentiation. However, in chronic injury, FAPs at the affected muscle displayed increased expression of genes associated with muscle atrophy, and their co-culture with myoblasts resulted in reduced fusion and myotube diameter[16]. This could be attributed to the paracrine signaling of dysfunctional FAPs. Aging MIME can decrease FAPs' production of IL-33 leading to deficiency in Tregs accumulation, resulting in an impaired muscle regenerative capacity[17], while muscular dystrophy MIM can induce excessive IL-33 signaling from FAPs leading to eosinophilia activation resulting muscle fibrosis[18]. As the quantities, the subtypes, and activities of FAPs can affect the recovery process, future work should characterize FAPs contribution to different types and at different stages of MIMEs as well as evaluate the effect of therapeutics on FAPs and modulating FAPs to promote a regenerative MIME. In summary, the findings from this work emphasize that efforts should be made to understand and modulate all actors in the affected MIMEs (niches, cells, and signaling) to boost functional recovery.

5.2 Future directions

As dECM gel injection has been used in human safety trials, the next step of this study should be to test dECM gel injection on a small cohort of patients suffering from re-tear of the RC tendons after repair and regrowth of healthy muscle[19]. The findings from human trials would add to our understanding of the safety and side effects of injectable dECM. Though some studies have reported the use of human-derived dECM including ours, availability can be limiting[20]. A major source of tissue for dECM applications comes from pigs due to their availability, size, and genetic relatedness to humans human[21]. The main limitation of pig dECM is the presence of foreign antigens present in xenogeneic tissues that can trigger an inflammatory immune response

when implanted[22]. A study reported that in general, solubilized dECM induces an M2-like phenotype, but exposure to different sources of xenogeneic dECM can induce M1-phenotype expression of macrophages [23]. To overcome this obstacle, one possibility is to leverage multiple emerging technologies to produce humanized skeletal muscle in pigs[24]. These pigs can be constructed with human cells from 'universal donors' or with personalized human cells derived from the patient. Beside serving as an allogenic source of dECM, it is also possible that differentiated human cells (satellite cells, progenitor cells) could be harvested from these chimeric animals to provide an ample source of cells such that combination therapies can be utilized. The feasibility of the production of humanized skeletal muscle in pigs relies upon three emerging technologies: CRISPR based gene-editing of porcine fibroblasts, SCNT (cell cloning) of edited porcine fibroblasts, and blastocyst complementation with hiPSCs[21]. Using the vacant niche approach, porcine embryos were gene-edited to lack skeletal muscle (vacant niche). Blastocyst complementation was then used to deliver exogenous stem cells (human pig chimeras) to the skeletal muscle null porcine embryo, the null phenotype was rescued. Human muscle is specified and differentiated following blastocyst complementation of the skeletal muscle null embryo with hiPSCs. The interspecies pigs (human:pig) generated with this niche based strategy result in donor cells contributed nearly exclusively to the skeletal muscle niche and not to other organs such as the brain or germ line. Lastly, human animal chimeras can be used, not only as a source of humanized muscle for transplantation, but also as humanized models for exploration of human myogenesis, MIMEs responses to injury and disease, as well as toxicology and therapeutic efficacy screens.

As shown in this study, manipulation of MIMEs using cytokines can also be an effective ad-on strategy to any standard of care therapies. Our sustained delayed delivery of IL-10 is a

proof of concept and can be translated into the clinic using a variety of engineered delivery vehicles. Dose control is also vital as cytokine concentrations above physiological levels have led to adverse effects including cancer, neurological problems and ectopic bone formation[25]. The field of engineered controlled delivery of bioactive molecules has shown promising accomplishments in both pre-clinal and clinical studies[26]. To fully exploit the versatility of ECM-based therapeutics, researchers have designed drug-loaded ECM to incorporate stimuli-responsive molecules (e.g., polymers, proteins and peptides) or nanostructured materials (e.g., iron oxide, gold nanoparticles, and graphene oxide) that respond to individual or combined stimuli. Some examples of the stimuli include light, magnetic, ultrasound, electric, ion, temperature, and enzyme triggered release[27]. Though in the context of muscle tissue, calcium-ion triggered release is a most fascinating topic as muscle's main function of contraction is not possible without calcium[28]. Although there are a variety of methods to manipulate the calcium levels in cells, mechanical stimulation or energy-based (magnetic, ultrasound) stimulation seemed to be most appropriate in for muscle target and can be performed by the patients at home[29]. As mentioned previously, there are many types of encapsulation that can be employed, though liposomes are among the most promising for intramuscular injection as well as the aforementioned calcium-triggered release[30].

Lastly, a new frontier of research using extracellular vesicles (EVs) have emerged as a more complex form of liposomes, but with a biological origin. Similarly to liposomes, numerous studies to date have reported the incorporation of drugs into EVs, to assess their suitability as drug delivery vehicles[31]. Furthermore, as the EVs are produced by cells, in addition to the incorporated molecules, other functional proteins can also be purposefully presented in the EVs. For example, EVs derived from antigen-presenting cells (APCs) (e.g., B-lymphocytes, DCs,

microglia, and macrophages) are enriched with major histocompatibility complex (MHC) proteins. These EVs carrying MHCs have been shown to stimulate $CD4^+$ T cells which play an important role in muscle repair. Besides proteins, EVs also carry a multitude of coding and non-coding RNAs, including mRNA, miRNA, circRNA, tRNA, snoRNA, and piRNA. Like proteins, specific functional RNAs are produced by specific sources of cells. For example, Treg-derived EV's ability to postpone graft rejection and extend host's survival was attributed to miRNAs[32]. Furthermore, therapeutic RNAs cargos can be loaded or engineered into the EV biogenesis process. Intra-tumoral injection of antisense RNA-loaded Red Blood Cell-derived EVs could efficiently inhibit breast tumor growth[33]. As the biogenesis of specific populations of EVs is increasingly understood, it is possible to specifically engineer and utilize these different populations to produce sequential EV therapeutics tailored to specific stages of injury/diseases[31]. These have resulted in highly encouraging proof-of-concept studies in preclinical models. Nonetheless, more effort needs to be made to achieve translational applications of EVs[31]. Increasingly detailed investigations into EV biogenesis, cargo sorting, EV subpopulations, and internalization/ trafficking pathways in recipient cells can provide more insight in employing EVs as bioactive payload carriers for regenerative medicine.

5.3 References

1. Heredia, J.E., *et al.* Type 2 innate signals stimulate fibro/adipogenic progenitors to facilitate muscle regeneration. *Cell* **153**, 376-388 (2013).

2. Gadani, S.P., Walsh, J.T., Smirnov, I., Zheng, J. & Kipnis, J. The glia-derived alarmin IL-33 orchestrates the immune response and promotes recovery following CNS injury. *Neuron* **85**, 703-709 (2015).

3. Novakova, S.S., *et al.* Repairing Volumetric Muscle Loss in the Ovine Peroneus Tertius Following a 3-Month Recovery. *Tissue engineering. Part A* **26**, 837-851 (2020).

4. Gilbert-Honick, J. & Grayson, W. Vascularized and Innervated Skeletal Muscle Tissue Engineering. *Advanced healthcare materials* **9**, e1900626 (2020).

5. Kasukonis, B., *et al.* Codelivery of Infusion Decellularized Skeletal Muscle with Minced Muscle Autografts Improved Recovery from Volumetric Muscle Loss Injury in a Rat Model. *Tissue engineering. Part A* **22**, 1151-1163 (2016).

6. Gilbert-Honick, J., *et al.* Engineering functional and histological regeneration of vascularized skeletal muscle. *Biomaterials* **164**, 70-79 (2018).

7. Pumberger, M., *et al.* Synthetic niche to modulate regenerative potential of MSCs and enhance skeletal muscle regeneration. *Biomaterials* **99**, 95-108 (2016).

8. Gilbert-Honick, J., *et al.* Adipose-derived Stem/Stromal Cells on Electrospun Fibrin Microfiber Bundles Enable Moderate Muscle Reconstruction in a Volumetric Muscle Loss Model. *Cell transplantation* **27**, 1644-1656 (2018).

9. Hwang, J.H., *et al.* Combination therapy of human adipose-derived stem cells and basic fibroblast growth factor hydrogel in muscle regeneration. *Biomaterials* **34**, 6037-6045 (2013).

10. Kosyakova, N., *et al.* Differential functional roles of fibroblasts and pericytes in the formation of tissue-engineered microvascular networks in vitro. *NPJ Regenerative medicine* **5**, 1 (2020).

11. Alheib, O., da Silva, L.P., Kwon, I.K., Reis, R.L. & Correlo, V.M. Preclinical research studies for treating severe muscular injuries: focus on tissue-engineered strategies. *Trends in biotechnology* (2022).

12. Qazi, T.H., *et al.* Cell therapy to improve regeneration of skeletal muscle injuries. *Journal of cachexia, sarcopenia and muscle* **10**, 501-516 (2019).

13. Kiran, S., Dwivedi, P., Kumar, V., Price, R.L. & Singh, U.P. Immunomodulation and Biomaterials: Key Players to Repair Volumetric Muscle Loss. *Cells* **10**(2021).

14. Joe, A.W., *et al.* Muscle injury activates resident fibro/adipogenic progenitors that facilitate myogenesis. *Nature cell biology* **12**, 153-163 (2010).

15. Feeley, B.T., *et al.* Human Rotator Cuff Tears Have an Endogenous, Inducible Stem Cell Source Capable of Improving Muscle Quality and Function After Rotator Cuff Repair. *The American journal of sports medicine* **48**, 2660-2668 (2020).

16. Madaro, L., *et al.* Denervation-activated STAT3-IL-6 signalling in fibro-adipogenic progenitors promotes myofibres atrophy and fibrosis. *Nature cell biology* **20**, 917-927 (2018).

17. Kuswanto, W., *et al.* Poor Repair of Skeletal Muscle in Aging Mice Reflects a Defect in Local, Interleukin-33-Dependent Accumulation of Regulatory T Cells. *Immunity* **44**, 355-367 (2016).

18. Kastenschmidt, J.M., *et al.* A stromal progenitor and ILC2 niche promotes muscle eosinophilia and fibrosis-associated gene expression. *Cell reports* **35**, 108997 (2021).

19. Traverse, J.H., *et al.* First-in-Man Study of a Cardiac Extracellular Matrix Hydrogel in Early and Late Myocardial Infarction Patients. *Jacc-Basic Transl Sc* **4**, 659-669 (2019).

20. Zhang, X., *et al.* Decellularized extracellular matrix scaffolds: Recent trends and emerging strategies in tissue engineering. *Bioactive materials* **10**, 15-31 (2022).

21. Greising, S.M., Weiner, J.I., Garry, D.J., Sachs, D.H. & Garry, M.G. Human muscle in gene edited pigs for treatment of volumetric muscle loss. *Frontiers in genetics* **13**, 948496 (2022).

22. Kasravi, M., *et al.* Immunogenicity of decellularized extracellular matrix scaffolds: a bottleneck in tissue engineering and regenerative medicine. *Biomaterials research* **27**, 10 (2023).

23. Dziki, J.L., *et al.* Solubilized extracellular matrix bioscaffolds derived from diverse source tissues differentially influence macrophage phenotype. *Journal of biomedical materials research. Part A* **105**, 138-147 (2017).

24. Maeng, G., *et al.* Humanized skeletal muscle in MYF5/MYOD/MYF6-null pig embryos. *Nature biomedical engineering* **5**, 805-814 (2021).

25. Carragee, E.J., Hurwitz, E.L. & Weiner, B.K. A critical review of recombinant human bone morphogenetic protein-2 trials in spinal surgery: emerging safety concerns and lessons learned. *The spine journal : official journal of the North American Spine Society* **11**, 471-491 (2011).

26. Qu, M., *et al.* Stimuli-Responsive Delivery of Growth Factors for Tissue Engineering. *Advanced healthcare materials* **9**, e1901714 (2020).

27. Serna, J.A., *et al.* Recent Advances on Stimuli-Responsive Hydrogels Based on Tissue-Derived ECMs and Their Components: Towards Improving Functionality for Tissue Engineering and Controlled Drug Delivery. *Polymers* **13**(2021).

28. Rudsari, H.K., Veletic, M., Bergsland, J. & Balasingham, I. Targeted Drug Delivery for Cardiovascular Disease: Modeling of Modulated Extracellular Vesicle Release Rates. *IEEE transactions on nanobioscience* **20**, 444-454 (2021).

29. Castellanos, I., Balteanu, B., Singh, T. & Zderic, V. Therapeutic Modulation of Calcium Dynamics using Ultrasound and Other Energy-based Techniques. *IEEE reviews in biomedical engineering* **9**, 177-191 (2016).

30. Lou, J. & Best, M.D. Calcium-responsive liposomes: Toward ion-mediated targeted drug delivery. *Methods in enzymology* **640**, 105-129 (2020).

31. Elsharkasy, O.M., *et al.* Extracellular vesicles as drug delivery systems: Why and how? *Advanced drug delivery reviews* **159**, 332-343 (2020).

32. Aiello, S., *et al.* Extracellular vesicles derived from T regulatory cells suppress T cell proliferation and prolong allograft survival. *Scientific reports* **7**, 11518 (2017).

33. Usman, W.M., *et al.* Efficient RNA drug delivery using red blood cell extracellular vesicles. *Nature communications* **9**, 2359 (2018).

APPENDIX: Protocol approval

UNIVERSITY OF ARKANSAS

Office of Research Compliance

To:	Jeff Wolchok
Fr:	Craig Coon
Date:	August 9th, 2018
Subject:	IACUC Approval
Expiration Date:	August 2nd, 2021

The Institutional Animal Care and Use Committee (IACUC) has APPROVED your protocol # **19002:** *Matrix Gel Efficacy Testing*.

In granting its approval, the IACUC has approved only the information provided. Should there be any further changes to the protocol during the research, please notify the IACUC in writing (via the Modification form) prior to initiating the changes. If the study period is expected to extend beyond August 2nd, 2021 you must submit a newly drafted protocol prior to that date to avoid any interruption. By policy the IACUC cannot approve a study for more than 3 years at a time.

The following individuals are approved to work on this study: Jeffrey Wolchok, Tyrone Washington, and John Kim. Please submit personnel additions to this protocol via the modification form prior to their start of work.

The IACUC appreciates your cooperation in complying with University and Federal guidelines involving animal subjects.

CNC/tmp

19002

UNIVERSITY OF ARKANSAS

Office of Research Compliance

To:	Jeff Wolchok
Fr:	Craig Coon
Date:	September 11th, 2018
Subject:	IACUC Approval
Expiration Date:	September 6th, 2021

The Institutional Animal Care and Use Committee (IACUC) has APPROVED your protocol # **19025:** *Synergizing Immunotherapy and Regenerative Medicine to Treat Muscle Injury*.

In granting its approval, the IACUC has approved only the information provided. Should there be any further changes to the protocol during the research, please notify the IACUC in writing (via the Modification form) prior to initiating the changes. If the study period is expected to extend beyond September 6th, 2021 you must submit a newly drafted protocol prior to that date to avoid any interruption. By policy the IACUC cannot approve a study for more than 3 years at a time.

The following individuals are approved to work on this study: Jeffrey Wolchok, Tyrone Washington, John Kim, and Tai Huynh. Please submit personnel additions to this protocol via the modification form prior to their start of work.

The IACUC appreciates your cooperation in complying with University and Federal guidelines involving animal subjects.

CNC/tmp